2016

Design of a solar cooling system for Iraq climate

Fakhraldin, Shahen Mohammed

Design of a solar cooling system for Iraq climate

By

Shahen Mohammed Fakhraldin

NO. 10341880

A thesis submitted to the Plymouth University in partial fulfilment for the degree of

Doctor of Philosophy

in

Mechanical Engineering

Faculty of Science and Engineering

School of Marine Science and Engineering

Plymouth University

July 2016

Design of a solar cooling system for Iraq climate

Shahen Mohammed Fakhraldin

Abstract

With the objectives of designing a solar cooling system with cold storage unit for the Iraqi climate, solar energy resources were assessed and methods were proposed to enhance harvesting the solar energy in the Iraqi climate. Where the results showed that adopting monthly average optimal tilt angles led to an increase in the amount of useful solar energy gained nearly 9%. A methodology of multi objective optimisation of solar absorption cooling system was then developed and demonstrated by applying it in a domestic application in Baghdad. Maximising the system performance in exergy, economic and environment were the objectives of the project. A decision-making tool was then implemented to select the most suitable design. The optimal proposed system has exergy efficiency of 56%, total cost rate of 4.19US$/hr, annual CO_2 emission of 32199kg and payback period of 18.7years. After analysing the optimal configuration of the system, a cold thermal energy storage unit with the solar absorption cooling system was suggested in order to store the cold energy produced by the system at times when the solar energy is available (at daytime) and use (discharge) it at times when there is no solar energy available (at night). Next, a new control strategy was developed and applied in the system to make it more cost effective. Five scenarios were considered to manage the quantity of charging of the cold storage tank according to the splitting rate of the mass of the supplied chilled water by the chiller to the cold storage tank and the building. Finally, the chosen optimal system that uses an efficient controlled cold thermal energy storage, has exergy efficiency of 69.4%, total cost rate of 4.25US$/hr and total avoided annual CO_2 emissions of 33.9% less than system without cold storage tank. Additionally, without any government

incentive, the payback was recorded 9.3years, which was 50% less than the system without cold storage tank.

List of Content

List of Figures

List of Tables

List of symbols

$\dot{E}$	Exergy rate (kJ/hr)
$\dot{E}_D$	Exergy destruction (kJ/hr)
$\dot{Q}$	Rate of heat transfer (kJ/hr)
$\dot{m}$	Mass flow rate (kg/hr)
$\dot{W}$	Work rate (kg/hr)
T_o	Ambient temperature (K)
$C^{\bullet}$	Cost rate (US$/hr)
$Z^{\bullet}$	Investment and maintenance cost rate (US$/hr)
C_{elec}	Electricity cost (US$/kW.hr)
op_{aux}	Heating rate in the auxiliary heater (kJ/hr)
m'	Optical air mass (-)
Ar	Area of the solar collectors (m^2)
AST	Apparent solar time (hr)
C	Cost (US$)
cp	Specific heat at constant pressure (kJ/kg.K)
crf	Capital recovery factor
E_b	Beam (normal) component of clear sky solar radiation (W/m^2)
E_d	Diffuse component of clear sky solar radiation (W/m^2)
E_t	Total clear sky solar irradiance (W/m^2)
Et_b	Tilted beam solar irradiance (W/m^2)
E_{td}	Tilted diffuse solar irradiance (W/m^2)
E_{tr}	Tilted ground reflected solar irradiance (W/m^2)
h	Specific enthalpy (kJ/kg)
H	Hour angle (°)
I_b	Direct beam solar irradiance on horizontal surfaces (W/m^2)
I_{bt}	Direct beam solar irradiance on tilted surface (W/m^2)

I_d	Diffuse solar irradiance on horizontal surfaces (W/m^2)
I_{dt}	Diffuse solar irradiance on tilted surfaces (W/m^2)
I_g	Global solar irradiance on horizontal surface (W/m^2)
I_G	Monthly average global solar irradiance (W/m^2)
I_o	Extraterrestrial solar irradiance on horizontal surface (W/m^2)
ir	Interest rate (%)
I_r	Ground reflected irradiance on tilted surfaces (W/m^2)
I_t	Total solar irradiance on tilted surface (W/m^2)
k	Diffuse index, the ratio between the diffuse irradiance and global irradiance (-)
k_b	Direct transmittance index, the ratio between the direct irradiance and extraterrestrial irradiance (-)
k_d	Diffuse transmittance index, the ratio between the diffuse irradiance and extraterrestrial irradiance (-)
k_t	Clearness index, the ratio of global irradiance to the extraterrestrial irradiance (-)
Kt	Daily clearness index (-)
k_t'	Normalised clearness index (-)
L	Latitude angle (°)
MABE	Mean absolute bias error (W/m^2)
MAPE	Mean absolute percentage error (%)
N	Operation hours of the system (hr)
n	System life span (year)
PW	Present worth (%)
pwf	Present worth factor (-)
Rh	Relative humidity (%)
RMSE	Root mean square error (W/m^2)
s	Specific entropy (kJ/kg.K)
SF	Solar fraction (-)
SP	Simple payback (year)
sv	Salvage value (%)

T	Temperature (K)
Tt, Tb	Top and bottom temperatures of the tank (°C)
V	Volume of the tank (m^3)
Z	Zenith angle (°)

Greek symbols

Ψ	Surface azimuth angle (°)
Ψ'	Specific unit exergy (kJ/kg)
ε	Exergy efficiency (%)
μ	Salvage value percentage (%)
μ_{CO_2}	CO_2 emissions factor (kg CO_2/kW.hr)
$\sum$	Inclination angle (°)
β	Altitude angle
γ	Control signal (-)
δ	Declination angle (°)
θ	Incidence angle (°)
ρ	Clear sky index (-)
σ_3	Variability index (-)
τ_b & τ_d	Beam and diffuse pseudo optical depths (-)
Φ	Persistence index (-)
Ω	Skartveit and Olseth variable (-)
Ω’	Maintenance factor (-)

Superscripts

CH	Chemical
KN	Kinetic
PH	Physical
PT	Potential

Subscripts

amb	Ambiant
aux	Auxiliary heater
c	cold
Chill	Chiller
coll	Collector
ct	Colling tower
CTES	Cold thermal energy storage
h	hot
HTES	Hot storage tank
inv	Investment
k	Component
op	Operation
opt	Optimal
pu	Pump

Acknowledgement

I did not notice that I have been in the UK for almost five years. I cannot say it is the best time in my life, but I would like to cherish this period that let me link with so many special people who made my life more meaningful!

First and foremost, I would like to thank my advisor Dr. Ming Dai, who truly has been the best mentor, helper, and friend throughout this process. I could not have imagined having a better advisor for my PhD study.

The financial support from Iraqi Ministry of Higher Education and Scientific Research is gratefully acknowledged.

I thank my mother who could always be counted on as a source of caring and support.

At the end, I would like express appreciation to my beloved wife Zaynab who spent sleepless nights with and was always my support in the moments when there was no one to answer my queries.

Author's Declaration

At no time during the registration for the degree of Doctor of Philosophy has the author been registered for any other University award without prior agreement of the Graduate Sub-Committee. This study was financed with the aid of a scholarship from the Ministry of Higher Education and Scientific Research, Iraq.

Word count of the thesis: 40420

Signed …….……..…...

Date …29/7/2016…….

Chapter One

Introduction

1.1 Introduction

Attempts to find alternative energy sources to fossil fuels began in the 1970s, particularly after the energy crisis when the Arab countries stopped exporting oil to Western countries that had supported Israel in the war of 1973. After that period, these attempts slowed because of the relatively lower prices of fossil fuels. Concerns increased again after the dramatic rise in fuel prices after the Gulf War II. Fossil fuel is considered one of the main factors of air pollution and climate change. Climate change has serious environmental, economic and social consequences, such as global warming and natural disasters.

Heating, refrigeration and air conditioning sectors have recently seen tremendous growth. In addition to their importance for human comfort, they have become essential for industrial applications such as in the food industry. For example, the sales of air-conditioning systems in China have doubled within the last five years, reaching 64 million units, eight times the sales in the USA in 2013 (Davis & Gertler, 2015). The share of buildings in global energy consumption is about 40% (Yang, Yan & Lam, 2014), with cooling and heating requirements as key participants. In the USA, nearly half of the energy consumed in residential buildings is used for indoor environment control (Koo et al., 2014), where 90% of the houses have air-conditioning units. In Arab Gulf states, in the summer months, 40-65% of the power consumption is used for air-conditioning systems, due to the fact that the summer is long with high temperatures, and may reach the fifties Celsius (Hasnain et al., 1999; Sebzali & Rubini, 2006). Said et al. (2015) add that 70% of the energy consumed in the residential sector is used for “comfort conditioning” in Saudi

Arabia. Said et al. also state that “Gulf countries are realising the fact that they might end up (in few years) consuming more than 80% of the fossil fuel they produce to meet domestic energy demand”. However, the power generation sector in Middle East countries, which currently relies on fossil fuels, needs more than 120 GW to cover the growing demand by 2017, and this would represent investments of up to 250 billion US$ (Griffiths, 2013). Additionally, crude oil and natural gas are expected to be depleted significantly over the next four decades (Agyenim, Knight & Rhodes, 2010). This significant increase in energy consumption due to air-conditioning demand leads to a substantial increase in greenhouse gas emissions, directly due to leakage of high global warming potential refrigerants that are used in air-conditioning systems, and indirectly due to the emissions related to using fossil fuel in electricity generation stations (Mugnier, 2015b). Thus, there is an urgency to develop environmentally friendly systems that use sustainable energies, such as solar energy. Solar energy is an important sustainable energy source that can be used as an alternative to conventional energy sources because it is free, plentiful, inexhaustible and reaches everywhere without the need for transmission and distribution. Additionally, the total energy consumed in the world within one year was estimated to be less to that received by the Earth during just one hour’s emissions from the sun (Thirugnanasambandam, Iniyan & Goic, 2010). The intermittent nature of solar energy is one of the main obstacles facing any of the solar energy projects, and most of the countries in the Middle East still sell electricity to consumers at subsidised prices. However, this policy has begun to change, as happened recently in Jordan and Iraq. The social, economic and environmental awareness, as well as scientific progress, have given a strong momentum in the setting up or planning to build solar energy projects in the Middle East region, such as the “Shams I” and “Masdar City” projects in the UAE (Alnaser & Alnaser, 2011). Obviously, these projects are favourably supported by the abundance of solar

energy (Trieb & Müller-Steinhagen, 2008) in these regions. Figure 1-1 illustrates the availability of annual average solar radiation on Earth, with the Iraq site for this research indicated.

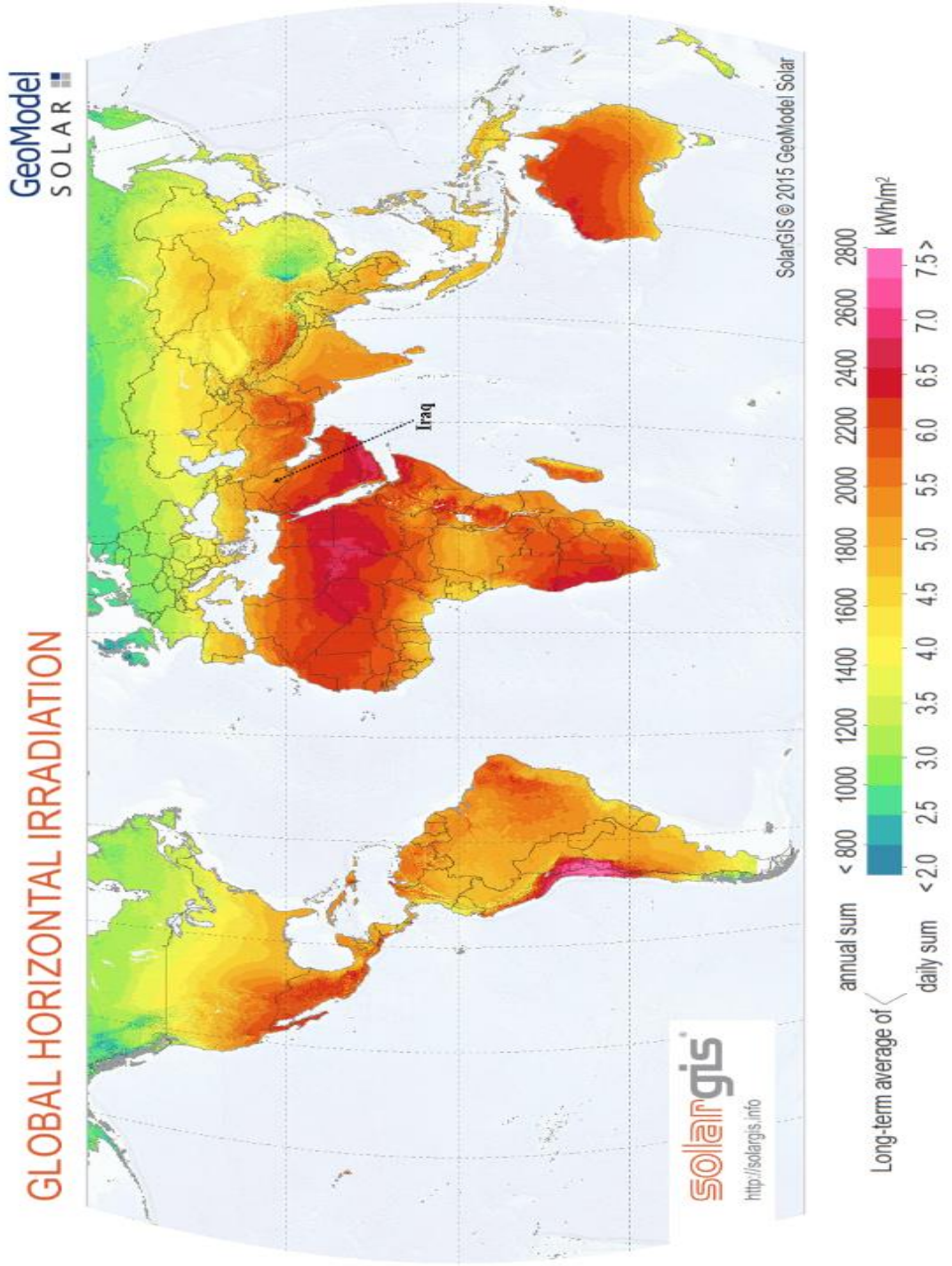

Figure 1-1 Annual availability of global solar irradiation and daily sunny hours on Earth, with the Iraq site for this research indicated (GoModel Solar).

1.2 Solar Cooling

Harvesting the sun's thermal and/ or photonic energy to produce a cooling effect can be defined as a solar air-conditioning system or solar cooling system. Besides its potential economical and ecological benefits, a solar cooling system has a distinct advantage over the other HVAC systems, that the maximum cooling load is demanded when solar energy is actually at its maximum availability, since the main cause of the heat gain in space, and buildings, comes from the sun.

There are several studies that have classified and listed various types of solar cooling systems, such as Sarbu & Sebarchievici (2013) and Hwang et al. (2008). Baniyounes et al. (2013) state that "The existing operated solar assisted air conditioning systems around the world can be classified into solar electric cooling technology and solar thermal cooling technologies. Solar electric cooling technology uses a conventional electric vapour compressor air conditioning process as an electrical energy is provided by solar photovoltaic (PV) panels. In solar thermal cooling technologies, solar heat is required to drive the cooling process. This can be done by collecting solar radiation using thermal solar collectors to convert it into thermal energy, and use this energy to drive thermally driven cooling cycles such as desiccant, absorption and adsorption cycles".

1.3 Aim and objectives of the research

The aim of this research is to propose the most suitable solar cooling system for a domestic application in Baghdad, Iraq. This will be done through the following detailed specific objectives:

- Review existing solar cooling systems to establish the fields that need more attention.

- Assess the solar energy resources and propose methods to enhance harvesting the solar energy in the Iraqi climate.
- Propose a methodology to design and assess a solar cooling absorption system based on exergic, economic and environmental aspects.
- Develop multi-criteria optimisation technique to optimise a solar absorption cooling system for a domestic application in Baghdad, Iraq.
- Present a new generic and simple control strategy for charging and discharging a water cold thermal energy storage used in a solar absorption cooling system.

This project aims to address the continuing demand for the various air conditioning systems in Iraq, due to the tremendous growth in the economy and expansion of business that has produced a large increase in the purchasing power in the past few years. Although there is a severe shortfall in electricity supply and poor security conditions, the demand is expected to continue for the next few years. The main drive of this study is to reduce the consumption of fossil fuels, thus minimising greenhouse gas emissions, as well as to propose an optimum solar cooling system according to the technical, economical and environmental aspects.

1.4 Outline

The design of a solar cooling system required a good knowledge of the state of the art of this technology, thus a literature review is presented in Chapter Two. Chapter Three then presents assessments of solar resources in Baghdad. The optimisation of the solar cooling absorption system, based on exergic, economic and environmental aspects, is described in Chapter Four. Chapter Five demonstrates a generic control strategy for solar cooling systems with cold thermal energy storage for residential applications. Finally, the major conclusions and future work recommendations are summarised in Chapter Six.

Chapter Two

Literature review

This chapter clarifies the reasons for choosing a solar thermal cooling system over PV (electric) solar cooling system and then shows why the absorption system is the preferred option. The state of the art on solar absorption system technology is presented, through reviewing previous research and studies that relate to this system.

2.1 Thermal vs electric (photovoltaic) solar cooling

Solar thermal and electric cooling systems are different in two ways, firstly, the means or tools used for the conversion of solar energy to thermal and/or to electric energy (solar collectors and PV panels); secondly, the generation of the cooling effect. In a solar thermal cooling system, a thermal driven chiller is used, while in solar electric cooling systems, traditional (electric driven) vapour compression chillers are used. Tyagi et al. (2013) reported that the efficiency of the PV panels commercially available is up to 17%, and this efficiency is in inverse relationship with the surrounding temperature and the intensity of incident solar irradiance; i.e this percentage goes down at higher temperatures. On the other hand, the efficiency of thermal collectors reaches higher than 50 %, and high temperature leads to an increase in the energy collected. Ullah et al. (2013) have reported that a solar thermal system is capable of exploiting 95% of observed solar energy. Lazzarin (2013) presented a comprehensive compression between these two technologies through thermodynamic and economic analysis. The investigation reported that the solar thermal cooling systems are better than solar electric cooling systems for water cooling systems. In addition, thermal solar systems used refrigerants that do not have any harmful effects on the environment, are free from Chlorofluorocarbons, and would satisfy all regulations

and rules of international conventions on reducing the depletion of the ozone layer and reducing global warming.

2.2 Solar thermal cooling

The phenomenon of sorption: physical or chemical attraction among substances, is the principle or mechanism for the production of cooling effect in solar thermal cooling systems (Fan, Luo & Souyri, 2007). There are many studies that reviewed and classified solar thermal systems and technology in detail, such as Ullah et al. (2013) and Wang et al. (2009). Existing solar thermal systems can be classified into two general types: open and closed systems. In open systems, the sorption process serves as a dehumidifier of the air (these systems are called the desiccant system), thereafter this dry air will be cooled and supplied to the building through an evaporative cooling process. In closed systems, the refrigerant is circulated in a closed loop and the cooling effect takes place though heat exchange between the refrigerant and the air supplied to the building (using fan coil units and air handling units). There are two technologies in closed systems: absorption and adsorption, and the main difference is in the nature of the sorbent. In the absorption system, the sorption process takes place between liquid (sorbent) and gaseous (refrigerant) substances, and the refrigerant undergoes a change in its phase, while in the adsorption system, the sorption process takes place between solid (sorbent) and gaseous (refrigerant) substances, without any changes in the nature of the substances.

Tsoutsos et al. (2003) indicated that the prevalence of absorption chillers in the market is considerably higher than adsorption chillers. Additionally, Henning (2007) and Calise (2010) reported that most of the solar cooling systems in the EU are based on the absorption system. Kim & Infante Ferreira (2008) reviewed the state of the art of current solar cooling systems, and reported that the absorption system has the lowest cost compared to the

adsorption and desiccant systems. In 2014, 2200 solar cooling systems were installed worldwide (Mugnier, 2015b), and currently solar absorption cooling technology is dominant over all other types of solar cooling technologies (Mugnier, 2015a).

2.3 Solar absorption system

Absorption systems were among the first systems used for refrigeration and air conditioning. They are also, currently, the most prevalent worldwide along with conventional vapour compression systems. The absorption (sorption) process with the aid of a heat source and a pump serves as the compressor in a vapour compression system (apart from this difference the other components are similar in both systems). Figure 2-1 shows the schematic diagram for the main components of the absorption and vapour compression systems. Absorption systems require only a small number of moving parts for their operation, which means quiet operation and low level of maintenance. Additionally, renewable energies, such as solar and biomass, and waste heat can be exploited to power absorption systems.

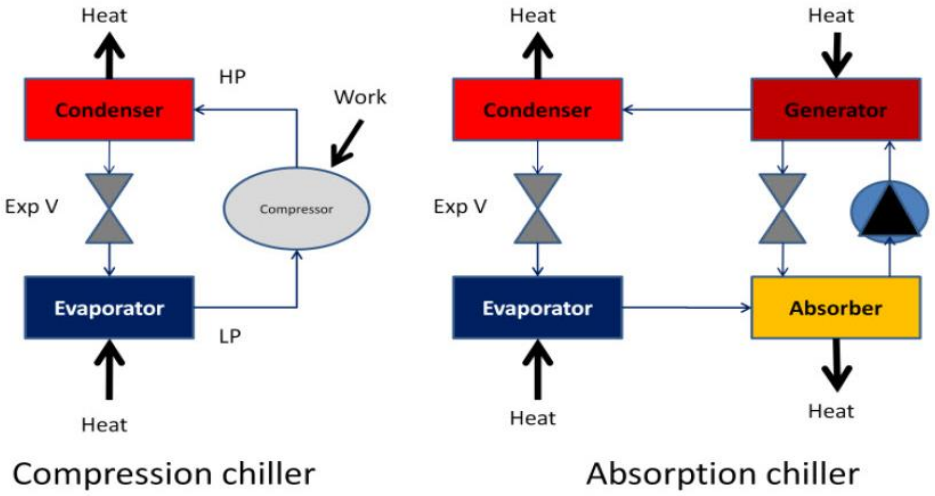

Figure 2-1 Schematic diagram for the main components of the absorption and vapour compression systems.

There are several types of working fluids used in absorption chillers; Karamangil et al. (2010) and Fan et al. (2007) reviewed those working fluids and they reported that the lithium bromide-water (LiBr-H_2O) solution pair is more suitable for air-conditioning applications than other working fluids. Figure 2-2 shows a solar assisted LiBr-H_2O absorption cooling system.

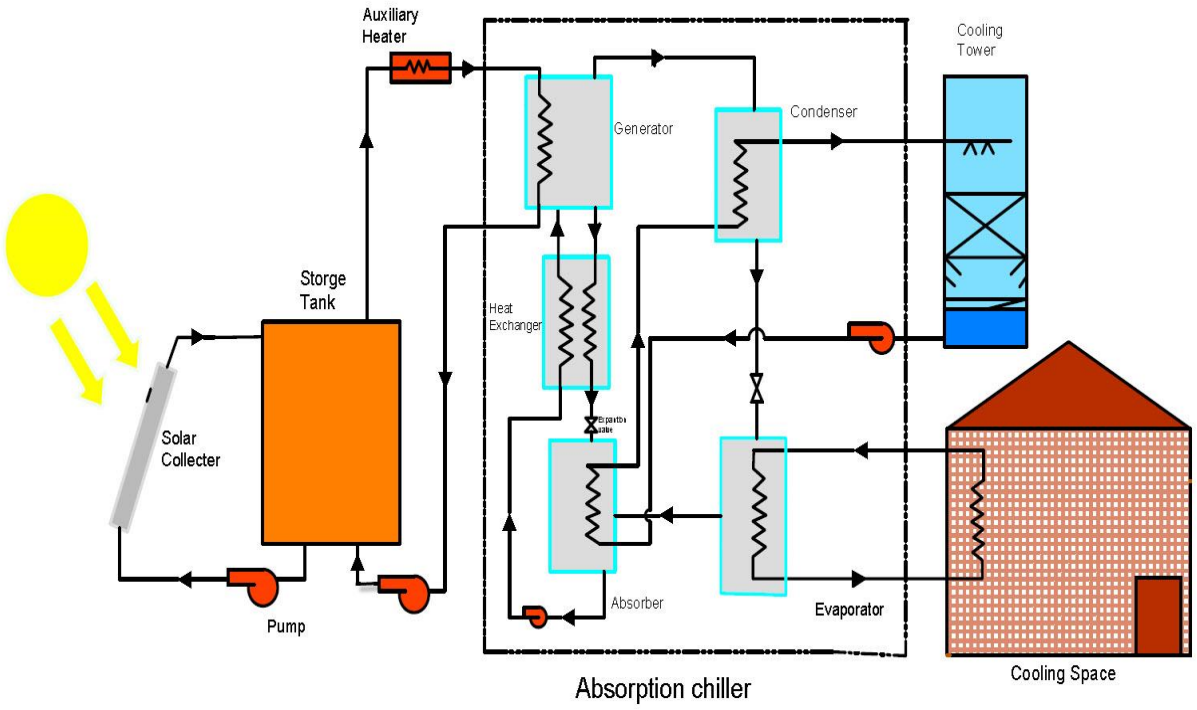

Figure 2-2 A solar assisted LiBr-H_2O absorption cooling system.

2.4 The operation of a solar single stage LiBr-H2O absorption chiller

In the evaporator, the water gains its latent heat from the warmer water that comes from the space to be cooled; as a result, the cooling effect will be supplied and the refrigerant undergoes a phase change to vapour. The water vapour flows to the absorber and is mixed with the strong LiBr-H_2O solution, where the vapour is turned to the liquid-phase and the solution goes back to be diluted. As a consequence of the mixing process, an amount of heat is liberated, where it is ejected to the cooling water from the cooling tower circuit. LiBr-H_2O solution is pumped to the generator through a heat exchange, which is preheated.

In the generator the solution is heated by the thermal energy that comes from the sun to release the refrigerant, thus the water is evaporated from the solution. The concentrated solution is returned to the absorber through the heat exchanger to repeat the absorption process, while the vaporised water flows to the condenser. In condenser, the water is condensed to a liquid state by ejection of its latent energy to the cooling water circuit that comes from the cooling tower. The water from the condenser is passed through an expansion valve on its way to the evaporator. When the solar energy is insufficient to raise the water temperature, the auxiliary heater is switched on to make up the shortfall in the energy. Due to the intermittent nature of the solar energy, hot thermal energy storage plays a vital role in decreasing and eliminating the non-uniform heat intensity that is supplied to the chiller. In addition to the hot storage tank, some solar absorption systems include a cold storage tank, as in Agyenim et al. (2010), which is used to store excess chilled water for later use in times of shortage.

There are two key criteria describing the energy performance of a solar absorption system: Coefficient of Performance (COP) and Solar Fraction (SF). COP indicates the rate of converting the thermal energy, which is supplied to the generator $Q_{generator}$, to cold energy; which is represented as the cold effect in the evaporative $Q_{evaporative}$.

$$COP = \frac{Q_{evaporative}}{Q_{generator}} = \frac{Q_{evaporative}}{Q_{solar} + Q_{\text{Auxiliary heater}}} \qquad \text{Equation 2-1}$$

where: $Q_{generator}$ is the summation of the solar energy Q_{solar} and the energy of the auxiliary heater $Q_{Auxiliary\ heater}$.

Solar fraction defines the participation ratio of the solar energy to the total hot energy demanded in the generator.

$$SF = \frac{Q_{solar}}{Q_{generator}}$$ Equation 2-2

2.5 Configurations of the solar absorption systems

There are several bases used to classify absorption systems, as can be seen in Labus et al. (2013). However, the absorption system can be broadly classified according to its configuration: the amount of effect and the number of stages (lifts). Amount of effect means the amount of input heat supplied to the absorption machine, while number of stages means the number of generator/absorber pairs in the absorption chiller (Eicker, 2009). The schemes of these arrangements can be seen in Wu & Eames (2000) and Srikhirin et al. (2001). Within these configurations, a single effect absorption chiller requires the lowest heat supply. Figure 2-3 shows COPs and heat supply temperature for single, double and triple effect LiBr–H_2O absorption systems (Balaras et al., 2007). Additionally, Ali et al. (2008) added that a single-effect LiBr–H_2O absorption system is considered the most prevalent "due to its low temperature operability". Single-effect absorption systems can be considered more suitable for domestic application as well as for medium sized buildings.

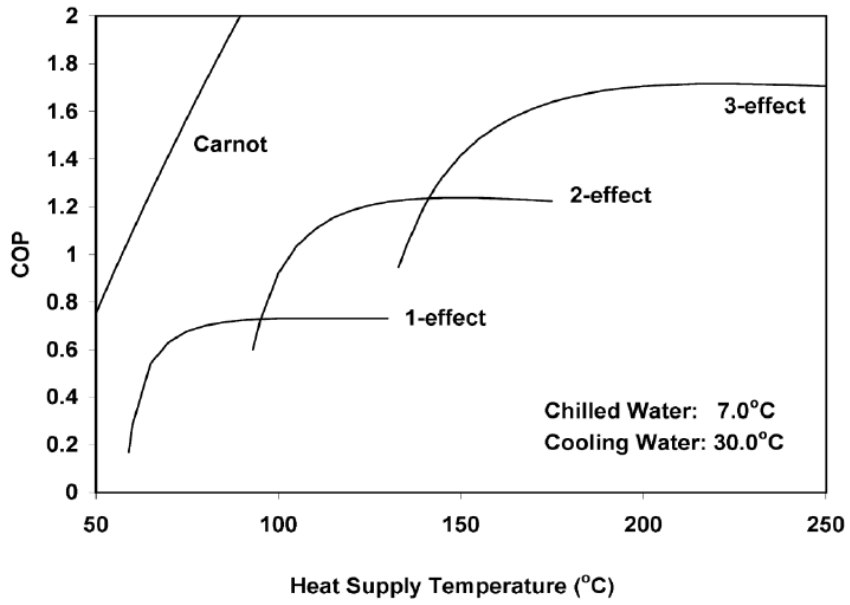

Figure 2-3 COPs and heat supply temperature for single, double and triple effect LiBr–H2O absorption systems (Balaras et al., 2007).

2.6 Solar thermal collector

Collectors can be defined as a special type of heat exchanger that converts the solar radiation to useful thermal energy. Generally, there are two types of solar collectors:

- Non-concentrating collectors: flat plate collectors FPC, evacuated tube collectors ETC and compound parabolic collectors CPC.
- Concentrating collectors: parabolic through collectors, linear Fresnel reflectors, parabolic dish reflectors, heliostat field collectors and pool collectors.

Kalogirou (2013) classified the types of solar thermal energy collectors and he identified the temperature ranges of each type, see Table 2-1. Mateus and Oliveira (2009) indicated that recent investigations were focusing on incorporating an evacuated tube solar collector with a single stage absorption chiller as the most promising configuration for solar absorption cooling systems.

Table 2-1 Solar thermal collectors and their temperature range (Kalogirou, 2013).

Motion	Collector type	Absorber shape	Concentration ratio	Temperature range(C^0)
Stationary	Flat Plate Collector (FPC)	Flat	1	30-80
	Evacuated Tube Collector (ETC)	Flat	1	50-200
	Compound Parabolic Collector (CPC)	Tubular	1-5	60-240
Single-axis tracking	Compound Parabolic Collector (CPC)	Tubular	5-15	60-300
	Linear Fresnel Reflector (LFR)	Tubular	10-40	60-250
	Cylindrical Trough Collector (CTC)	Tubular	15–50	60–300
	Parabolic Trough Collector (PTC)	Tubular	10-85	60-400
Two-axis tracking	Parabolic Dish Reflector (PDR)	Point	600-2000	100-1500
	Heliostat Field Collector (HFC)	Point	300-1500	150-2000
Note: Concentration ratio is defined as the aperture area divided by the receiver/absorber area of the collector				

Figure 2-4 shows a schematic diagram of the evacuated tube collector. A non-toxic liquid is placed in a hollow copper heat pipe under vacuum conditions. The absorber of the collector starts to absorb the sunlight and this leads to the non-toxic liquid evaporating, when the vapour rises to the head of the copper pipe, which is in contact with the system fluid. At the top of the pipe's head the vapour condenses and releases the heat to the system fluid, and then the condensate liquid flows back to the bottom of the pipe and the whole process will be repeated.

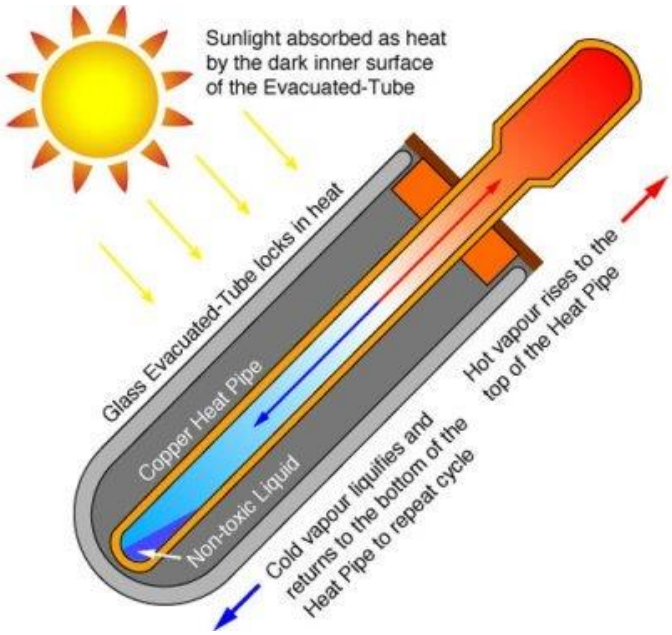

Figure 2-4 Schematic diagram of the evacuated tube collector (Kohlenbach & Jakob, 2014).

2.7 Experimental investigations

It is very important to review the studies on the existing solar absorption chillers in order to identify the components of the system and methods of control, in addition to establishing the fields that need more attention.

Hidalgo et al. (2008) and Syed et al. (2005) examined the impact of choosing an inappropriate size of solar absorption chiller on the primary energy consumption and CO_2 emissions. A 35kW single-stage LiBr-H_2O absorption chiller energised by hot water from a hot storage tank was used to meet the demand for cooling in a single detached house. 50m^2 flat solar collectors were used to heat up the hot storage tank. The results showed the seasonal COP of the chiller reached 0.33. Pongtornkulpanich et al. (2008) analysed a 35kW (10TR) single-effect LiBr-H_2O solar absorption chiller under the climate conditions of Thailand. The chiller was coupled with 72m^2 roof-mounted evacuated tube collectors, a thermal stratification hot water storage tank 400l, a heat backup, a cold storage tank of 200l and five fun coils. The system was found to satisfy the demand. Ketjoy et al. (2013),

however, reported that the aforementioned system does not work optimally; they found the daily rate of COP equal to 0.33 compared to the nominal COP of 0.7. Mammoli et al. (2010) and Ortiz et al. (2010) described 70kW of single-effect LiBr-H_2O solar absorption chiller using a thermal collector system that consisted of 108m^2 of evacuated tube collectors and 124m^2 of flat plate collectors, in addition to large hot and cold storage tanks, 34m^3 and 50m^3, respectively. They found the system covered only 18% of the demand for cooling and the biggest source of heat loss was the hot storage tanks. Eicker & Pietruschka (2009) reported that enlarging the hot storage tank leads to a decline in performance. Marc et al. (2010) and Praene et al. (2011) presented a 30kW single-effect LiBr-H_2O solar absorption system, installed in a tropical climate, that did not have auxiliary heater. 90m^2 flat plate collectors were used to energise the system, which also contained a 1500l hot water tank and a 1000l cold water tank. They found that 20kW of refrigeration were enough to maintain the desired conditions and the system was oversized. However, the investment costs of the aforementioned system were almost three times larger than a similar system reported by Pongtornkulpanich et al. (2008). Li & Sumathy (2001) succeeded in designing and fabricating a 4.7kW single-effect LiBr-H_2O absorption chiller. They found the system had the ability to generate cooling effects even on cloudy days. Hang & Qu (2010) stated that the cold storage could stabilise the operation of the system. Agyenim et al. (2010) used a cold storage tank to accommodate the excessive cool production from a 4.5kW single-effect LiBr-H_2O absorption system that did not have heat backup, and a 0.58 average COP was measured. Hammad & Zurigat (1998) succeeded in manufacturing and testing a 1.5RT single-effect LiBr-H_2O absorption system. They found 14m^2 of flat plate collectors was able to make the system work continuously around 4-5 hours per day during April and May in Amman, Jordan, depending solely on the sun. Monné et al. (2011) reported that an oversized solar domestic hot water system using 37.5m^2 flat solar collectors was upgraded

to include a 4.5kW single-effect LiBr-H_2O absorption chiller with a dry cooling tower to exploit the surplus energy. However, after two years, the investigations showed that a new problem had appeared: the performance of the absorption system was significantly influenced by the ambient temperature in an inverse relationship. However, due to the presence of a well near the building, a geothermal system was adopted as an alternative dry cooling tower. Implementing a dry cooling method increases consumption of electricity as well as increasing the initial costs of the solar absorption system compared with the wet cooling tower. Moreno et al. (2010) introduced the preliminary experimental results of a solar absorption system that uses a dry cooling tower as the heat reject unit. The inability of the chiller to produce the desired chilled water temperature was noticed when the ambient temperatures close to forty degrees, which was a normal consequence of using the dry cooling method. A summary of characteristics and operation temperatures for existing single-effect LiBr-H_2O solar absorption systems is reported in Zhai et al. (2011), see Table 2-2.

Table 2-2 Summary of characteristics and operation temperatures for existing single-effect LiBr-Water solar absorption systems (Zhai et al., 2011).

Operation temperature °C			*COP*	Solar collecting efficiency %
Hot water	Chilled water	Cooling water		
65 - 100	7- 15	26 - 32	0.33 – 0.7	35 - 50

Iraq is one of the leading countries in the field of solar cooling in the Middle East. A solar absorption system consists of two absorption chillers of 60TR refrigeration each, and 1587 evacuated tube solar collectors; each has 1.33m^2 area, has been used to fulfil the air conditioning requirements in the Solar Energy Research Center (Energy and Environment Research Center currently) building in Baghdad, see Figure 2-5. This system, which was inaugurated in the early eighties, is considered one of the largest buildings in the world

that uses solar cooling. The building consists of five floors with 3700m^2 air conditioned area. 64% of collectors are erected on the front surface of the building that faces 22° east of south with a slope of 45°; these are shown in Figure 2-5, while the remaining collectors are situated in the front space of the building with a slope of 17°; these are not shown in the figure.

Figure 2 5 Energy and environment research centre building in Baghdad, Iraq.

Al-Karaghouli et al. (1991) evaluated the performance of this system and found the rate of participation of solar energy in the generation of the cooling exceeded 60%.

The Iraqi solar house is another project that has used an absorption solar cooling system for providing the cooling requirements. The system consists of a 35kW single-effect LiBr-H_2O absorption chiller with 128 flat solar collectors (each has 1.89m^2 area), and 20m^3 hot storage tank (Al-Karaghouli, Al-Hamdani & Al-Sinan, 1989).

To sum up, selecting the appropriate size of chiller is essential in order to harness the whole capability of the absorption chiller and to achieve an efficient solar cooling system. In

addition, enlarging the hot storage tank to store more solar energy may not lead to an increase in the performance, but may lead to an increase in the heat losses. Additionally, using a dry cooling tower as a heat rejection sink, leads to reduced performance of the whole system as the ambient temperature increase. However, the areas that suffer from water scarcity cannot employ wet cooling systems, and the geothermal system could be considered as an excellent alternative. Moreover, the cold storage tank could be as promising solution to improve the performance of solar absorption systems. More importantly, the size of the chiller could be less than maximum cooling load when the cold storage tank is used, thereby reducing the initial cost of the whole system (Hang & Qu, 2010).

2.8 Theoretical investigations

Modelling of solar absorption systems is very important to estimate their performances and analyse their reaction in different situations. Ghaddar et al. (1997) presented a simulation of a 10.5kW single-effect LiBr-H_2O absorption system under Beirut climate conditions; flat solar collectors plus a hot thermal storage tank were used to actuate the chiller. The results of the simulation showed that at least 23.3m^2 of solar collectors are needed for each one ton of refrigeration. Additionally, the system needs a hot storage tank with a volume from 1m^3 to 1.5m^3, in order to enable the system to work autonomously up to seven hours each day. Florides et al. (2002) modelled and simulated a 65000kJ/hr single effect LiBr-H_2O absorption chiller, that was assumed to satisfy the cooling demand of a typical house in Nicosia, Cyprus. The parametric study showed the compound parabolic collectors of 15m^2 area with a slope of 30° from the horizontal, 0.6m^3 hot storage tank and an auxiliary boiler were desired for the system to work ideally. Atmaca & Yigit (2003) presented a simulation of a 10.5kW single effect LiBr-H_2O absorption system with different types of

solar collectors under climate condition of Antalya, Turkey. The report revealed that the best choice is to use a vacuumed tube solar collector type. Assilzadeh et al. (2005) presented a simulation of a 3.5kW single effect LiBr-H_2O solar absorption system in Malaysia. Figure 2-6 shows a flowchart of the modelling and simulation methodology.

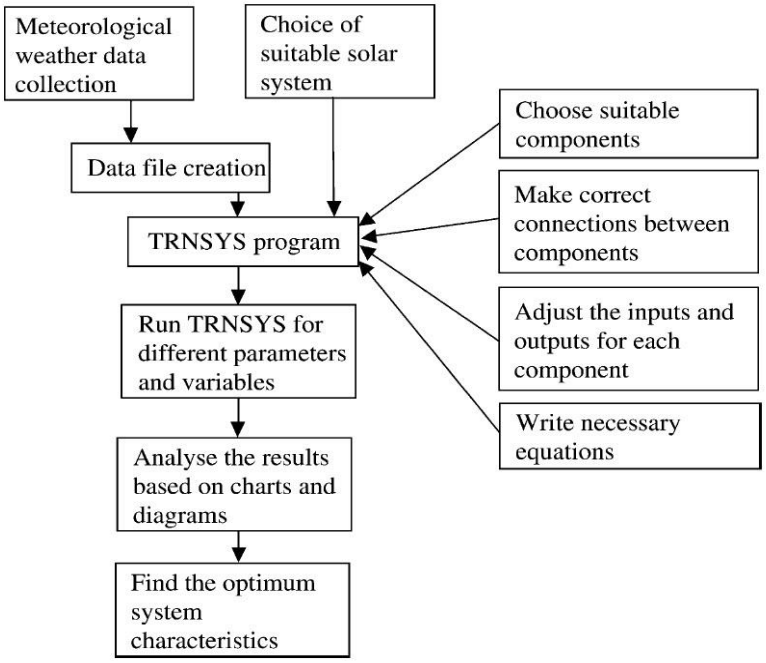

Figure 2-6 A flow chart of the modelling and simulation methodology of the work done by Assilzadeh et al. (2005).

Joudi & Abdul-Ghafour (2003) carried out a simulation of a 35kW single effect LiBr-H_2O solar absorption system under Baghdad climate conditions, in order to find the minimum recommended values for the area of the solar collector area and the volume of the hot storage tank. In order to evaluate the suitability of solar cooling for Tunisia's climate, Balghouthi et al. (2005) and (2008) carried out a simulation of a solar absorption system. They found that a 11kW single effect LiBr-H_2O absorption system needs a flat plate solar collectors with an area of 30m^2 and a 0.8m^3 hot storage tank to serve a typical residential house with an area of 150m^2. Eicker & Pietruschka (2009) carried out simulations of a solar powered absorption system for buildings in different cities in Europe. These buildings

were characterised by the same maximum cooling load; they discovered that to reach to the same solar fraction in each city, the chiller needs different sizes of solar collector and hot storage. Tsoutsos et al. (2010) examined several design configurations of solar absorption system that will be used to provide the cooling loads of a hospital in Sitia, Greece. They found a 70kW single effect LiBr-H_2O absorption chiller that was energised by a 500m^2 of flat solar collectors with the aid of an 87kW auxiliary heater and a 50kW vapour compression chiller as a backup, was the best option. The annual Solar Fraction of the proposed system was found to be 0.74. Thereafter, the authors implemented simulations for the same hospital in different locations in Greece and Switzerland.

The effect of the purity of atmospheric air in Tehran, Iran, (clearness index, ratio of global solar irradiance to the extraterrestrial solar irradiance on horizontal surface) on the amount of heat energy required from the auxiliary heater of a solar absorption system has been calculated by Ardehali et al. (2007). The results showed the heat required from the auxiliary heater more than doubled when the clearness index was minimized by 17% (due to the smog and pollutants). Results reported by Martínez et al. (2012) showed that only 29% of the solar energy fallen on the collector was transferred to the hot storage tank. Arsalis & Alexandrou (2015) suggested changing the slope of the solar collectors to energises a single-effect, LiBr–H2O absorption chiller in a monthly average. A case study for a single-family residential property in Nicosia, Cyprus was presented.

A solar absorption system for a family house has been modelled by Granjeon et al. (2013). The study recommended a chilled water supply of 18°C to cool the house, and in order to evaluate the economic viability of the system, the payback period should be defined in future. Belmonte et al. (2014) presented a simulation for a solar absorption system used for a residential purposes under Spain climate. They fixed the operation period between 9am to 8pm.

Gebreslassie et al. (2009) presented an approach to optimising the absorption cooling system by using a multi-objective function that reduced the environmental impact and the cost. Al-Alili et al. (2010) proposed a methodology to optimise a solar absorption system for a building in the UAE. They coupled the TRNSYS and MATLAB to implement a multi-objective criteria optimisation: both minimising the cost and the energy consumed by the auxiliary heater. Later, Al-Alili et al. (2012) analysed a solar absorption system according to its performance and the CO_2 emissions. Calise et al. (2010) used the economic aspect as an objective function to optimise a single-stage LiBr–H_2O absorption system. A built-in TRNSYS plugin TRNOPT was used to do the optimisation. Boopathi Raja & Shanmugam (2012) reviewed the research done in the field of solar absorption systems and presented some ideas to reduce the cost of the system. Government incentives are necessary to reduce the payback period and make them cost-competitive (Hang, Qu & Zhao, 2011). Hang et al. (2013) observed that the assessment of any solar absorption cooling system should contain environmental aspects beside the aspects of energy and cost; they presented a multi-objective optimisation for a solar absorption system in terms of energy, economy and environmental aspects in four cities in the USA. An environmental life cycle assessment of a solar cooling system has been done by Bukoski et al. (2014). Dincer & Rosen (2011) stated "exergy analysis yields efficiencies that provide a true measure of how nearly actual performance approaches the ideal and identifies more clearly than energy analysis the causes and locations of thermodynamic losses". Onan et al. (2010) studied the hourly exergy loss of a solar assisted absorption cooling system and they observed that the solar collector has the highest exergy loss. Bellos et al. (2016) have used exergic analysis to evaluate a solar absorption system with different collector types, and they found that the evacuated solar tube collectors are most suitable to drive solar absorption chillers from exergic and financial criteria. Recently, Abdullah (2016) has

presented a multi-objective of a solar cooling system based on exergic and economic aspects. It is worth mentioning here, that the TRNSYS (TRaNsient System) Simulation program has been used to model the systems investigated by Assilzadeh et al. (2005), Eicker & Pietruschka (2009), Al-Alili et al. (2010) & (2012), Hang et al. (2013) and Abdullah (2016), and the outcomes of TRNSYS then used according to the purpose of each study.

Several papers have reviewed and demonstrated the projects and the investigations in the field of solar absorption cooling systems, such as Wang et al. (2009), Zhai et al. (2011), Hassan & Mohamad (2012) and Labus et al. (2013). They have concluded that the investigated systems are of limited success, and still unsatisfactory if the economic performance (the initial cost and payback period) is considered, even though many of these systems have proven operationally successful, where the investment payback period is generally greater than the life span of the system (Lentz et al., 2014). Thus, government subsidies and incentives, in addition to energy tax, are necessary to reduce the payback period and make solar absorption systems more competitive with conventional cooling systems (Hang, Qu & Zhao, 2011). Labus et al. (2013) also observed "appropriate standards, test procedures and best practices guides together with intensified work on simulations, optimization and control strategies improvement are some of the needs which are necessary to accelerate the progress and to fill the gap with respect to the conventional systems". However, these reviews showed that the focus, as design and operation control, is mainly on hot energy (solar collector, hot thermal energy storage and auxiliary heater) and chiller (absorption chiller and cooling tower) sides, and there is a lack of information about the cold energy side (cold thermal energy storage) in design and control strategies, especially for residential applications that need cooling during the night in climates such

as the Middle East. In the next section, the principle, types and applications of cold storage tank in addition to the control strategies will be explained.

2.9 Cold thermal energy storage

Usually, the working day is divided into peak hours where the electricity demand of the domestic and industrial users is high, and off-peak hours where the demand is low. Therefore, discounted (cheap) electricity prices during off-peak hours have been offered by the utility companies to encourage users to use electricity at those times, thus shifting the demand to the off-peak hours. The disparity of the electricity price between peak and off-peak hours could reach more than 7 times, as shown in Figure 2-7. At peak hours, the electricity supply company in the region might have to purchase power from another company (or several companies at the same time), hence "the price of the electricity corresponds to the scarcity of electricity during that time" (Cole et al., 2015). As the power consumption of air-conditioning systems has influential weight (in the summer months, especially in warmer climates, up to about 50% to 70%, whether in the domestic (Said, El-Shaarawi & Siddiqui, 2015) or commercial (Boonnasa & Namprakai, 2010) applications) in energy demand at peak hours (expensive hours), transferring this demand to less expensive hours would be very desirable, and thermal energy storage technologies can be used for this purpose.

Cold Thermal Energy Storage (CTES) is the concept of producing and storing cold energy for future use. The basic idea of the CTES is using a tank for storing cold thermal energy at off-peak hours, which is also the hours when demand for cooling effects is low, and discharging the cold thermal energy later at peak hours, when the demand for electricity and cooling effects is high. Figure 2-8 shows a simplified schematic of the difference between a traditional air conditioning system and an air conditioning system with CTES.

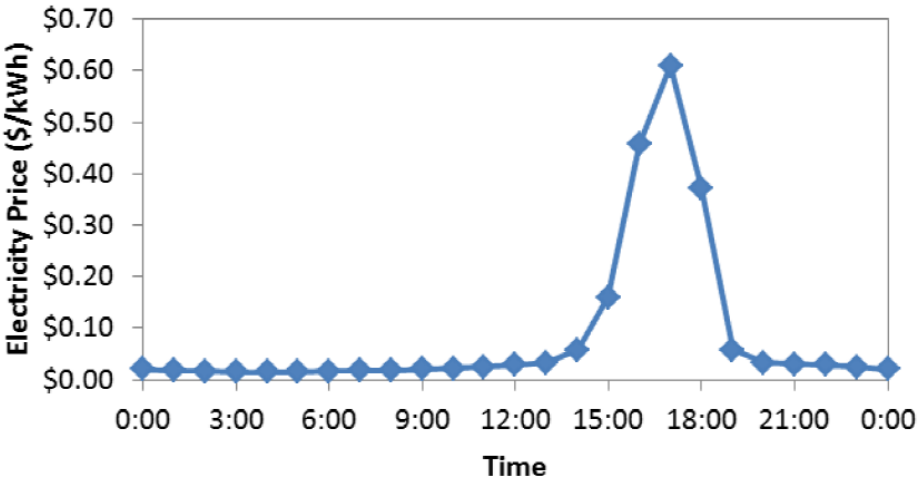

Figure 2-7 Electricity price on 25 June 2012 in Austin the capital of Texas state, USA (Cole *et al.*, 2015).

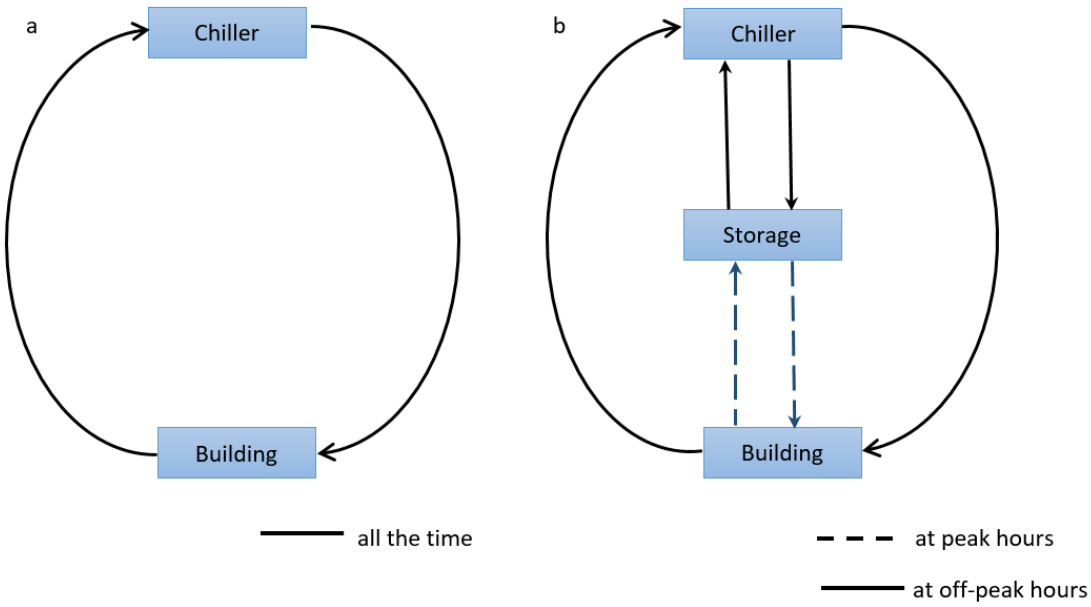

Figure 2-8 shows a simplified schematic of the difference between (a) a traditional air conditioning system and (b) an air conditioning system with CTES.

Decoupling between the generation and the consumption of the cold energy can provide backup options and more flexibility to the operation of the air-conditioning systems, as well as being able to reduce the size of the chiller (Zhang et al., 2011). Actually, some of the utility companies in the USA offer incentives when using TES systems (Krarti, 2010), where "retrofits are usually eligible for higher incentives than new construction" (Dincer & Rosen, 2011).

Generally, chilling (sensible energy storage) or freezing (latent energy storage) water are used widely to store the cold thermal energy (however, eutectic salt solutions, phase change materials, can be used as well as latent energy storage) (Rismanchi et al., 2012). In the latent energy storage system, the energy is stored at a constant temperature, by changing the phase of water to ice, instead of changing (reducing) the temperature as in the sensible energy storage systems. There are many practical and thermodynamic reasons, such as being harmless, inexpensive and available, as well as being compatible with most available equipment used either for producing or storing cold thermal energy, that have led to water being the most frequently chosen energy storage medium (Dincer & Rosen, 2011). In ice CTES, in order to produce the ice, the chiller must be capable of producing temperatures lower (between -6°C and -3°C (Sebzali & Rubini, 2006)) than are required in water CTES (the required temperature in a water CTES system is the same as the temperatures that can be produced by a non-storage chiller for air conditioning purposes), thereby necessitating larger and more expensive chillers. In addition to that, reducing the evaporator temperature of a chiller leads to a decrease in the efficiency of that chiller, where "the chiller operates at low efficiencies when it is used to charge an ice storage tank rather than to meet the space cooling load directly" (Krarti, 2010), which could be 70% less than the efficiency of the chiller used water CTES (Dincer & Rosen, 2011). Therefore, water CTES is preferred for a single residential house.

Besides incurring extra initial costs, using CTES leads to increased complexity of air-conditioning systems, so that the systems with CTES could actually require more energy than non-storage cooling systems (Krarti, 2010) which means extra operational costs. Therefore, efficient control (operational) strategies are essential to manage charge (storing the cooling energy), standby and discharge (using the stored cooling energy) times (Zhao et al., 2015), not simply to prevent any increase in the operational costs, but to reduce them

as well. Thus, the extra expenses (investment costs) can be recovered in a shorter period. Generally, the control strategies of CTES can be classified as conventional and non-conventional control strategies, and both strategies will be explained in the following two sections.

2.9.1 Conventional control strategies

Conventional control strategies can be divided into two types: full and partial tank. In Full tank control strategy, the chiller charges the CTES at off peak hours and then stops working at peak hours, while the CTES discharges at peak hours and provides all the cold effects required by the building. In partial tank strategy control strategy, the chiller works 24 hours and the size of the tank (storage) and the capacity of the chiller are smaller than the full tank CTES system. The partial tank is classified into two types of operations (Dincer & Rosen, 2011): load levelling and demand limiting, and the major difference between these two types are the size and the operation of the chiller. The chiller operates at its maximum capacity for the whole day in the load levelling type (supply the required load is split between the chiller and the storage in a fixed ratio for example 60% by the chiller and 40% by the storage), while it operates at reduced capacity at peak hours in the demand limiting type (in order not to allow the demand for electricity to exceed a certain limit). Usually, the chiller capacity of the demand limiting operation is between chiller capacity for the full tank and load levelling strategies (load levelling CTES system has the smallest chiller) (Sebzali & Rubini, 2006). Figure 2-9 illustrates the types of conventional strategies of CTES as well as the basic operation mechanism of full tank, load levelling and demand limiting CTES.

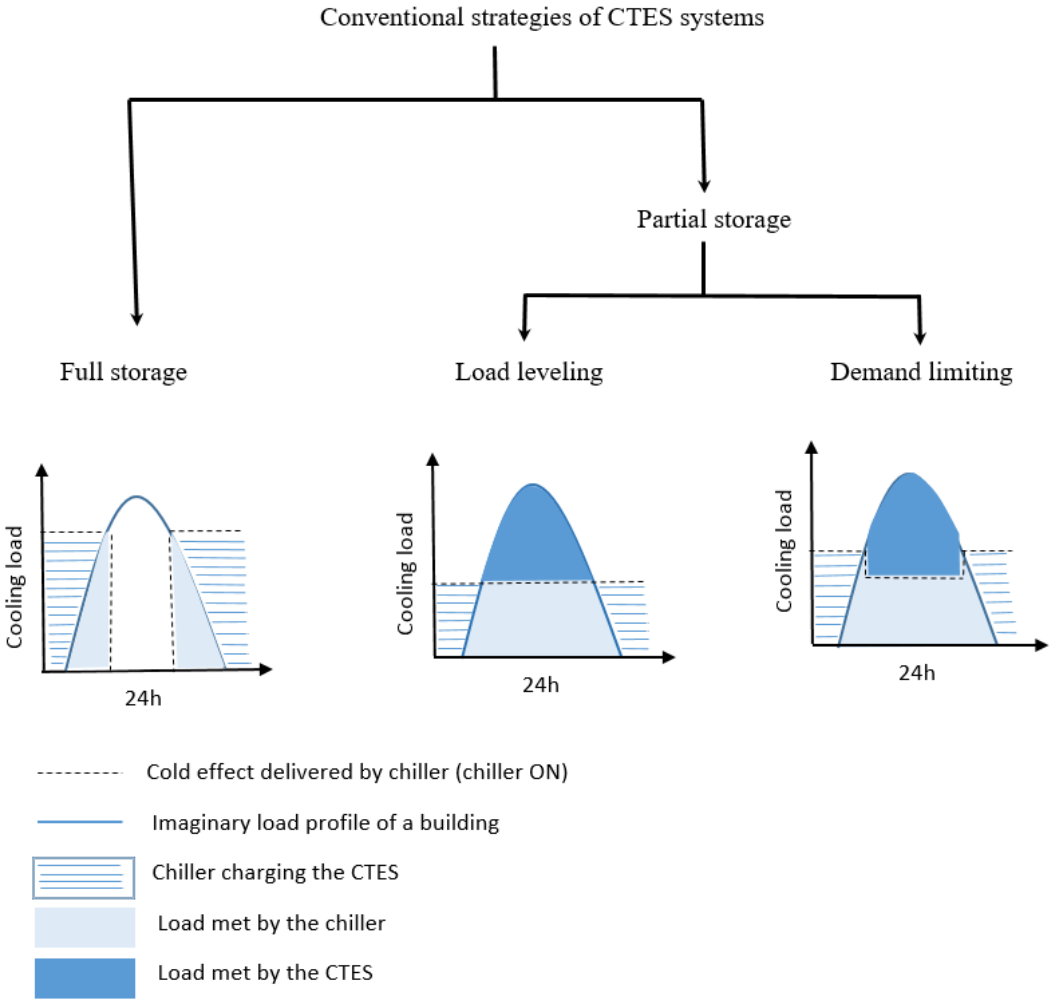

Figure 2-9 Types of conventional strategies of CTES and the basic operation mechanism of full tank, load levelling and demand limiting CTES.

There are alternative control strategies for the partial tank, chiller priority and storage priority (Brown, 2000). In chiller priority, the chiller provides the required cooling load while the storage works when the demand is exceeding the capacity of the chiller. On the other hand, in storage priority, the storage provides as much of the cooling load as it can and the chiller works only when the load is exceeding the available stored cold energy. Practically, the chiller priority partial tank CTES is used more commonly (Gaspar & Silva, 2015). Although the partial tank operation strategies incur less initial investment, they cannot transfer as much as the load shifted by full tank operation, and they are not applicable (unsuitable) with the chillers that are able to provide the maximum cooling load of the building.

In Kuwait, depending on the rate of reduction in the peak power required and the energy consumption, it was found that full storage was the most suitable operation strategy (Sebzali & Rubini, 2007), when a CTES with different operating strategies (full storage and load levelling and demand limiting partial storages) was compared with a non-storage air conditioning system (the chiller in all cases was able to provide the peak load required). Boonnasa & Namprakai (2010) investigated the feasibility of using a CTES for academic buildings for different electric tariffs. The mechanism of charging and discharging the full storage CTES was as follows:

- In charge period (off peak period), chilled water that comes from the chiller charges the CTES and simultaneously provides the cold load of the buildings directly.
- In discharge period (peak period), the chiller turns off and the CTES provides the cooling effects.

Al-Zahrani et al. (2012), for a residential application, used the temperature of the water in the CTES as an indicator to turn the chiller ON and OFF, they proposed the following control function:

If $\gamma_{Chiller} = 1$ and $T_{CTES} > 16$°C then $\gamma_{Chiller} = 1$, otherwise $\gamma_{Chiller} = 0$ Equation 2-3

If $\gamma_{Chiller} = 0$ and $T_{CTES} \geq 12$°C then $\gamma_{Chiller} = 1$, otherwise $\gamma_{Chiller} = 0$ Equation 2-4

Where: $\gamma_{Chiller}$ is the control signal of the chiller operation (1 means ON and 0 means OFF) and T_{CTES} is the average temperature of the water in CTES.

Hasnain & Alabbadi (2000) reviewed the existing CTES projects in Saudi Arabia, and they anticipated that there could be 10% to 20% reduction in peak electric demand when using the CTES. They also mentioned, however, that the CTES technologies are more prevalent

in countries where there is a difference in the price of electricity between the peak and off peak times. Therefore, due to the absence of this disparity in the prices in Saudi Arabia, "there are no direct cash benefits offered by the utility for demand-management measures". For different electric tariffs, the economic feasibility of the use of full and partial storage schemes with the air conditioning system of the Sacred Mosque of Mecca, Saudi Arabia, has been investigated by (Habeebullah, 2007). With different prices for day and night, the results showed that adopting full storage, compared to partial storage, reduced the electric daily bill significantly. However, with a fixed price, the current situation in Saudi Arabia (as well as in Iraq), there was "no gain" in using full nor partial CTES systems economically (similar to the results of Hasnain & Alabbadi's study).

2.9.2 Non-conventional control strategies

Some researchers named these strategies 'optimal control strategies' (Krarti, 2010). The prediction of the cooling load of the building, energy (electric) price rate and the weather are the main requirements of these controls. Maluleke (2002) defined optimal control as the control that "entails sequential decision making over a simulation period in order to arrive at a control trajectory that would lead to the least integral cost of electricity over the simulation horizon". In other words, it is the optimal charging and discharging process of the CTES, which relies on using updated predicted data over a marching horizon "fixed look-ahead time window" for each time step (Henze, Dodier & Krarti, 1997). However, in the last decade, the term 'optimal control' is no longer used, as this kind of control has been further developed and become a sophisticated control process called model predictive control (MPC), used widely in chemical plants and oil refineries.

In MPC, a model of the plant (the system to be controlled) is used to predict the future response of the original plant within a certain horizon to forecast data, such as energy price and weather, in order to generate control actions that minimize the objective function (such

as a function of cost or consumed energy) for the next time instant. Then, in the next time instant (current time step), the prediction horizon is moved forward and the process is repeated with new forecast data to generate the next control signals; Figure 2-10 shows a simplified schematic of a model predictive controller configuration. Yudong et al. (2009) and (2012) used the MPC and a simple model of a chiller system with CTES to minimise the cost of the electricity. They found the cost can be reduced by a quarter compared to the original system's manual controlling. Beghi et al. (2014) compared three conventional control strategies of partial tank CTES (chiller priority, storage priority and load levelling) with MPC, and they found that MPC was more efficient in reducing the cost of electricity in the days where the cooling load demands were low. Cole et al. (2012) presented a literature review about using the MPC in TES systems, and they reported that the benefit of implementing a water CTES system for university buildings has been investigated, and the results showed that the water CTES with storage priority control and MPC can reduce the operation cost by 34% and 42%, respectively, compared to the non-storage system. Later, Cole et al. (2014) stated that the major challenge of MPC is generating an appropriate system model to study the future response of the system, as the comprehensive validated models that already exist in advanced simulation tools, such as TRNSYS (Klein et al., 2012) and EneryPlus (DOE, 2012), are not suitable, where the complexity of the system models should be reduced and simplified for the proposed MPC process.

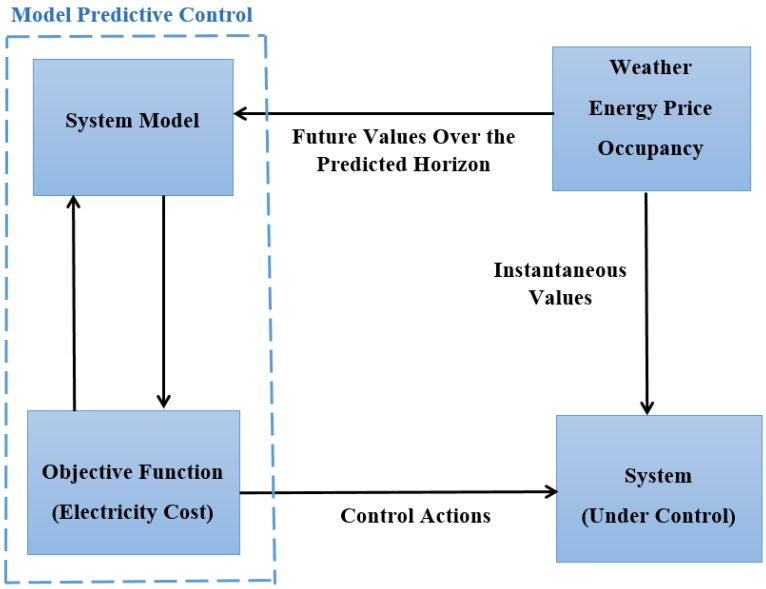

Figure 2-10 Simplified schematic of Model Predictive Controller configuration.

The same concept (utilising simplified system models) was proposed in Afram & Janabi-Sharifi (2014) and Touretzky & Baldea (2014). Afram & Janabi-Sharifi presented a literature review of the studies that investigated using the MPC for heating, ventilation and air-conditioning (HVAC) systems control. However, Zakula et al. (2014) added that in spite of these numerous studies, "currently there is no commercially or publicly available software that allows the analysis of building systems that employ MPC".

It should be mentioned here that because these simplified system models must accurately simulate the original system, they need to be validated. That means that if the system (under control) is subjected to an optimization process such as the genetic algorithm optimization in order to determine the ideal physical design of the system (for example, the optimal volume of water CTES), then in each case (population) a simplified system model should be proposed and validated. Thus the whole process becomes futile, unreasonable and does not lead to the desired goal. Therefore, there should be a trade-off between the complexity and the benefits of using a particular control strategy (Silvetti, 2002).

In solar cooling systems, the best known approach is to supply the cooling effects directly without using “cold tank”, as reported in Hidalgo et al. (2008), Monné et al. (2011), Al-Alili et al. (2012), Ghiaus & Jabbour (2012) and Shirazi et al. (2016b). However, there are numerous studies that presented solar absorption systems (some of these systems are already existed) in co-operation with a cold tank (usually the cold tank term is used more than CTES term in solar cooling systems, and this study will use both terms in this section). Table 2-3 lists a summary of some these research studies that use CTES.

Table 2-3 Summary of the some of the research studies that use CTES.

Reference	Building type	Purpose of using the Cold tank
Calise et al. (2010), (2011)	Office	The chiller provides the chilled water to the building through the cold tank
Ortiz et al. (2010) & Mammoli et al. (2010)	University	Cold tank is charged at nighttime by a conventional chiller, the solar absorption is activated at daytime to provide the chilled water to the building through the cold tank.
Hang & Qu (2010)	Office	The chiller provides the chilled water to the building through the cold tank
Marc et al. (2010), (2012), (2012) & Praene et al. (2011)	Classrooms	The chiller provides the chilled water to the building through the cold tank
Agyenim et al. (2010) & Agyenim (2016)	Office	The chiller provides the chilled water to the building through the cold tank
Hang et al. (2011)	Office	The chiller provides the chilled water to the building through the cold tank
Ayadi et al. (2012)	Office	Connecting tank between the solar absorption system and a backup compression chiller, the chilled water is delivered through the cold tank
Martínez et al. (2012)	Laboratories	The chiller provides the chilled water to the building through the cold tank
Granjeon et al. (2013)	Residential	The chiller provides the chilled water to the building through the cold tank
Best B. et al.(2013)	Food company	The chiller provides the chilled water to the building through the cold tank
Drosou et al. (2014)	Healthcare centre and Residential flats	Connecting tank between the solar absorption system and a convention chiller, the chilled water is delivered through the cold tank
Arsalis & Alexandrou (2015)	Residential	The chiller provides the chilled water to the building through the cold tank
Xu et al. (2015)	Laboratory	The chiller provides the chilled water to the building through the cold tank
Said et al. (2015)	Residential	The chiller provides the chilled water to the building through the cold tank
Reda et al. (2016)	Office	The chiller provides the chilled water to the building through the cold tank

From Table 2-3, the general trend in using the CTES in solar cooling systems is that the chiller provides the chilled water to the building through the cold tank; Figure 2-11 illustrates a solar absorption system that uses a cold tank. The cold tank is continuously charging throughout the period of operation of the chiller and is not used when the chiller turns off (when the solar energy is not available to activate the chiller), where none of these studies have mentioned the mechanism of discharging the stored energy from the cold tank, especially at night, when the cold effects are still needed in residential buildings as in the Middle East. In other words, the chiller, beside its main job of providing the cold effects in the building, is used to maintain the temperature of the chilled water in the CTES as cold as possible (as if the cold tank has become an extra cooling load that has to be provided by the chiller). Hang & Qu (2010) found insignificant effects of increasing the size of the cold tank from $4m^3$ to $20m^3$ on the system performance. More recently, Abdullah (2016) has discovered that there is "no advantage" from changing the size of the cold tank in a solar cooling system. As mentioned before, more energy may actually be consumed in the cooling systems with CTES compared to the non-storage cooling systems. Therefore, efficient control strategies for the cold tank are essential (as they are in conventional cooling systems) to make it capable of enhancing the performance of solar cooling systems rather than being a burden on the system.

The concept of using CTES with solar cooling systems is the opposite of the conventional cooling system (that is activated by electric energy only), where the working hours of the solar cooling systems can be divided into the following:

- Inexpensive period (hours) in the daytime when solar energy is available and can activate the system.
- Expensive period (hours) at night when the system relies on external energy to activate and produce the required cooling loads.

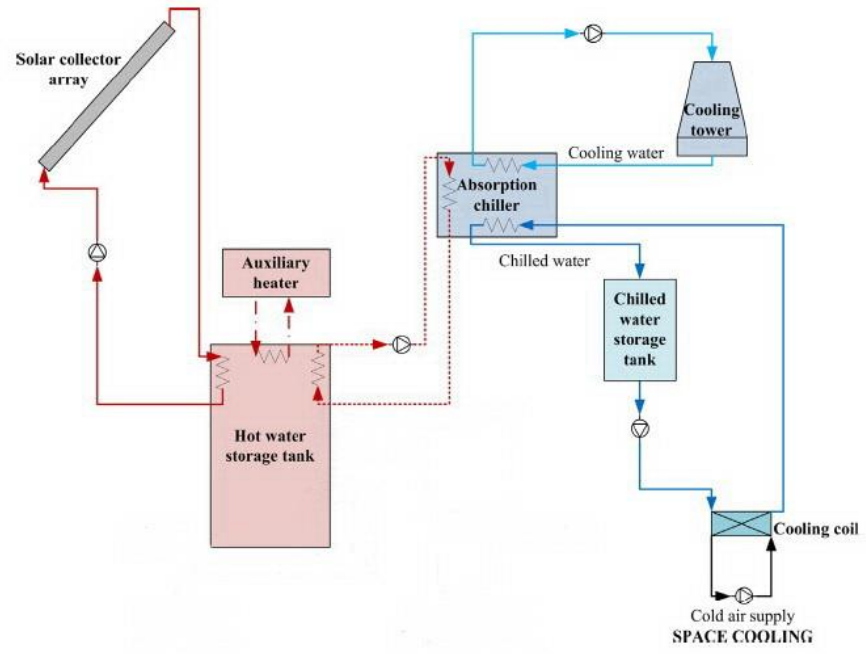

Figure 2-11 Schematic of a solar absorption cooling system that supplies the chilled water through a chilled water storage tank, adopted from Arsalis & Alexandrou (2015).

Although a few papers, such as Al-Ugla et al. (2015), have mentioned that the stored cold thermal energy will be used later at night, still there is no clear procedure or methodology that describes the control mechanism of the CTES. Additionally, no study has pointed out the benefits of transferring or shifting the demanded cooling load for building from night time (expensive period) to daytime (inexpensive period).

2.11 Summary

This chapter has clarified the major differences between the thermal and electric solar cooling systems. The technologies of the thermal cooling systems were presented; that made it clear that solar absorption cooling technology is currently dominant over all types. The operation of solar absorption chillers was explained. A literature review of the studies that have been done on the solar absorption systems as well as on the principle, types, applications and the control strategies of the cold storage tank were presented, and the following points have been concluded:

- Solar energy resources should be assessed in order to find methods to enhance harvesting the solar energy.
- Each location has its own characteristics and requirements, and a successful system is site specific and cannot be applied to another location.
- Solar absorption cooling systems are still immature economically, in that the investment payback period is generally greater than the life span of the system, and government incentives are necessary to reduce the payback period and make them cost-competitive.
- The focus, as design and operation control, is mainly on the hot energy (solar collector, hot thermal energy storage and auxiliary heater) and chiller (absorption chiller and cooling tower) sides, and there is a lack of information about the cold energy side (cold thermal energy storage) in design and control strategies, especially for residential applications that need cooling during the night in hot climates, such as in the Middle East countries.
- The concept of using cold thermal energy storage with solar cooling systems is the opposite of the conventional cooling system that is activated by electric energy only.
- Lack of a general control strategy for the operation of a solar cooling system with a cold storage unit.

Chapter Three

Solar resources assessments

In this chapter, solar energy resources were assessed and methods were proposed to enhance harvesting the solar energy in the Iraqi climate. The intensity of solar radiation incident upon any surface is increased when a slope (tilt) is given to the surface from the horizon. Thus, it is important to know the solar irradiance flux on a tilted surface. However, this kind of data is seldom available, therefore correlations are used to calculate the solar irradiance on a tilted surface, and these correlations need to know global solar irradiance components, diffuse and direct normal irradiance.

This chapter is divided into three parts: the assessment of the horizontal diffuse solar irradiance models, the feasibility of using of ASHRAE clear sky model in Baghdad and proposing a methodology to estimate the solar irradiance fallen on a tilted surface and searching for the optimal tilt angles for the solar collectors. It must be mentioned here that the ASHRAE clear sky model will be used as one of the ways to evaluate the results of the proposed methodology of the solar irradiance fallen on a tilted surface.

The outcomes of this chapter can be considered as a guide in the designing of solar powered systems for Baghdad’s climate, which in turn could increase the exploitation of solar energy and hopefully accelerate Iraq's transformation to an eco-friendly country.

3.1 Modelling the hourly diffuse solar irradiance on horizontal surfaces

The main objective of this section is to give a comprehensive description of the variation of the diffuse solar irradiance on horizontal surfaces in Baghdad, the capital of Iraq. An evaluation of the estimated diffuse solar irradiance on a horizontal surface based on nine models has been carried out. MABE, RMSE and MAPE statistical indicators were used to determine the performance of each model compared to recently collected data. However, none of these models obtained the top scores in all these tests. This gave us the motivation to propose a new model that can be suited to the climate of Baghdad. Four new potential regressions have been proposed. The optical air mass, the solar altitude angle and the ambient temperature were utilised as the second parameters besides the clearness index. These potential models were analysed to choose the most suitable model.

3.1.1 Introduction

Reliable and detailed solar irradiation data is a crucial element in the design, evaluation and optimisation of the performance of any application of solar systems. In addition, solar radiation data are used directly in the design of sustainable buildings, whether domestic or commercial buildings (Marion & Wilcox, 1995). In the past few years, moreover it has been used to convert energy-consuming buildings to energy-producing buildings by integrating solar applications, such as PV cells and solar thermal collectors, in the external finishing crust of the building (Munari Probst & Roecker, 2007). Most meteorological stations measure the global solar irradiance (total solar irradiance falling on a horizontal surface), and few stations also measure both or one of the global irradiance components: diffuse and direct beam irradiance (shown in Figure 3-1), because the instruments that measure these components are expensive and need expensive maintenance and calibration processes (Ruiz-Arias et al., 2010).

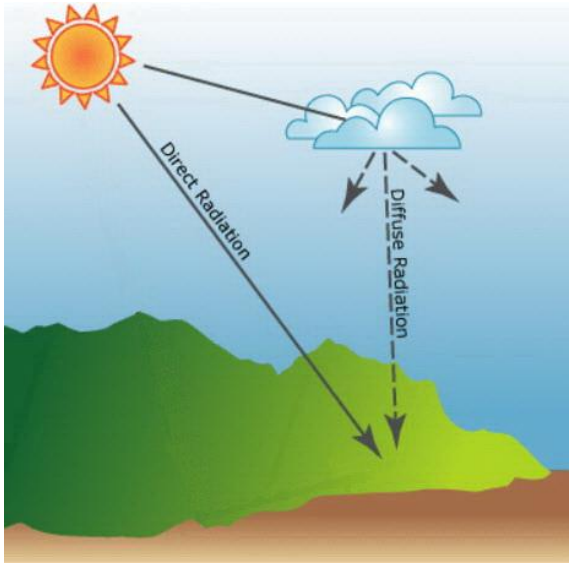

Figure 3-1 The components of global solar irradiance.

It is an established fact that the intensity of solar radiation incident upon any surface is increased when a slope (tilt) is given to the surface from the horizon. Consequently, most solar energy applications use tilted solar panels. Thus, it is important to know the solar irradiance flux on a tilted surface. However, this kind of data is seldom available, therefore correlations are used to calculate the solar irradiance on a tilted surface (El-Sebaii et al., 2010). On an overall basis, these correlations frequently need to know global solar irradiance components, diffuse and direct normal irradiance.

Since the middle of the last century, many models have been proposed to compute the global solar irradiance components. Many of these models are based on several meteorological and geographical parameters (air temperature, relative humidity, sunshine hours, latitude, longitude,....etc.) (Muzathik et al., 2011). Perez et al. (1990a) reported that in 1954 Black et al. introduced the clearness index, k_t (the ratio of global solar irradiance to the extraterrestrial irradiance on the horizontal surface) as a criterion to determine the characteristics of solar irradiance. Liu & Jordan (1960) in their pioneer study to estimate the solar diffuse irradiance, introduced the terms diffuse transmittance index k_d (ratio of diffuse irradiance to extraterrestrial irradiance) and diffuse index k (ratio between diffuse

irradiance and global irradiance). Since then, the terms clearness index and diffuse index have been used in many (universal, or specific site) models that have been developed to estimate solar irradiance information. However, the increasing use of simulation tools for solar applications has led to the need to provide accurate detailed data (global irradiance and its components) with short time scales (hourly or even less) (Torres et al., 2010).

This research is focused on the models that deal with global solar irradiance and its diffuse component (the direct irradiance component could be easily determined by subtracting the diffuse component from the global irradiance). Orgill & Hollands (1977), Erbs et al. (1982), Spencer (1982) and de Miguel et al. (2001) presented correlations to determine diffuse index k as a function of clearance index k_t. Erbs et al. (1982) found that their results were similar to Orgill & Hollands' (1977) results; their proposed model has a weakness at high values of k_t. Spencer (1982) reported that latitude L has a clear influence on the diffuse irradiance. In addition, de Miguel et al. (2001) demonstrated the influence of the solar altitude β on k_t, and they suggest considering this influence in future research. It must be mentioned here that this type of correlation, which depends only on k_t, is characterised by simplicity and ease of use because it needs only the knowledge of global solar irradiance.

Iqbal (1980) introduced the solar altitude angle as the second parameter (predictor) beside k_t in a regression to estimate the diffuse index. He deduced that the universal model is not possible and they remain dependent on the site-characteristics. Solar altitude and clearness index were used to predict diffuse index in an analytical model that was proposed by Skartveit & Olseth (1987). Hollands & Crha (1987) have extended the model of Orgill & Hollands (1977); they showed that considering the ground reflectance as the second predictor led to improving a model that was based only on the clearness index. Reindl et al. (1990) used extra meteorological parameters to describe the diffuse irradiance through adoption of total 28 potential predictors that are measured widely at meteorological

stations. Thereby, a model based on clearness index, solar altitude, ambient temperature T_{amb} and relative humidity Rh is built. Furthermore, in the absence of temperature and humidity data, a second model based on the clearness index and the sun altitude is proposed as well. Then, just for the sake of evaluating those models, a third model that depends solely on the clearness index is suggested. The predictability improvement was about 14% & 9% when using the first and second model, respectively. Furthermore, the first model was found to be better than the model of Erbs (1982) by 26%. Perez et al. (1990a) indicated the possibility of obtaining the same k_t in different conditions when the models based only on k_t are used, also adding the solar altitude angle parameter does not enhance these models because the solar altitude angle β is included "implicitly" in k_t. Therefore, they suggested utilising k_t`, a new expression of the clearness index that does not depend on the zenith angle Z (or in other words not depending on the solar altitude angle β because $Z=90°–\beta$). Additionally, Perez et al. stated that the improvement of models that are based only on k_t could be achieved by the use of extra meteorological parameters when they are available. Perez et al. (1992), as a complement to the preceding research, utilized kt`, stability index, dewpoint temperature and the zenith angle to present "four dimensional Look-up" tables, in order to estimate the direct solar irradiance (as previously mentioned, the difference between the global and direct irradiance is the diffuse irradiance). This proposed model was based on the DISC model proposed by Maxwell (1987). Maxwell introduced the DISC model to estimate the direct transmittance index k_b (ratio between direct irradiance and extraterrestrial irradiance) by correlating the best fit polynomial of the results of a clear sky model presented by Bird & Hulstrom (1981). The resulting model (DISC model) was in terms of k_t and air mass m'.

Instead of using extensive look-up tables as suggested by Perez et al. (1992), Skartveit et al. (1998) preferred to build an analytical model that takes into account the abrupt change

in the conditions to estimate diffuse index *k*. The proposed model is considered an improvement on the model Skartveit & Olseth (1987). The clear sky index ρ is suggested to neutralise the clear index from the sun altitude. This clear sky index in turn is used to determine another index called the hour-to-hour (hourly) variability index σ_3, which considers the effect of the presence of clouds. Boland et al. (2001) employed logistic function technique to present a single regression for diffuse index *k* in term of the clearness index. They then demonstrated that the model is improved when the apparent solar time *AST* is taken as the second predictor (they state that the apparent solar time is more influential than the solar altitude).

Muneer & Munawwar (2006) showed that the inclusion of the sunshine fraction, cloud cover, and air mass led to significant improvement in a set of k_t based models. They also found that these models were site-dependency. Jacovides et al. (2006) preferred the classical approach, where they proposed piecewise correlations using the clearness index as the only indicator to predict diffuse irradiance. After evaluation of models of de Miguel et al. (2001), Erbs et al.(1982), Orgill & Hollands (1977) and Reindl et al. (1990), Jacovides et al. (2010) found that these models can be used for other sites. Ruiz-Arias et al. (2010) used the clearness index to present a model based on the sigmoid function (sigmoid function is a special case of the logistic function) . Ruiz-Arias et al. preferred not to use any extra parameters in their regression in order to make it simple and more general. Nevertheless, the air mass m' is added as an extra predictor to propose a second regression. However, the results showed that the first model was found better than the second model.

Boland et al. (2008) continued the work of Boland et al. (2001), where they indicated the potential of a logistic regression that encompasses the solar altitude, daily clearness index K_t and the hourly clearness index k_t. Later, Ridley et al. (2010) proposed a multiple predictor model, based on logistic function, including these parameters plus another two

parameters: the apparent solar time (as suggested in (Boland, Scott & Luther, 2001)) and a new predictor named persistence index Φ. Persistence index is the mean of "both a lag and a lead" of the clearness index, except sunrise and sunset hours, where it is, respectively, the next hour or the hour before the clearness index at sunrise and sunset. This model is named BRL (acronym of the authors Boland, Ridley & Lauret). As an extension of the previous model, Lauret et al. (2013) adopted a Bayesian inference statistical approach to estimate the coefficients of the BRL (the original coefficients were calculated by using the minimum least squares method (Ridley, Boland & Lauret, 2010)). Lauret et al. said that the use of the new statistical approach led to obtaining "a less biased model".

As for Iraq, only one study has been found, that was based on a data bank of hourly collected measurements of the globe and diffuse irradiances to describe the hourly diffuse irradiance, where Al-Riahi et al. (1992) proposed piecewise regressions based on the clearness index to estimate the diffuse solar radiance in Baghdad.

Most of the studies previously mentioned have compared their models with other models. Meanwhile, a number of studies have made a comparison between difference models to recommend the best one. Table 3-1 shows a summary of some of these recommendations.

Table 3-1 Summary of some recommended models.

Authors	Location	Recommended model	Additional indicators beside the clearness index
Perez et al. (1990b)	Europe and the USA	Maxwell (1987)	m'
Batlles et al. (2000)	Spain	Louche et al. (1991)	--
de Miguel et al. (2001)	North Mediterranean Belt area	Hollands et al. (1987)	ground albedo
Notton et al. (2004)	Ajaccio, France	de Miguel et al. (2001)	--
Elminir (2007)	Egypt	Erbs et al. (1982)	--
Ineichen (2008)	Worldwide	Perez et al. (1992)	k_t`, stability index, dewpoint temperature & Z
Torres et al. (2010)	Pamplona, Spain	BRL (the old) (2010)	K_t, AST & Φ
Lauret et al. (2010)	Worldwide	Skartveit et al. (1998)	(β, ρ & σ_3)
Dervishi et al. (2012)	Vienna, Austria	Reindl et al. (1990)	β, T_{amb} & Rh

The models that are mentioned in the literature are a small part of a large number of models that exist; however, it might be sufficient to understand that the use of the clearness index is probably inadequate to describe the variation of diffuse irradiance, and engaging extra indicators would be useful to enhance the predictability of any regression.

The main objective of this work is to reach a comprehensive description of the variation of the diffuse solar irradiance on horizontal surfaces in Baghdad, the capital of Iraq, which in turn can be used as a tool to enhance harvesting the solar energy in the Iraq. The following steps show how the work is organised. First, the site and data quality are presented. Second, various widely used models are used to estimate the hourly diffuse irradiance, and the results are analysed to show the applicability of these models for the Baghdad climate. Third, new diffuse irradiance regressions are proposed, and the performance of these new models is quantified to identify the most accurate model.

3.1.2 Site and data quality

Iraq is located in the northern part of the area of semi-tropical weather in terms of the temperatures which from March to November are higher than 20 degrees Celsius. It is also considered as a continental climate where it is characterised by rainy winters (especially in the north of Iraq) with moderate to relatively cold temperatures, and by hot, dry and clear skies summers; in addition to two short transition seasons, autumn and spring. Temperatures frequently exceed 35°C during summer and can be extremely high in June, July and August, exceeding 50°C, while in winter temperatures are usually above freezing. Geographically, Iraq is divided into mountainous areas in the north and east (with abundant rainfall), desert areas in the west to the south (with a lack of rain) and fertile alluvial plains that separate the mountainous and desert areas; the Tigris and Euphrates rivers pass through this region.

Baghdad (33° 19' N, 44° 25' E & 34 m above mean sea level) is located in the middle of Iraq within the alluvial plains; the Tigris River divides it into two parts, east and west. Baghdad's climate can be considered as semi-arid (Al-Riahi, Al-Jumaily & Kamies, 2003). Figure 3-2 shows the average high temperature distributions and the number of rainy days in Baghdad for each month of the year 2015, showing the height of the average temperature in the summer months in addition to the low number of rainfall days in the winter months. The winter lasts no more than three months, from early November to late February.

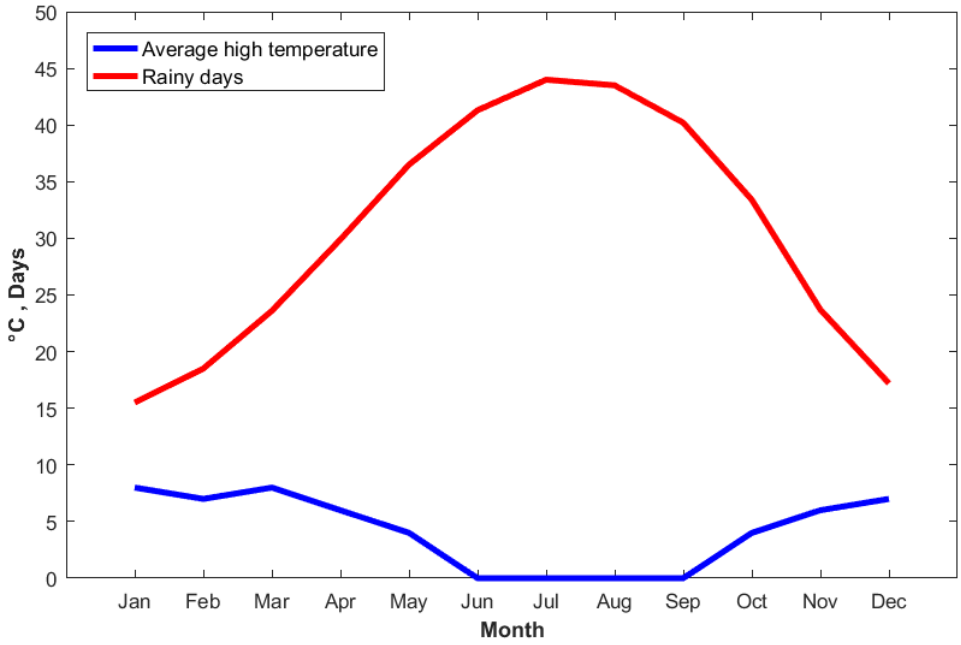

Figure 3-2 Chart showings the average high temperature distributions and the number of rainy days in Baghdad in the year 2015.

In order to carry out this study, data sets from 1st of March to 31th of October 2012 are used. The data quality process consisted of three stages:

- First, eliminating the days that included a shortage of readings (Al-Riahi, Al-Hamdani & Tahir, 1992).
- Second, ignoring data when the clearness and diffuse indices values were higher than one (Muneer & Munawwar, 2006; Ruiz-Arias *et al.*, 2010).

$$0 < k_t \leq 1 \qquad \text{Equation 3-1}$$

$$0 < k \leq 1 \qquad \text{Equation 3-2}$$

- Third, neglecting data when the solar altitude angle less than 5° (Dervishi & Mahdavi, 2012; Posadillo & López Luque, 2009).

$$\beta > 5^{\circ} \qquad \text{Equation 3-3}$$

Consequently, 2540 hours of data have been used in this study.

3.1.3 Models and evaluations

3.1.3.1 Models

The need for accurate data within short periods of time in the design and evaluation of projects that use solar energy was the motivation to focus on hourly diffuse models. Nine models have been selected and evaluated in order to find the appropriate model for the Baghdad climate. The criteria used in the selection of these models were:

- The availability of all analytical equations and the presence of the required input data (or the possibility to find it through additional corrections).
- These models can be used globally (except for Al-Riahi et al. model (1992)).
- On the basis of the quality of the results that have been found in the original studies of these models and the evaluations of these models in other studies.

The following subsections are a brief review of the mathematical equations of these models:

A) Maxwell model (MX) (1987)

$$k = 1 + \frac{k_b}{k_t} \qquad \text{Equation 3-4}$$

$$k_b = kn_c - \left(a + b * e^{m'c}\right) \qquad \text{Equation 3-5}$$

Where (kn_c) is the best-fit polynomial of the results of a clear sky model that was proposed by Bird & Hulstrom (1981), and can be calculated by:

$$kn_c = 0.866 - 0.122\,m' + 0.0121\,m'^2 - 0.000653\,m'^3 + 0.000014\,m'^4 \qquad \text{Equation 3-6}$$

The air mass m' is calculated from (Kasten & Young, 1989):

$$m' = \frac{1}{\sin(\beta) + 0.50572\ (6.07995 + \beta)^{-1.6364}}$$ Equation 3-7

And *a, b & c,* which depend on the clearness index, are obtained from:

$$Interval \quad k_t \le 0.6: \begin{cases} a = 0.512 - 1.56k_t + 2.286k_t^{\,2} - 2.222k_t^3 \\ b = 0.370 + 0.962k_t \\ c = -0.280 + 0.932k_t - 2.048k_t^2 \end{cases}$$ Equation 3-8

$$Interval\ k_t > 0.6: \begin{cases} a = -5.743 + 21.77k_t - 27.49k_t^2 + 11.56k_t^3 \\ b = 41.40 - 118.5k_t + 66.05k_t^2 + 31.90k_t^3 \\ c = -47.01 + 184.2k_t - 222.0k_t^2 + 73.81k_t^3 \end{cases}$$ Equation 3-9

Furthermore, values of the solar altitude angle β are calculated from the following equation (ASHRAE, 2009):

$$\beta = \sin^{-1}(\cos(L)\cos(\delta)\cos(H) + \sin(L)\sin(\delta))$$ Equation 3-10

where L, δ and H are latitude angle, solar declination angle and hour angle, respectively.

B) Reindl et al. models (1990)

- **Reindl 1 (RE1)**

Interval $0 \le k_t \le 0.3$; constraint $k \le 1$:

$$k = 1 - 0.232k_t + 0.0239\ \sin(\beta) - 0.000682\ T_{amb} + 0.0195\frac{Rh}{100}$$ Equation 3-11

Interval $0.3 < k_t < 0.78$; constraint $0.1 \le k \le 0.97$:

$$k = 1.329 - 1.716k_t 0.267\ \sin(\beta) - 0.00357T_{amb} + 0.106\frac{Rh}{100}$$ Equation 3-12

Interval $0.78 < k_t$; constraint: $0.1 \le k$:

$$k = 10.426k_t - 0.256\ \sin(\beta) + 0.00349T_{amb} + 0.0734\frac{Rh}{100}$$ Equation 3-13

- **Reindl 2 (RE2)**

Interval $0 \le k_t \le 0.3$; constraint $k \le 1$:

$$k = 1.020 - 0.254k_t + 0.0123\sin(\beta)$$ Equation 3-14

Interval $0.3 < k_t < 0.78$; constraint $0.1 \le k \le 0.97$:

$$k = 1.400 - 1.749k_t + 0.177\sin(\beta)$$ Equation 3-15

Interval $0.78 < k_t$; constraint: $0.1 \le k$:

$$k = 0.486k_t - 0.182\sin(\beta)$$ Equation 3-16

- **Reindl 3 (RE3)**

Interval $0 \le k_t \le 0.3$; constraint $k \le 1$:

$$k = 1.020 - 0.248k_t$$ Equation 3-17

Interval $0.3 < k_t < 0.78$; constraint $0.1 \le k \le 0.97$:

$$k = 1.45 - 1.67k_t$$ Equation 3-18

Interval $0.78 < k_t$; constraint: $0.1 \le k$:

$$k = 0.147$$ Equation 3-19

C) Al-Riahi et al. model (AR) (1992)

Interval $k_t < 0.25$:

$$k = 0.932 \qquad \text{Equation 3-20}$$

Interval $0.25 \le k_t \le 0.7$:

$$k = 1.293 - 1.631 k_t \qquad \text{Equation 3-21}$$

Interval $k_t > 0.7$:

$$k = 0.151 \qquad \text{Equation 3-22}$$

D) BRL model (BRL) (2013)

$$k = \frac{1}{1 + e^{-5.38 + 6.63 k_t \, 0.006 AST - 0.007 \beta + 1.750 k_t + 1.31 \phi}} \qquad \text{Equation 3-23}$$

where the persistence index is obtained from:

$$\phi = \begin{cases} \dfrac{k_{t-1} + k_{t+1}}{2} & sunrise < time < sunset \\ k_{t+1} & time = sunrise \\ k_{t-1} & time = sunset \end{cases} \qquad \text{Equation 3-24}$$

and the daily clearness index is calculated from

$$K_t = \frac{\sum_{sunrise}^{sunset} I_g}{\sum_{sunrise}^{sunset} I_o \sin(\beta)} \qquad \text{Equation 3-25}$$

E) Skartveit et al. model (SK) (1998)

The hourly variability index (σ_3) is equal to:

$$\sigma_3 = \begin{cases} \sqrt{\dfrac{(\rho-\rho_{-1})^2+(\rho-\rho_{+1})^2}{2}} & for\ sunrise < time < sunset \\ |\rho-\rho_{\pm 1}| & for\ sunrise\ and\ sunset\ hours \end{cases}$$ Equation 3-26

the clear sky index (ρ) is defined as follows:

$$\rho = \frac{k_t}{k_1}$$ Equation 3-27

and k_1 is equal to:

$$k_1 = 0.83 - 0.56e^{-0.06\beta}$$ Equation 3-28

- **For invariable hours (when $\sigma_3 \approx 0$ or $0.9 < \sigma_3 < 1$)**

- *Interval* $k_t \le 0.22$

$$k = 1$$ Equation 3-29

- *Interval* $0.22 \le k_t \le k_2$

$$k(k_t, \beta) = 1 - (1 - d_1)\left(0.11\sqrt{K} + 0.15K + 0.74K^2\right)$$ Equation 3-30

where:

$$K = 0.5\left(1 + \sin\left(\pi\left(\frac{k_t - 0.22}{k_1 - 0.22}\right) - \frac{\pi}{2}\right)\right)$$ Equation 3-31

$$k_2 = 0.95k_1$$ Equation 3-32

$$d_1 = 0.07 + 0.046\left(\frac{90-\beta}{\beta+3}\right)$$ Equation 3-33

and $d_1 = 1$ *for* $\beta \leq 1.4^{\circ}$

- *Interval* $k_2 \leq k_t \leq k_{\max}$:

$$k = d_2 k_2 \left(\frac{1 - k_t}{k_t (1 - k_2)} \right)$$ Equation 3-34

where $d_2 = k(k_2, \beta)$ is calculated from equations 3-30, 3-31, 3-32 and 3-33, and (k_{max}) is defined as:

$$k_{\max} = \left(\frac{k_{b\max} + \frac{d_2 k_2}{1 - k_2}}{1 + \frac{d_2 k_2}{1 - k_2}} \right)$$ Equation 3-35

where:

$$k_{b\max} = 0.81^{\alpha}$$ Equation 3-36

with:

$$\alpha = \left(\frac{1}{\sin(\beta)} \right)^{0.6}$$ Equation 3-37

- *Interval* $k_t \geq k_{\max}$:

$$k = 1 - k_{\max} \frac{1 - d_{\max}}{k_t}$$ Equation 3-38

where:

$$d_{\max} = \frac{d_2 k_2 (1 - k_{\max})}{k_{\max} (1 - k_2)}$$ Equation 3-39

- **For variable hours (when $\sigma_3 > 0$)**

The term $\Delta(k_t, \beta, \sigma_3)$ is added to equations 3-29, 3-30, 3-34 and 3-38:

$$\Delta(k_t, \beta, \sigma_3) = -3k_L^2(1-k_L)\sigma_3^{1.3}, \quad \text{for } 0.14 \le k_t \le k_x \qquad \text{Equation 3-40}$$

$$\Delta(k_t, \beta, \sigma_3) = 3k_R(1-k_R)^2\sigma_3^{0.6}, \quad \text{for } k_x \le k_t \le (k_x + 0.71) \qquad \text{Equation 3-41}$$

$$\Delta(k_t, \beta, \sigma_3) = 0, \quad \text{for } k_t \le 0.14 \text{ and for } k_t \ge (k_x + 0.71) \qquad \text{Equation 3-42}$$

where:

$$k_x = 0.56 - 0.32e^{-0.06\beta} \qquad \text{Equation 3-43}$$

$$k_L = \frac{(k_t - 0.14)}{(k_x - 0.14)} \qquad \text{Equation 3-44}$$

$$k_R = \frac{(k_t - k_x)}{0.71} \qquad \text{Equation 3-45}$$

F) Ruis-Aruiz et al. model (2010)

- **Ruiz-Arias 1 (RU1)**

$$k = 0.952 - 1.041e^{-e^{(2.3-4.702k_t)}} \qquad \text{Equation 3-46}$$

- **Ruiz-Arias 2 (RU2)**

$$k = 0.952 - 1.041e^{-e^{(2.808-5.759k_t+2.276k_t^3-0.125m'+0.013m'^2)}} \qquad \text{Equation 3-47}$$

3.1.3.2 Evaluations of models

In order to evaluate the performance of the models that have been mentioned, the diffuse irradiance on horizontal surfaces $I_{d(estimated)}$ are calculated and then compared to the

counterpart of measured data $I_{d(measured)}$. The comparison was done by using three widely used statistical tests, mean absolute bias error MABE, root mean square error RMSE and mean absolute percentage error MAPE, in the realm of the solar irradiance estimation. The MABE test shows the average difference of the predicted data from the measured data. The RMSE test presents "the standard deviation of the random component in the data", and the normalised RMSE indicate the short term of the performance of the model. The MAPE test indicates the performance of predictability of the regression. Whenever the values of these tests are small and close to zero, whenever the model is better. The following equations show how to measure these statistical indicators:

$$MABE = \frac{\sum \left| I_{d(estimated)} - I_{d(measured)} \right|}{nd} \quad \text{Equation 3-48}$$

$$RMSE = \sqrt{\frac{\sum \left(I_{d(estimated)} - I_{d(measured)} \right)^2}{nd}} \quad \text{Equation 3-49}$$

$$MAPE = \frac{\sum \left| \frac{I_{d(estimated)} - I_{d(measured)}}{I_{d(measyred)}} \right| 100\%}{nd} \quad \text{Equation 3-50}$$

where *nd* is the number of data.

The results of the evaluation are reported in Table 3-2 and illustrated in Figure 3-3 as well. Of course, the best model is the model that has the lowest value in these statistical tests. However, the rudimentary impressions that can be reached from examining Figure 3-3 are the failure of the Maxwell, Reindl 2, BRL, Reindl 3 and Skartveit models and the possibility of success of the Al-Riahi, Ruiz-Arias1, Ruiz-Arias1 and Reindl 1 models.

With regards to the MBE test, the lowest value was found to be 9.14W/m^2 and that was for Ruiz-Arias 1 model, while the value of 52.4W/m^2 was the worst and the highest value, and that was for Reindl 2 model. As for RMSE results, Al-Riahi model was the best model

where it scored 19.48W/m^2, whereas the highest value was 75.14W/m^2 and that was for Maxwell model. MAPE results revealed that the best and the worst performance were in Ruiz-Arias 1 and Reindl 2 models, respectively, where it ranged from 11% for Ruiz-Arias 1 model to 34.03% for Reindl 2 model. In addition, it can be observed the slight difference between the result of Al-Riahi model that scored 11.14% and the result of Ruiz-Arias 1 model. It is worth mentioning here that a 10% error can be considered reasonable and acceptable in the field of solar radiation (Muzathik *et al.*, 2011).

Table 3-2 Results of MABE, RMSE & MAPE tests for the nine models.

Models	Abbreviation	MABE (W/m^2)	RMSE (W/m^2)	MAPE (%)
Maxwell	MX	50.15	75.14	31.40
Reindl 1	RE1	22.00	28.76	15.26
Reindl 2	RE2	52.40	67.28	34.03
Reindl 3	RE3	37.12	45.78	25.25
Al-Riahi	AR	17.05	19.48	11.14
BRL	BRL	35.94	51.21	24.48
Skartveit	SK	13.07	38.03	17.34
Ruiz-Arias 1	RU1	9.14	20.62	11.00
Ruiz-Arias 2	RU2	12.81	26.39	13.79

Nevertheless, the failure of these two models, Al-Riahi and Ruiz-Arias 1, in one or two of the statistical tests was sufficient reason to not consider one of these two regressions as a suitable model for Baghdad climate, and this was the motivation for proposing a new model that can be successful in these statistical tests, besides its ability to describe the diffuse solar irradiance in Baghdad better than other models.

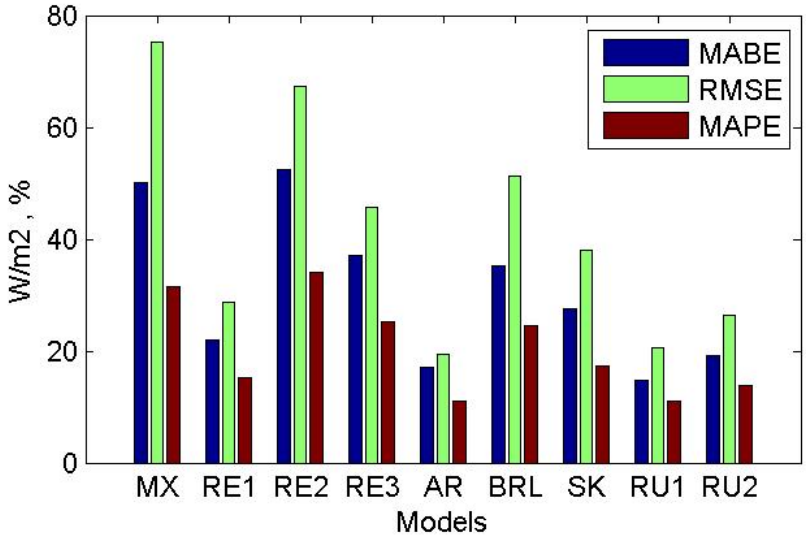

Figure 3-3 Results of the evaluation of the nine models.

3.1.4 The proposed regression

The purpose of this paragraph was to use recently collected data (from March to October 2012) to build a regression for the diffuse index for Baghdad, Iraq. Our concern was the potential of using ten-month period data for proposing a new model. However, the reports have revealed the possibility of using it. Boland et al. (2001) used 75 days to propose their model. (Perez *et al.*, 1990b) stated that a six month period is enough to delineate "the prevailing relationship between solar radiation components at a given site". Furthermore, Perez et al. (1992) used six-month period data from three different locations in their data set to construct their model.

Our attention focused on the proposed model being easily applicable and requiring a minimal number of parameters. The current literature showed the easiest regression is either traditional piecewise (Al-Riahi, Al-Hamdani & Tahir, 1992; Reindl, Beckman & Duffie, 1990) or logistic correlation (Lauret, Boland & Ridley, 2013; Ruiz-Arias *et al.*, 2010). However, logistic correlation is simpler than piecewise correlation because it consisted of one equation and there is no need to be divided it three intervals with start and end points as in the piecewise correlation. Furthermore, the sigma function (one of the

forms of the logistic equation) proposed by Ruiz-Arias et al. (2010) recorded the best scores in two tests. Consequently, the logistic correlation was adopted and the following are the two forms of the proposed model:

$$k = a_0 - a_1 e^{-e^{(a_2 + a_3 k_t)}} \quad \text{Equation 3-49}$$

$$k = a_0 - a_1 e^{-e^{(a_2 + a_3 k_t + a_4 k_t^2 + a_5 P + a_6 P^2)}} \quad \text{Equation 3-50}$$

where a_0, a_1, a_2, a_3, a_4, a_5 and a_6 are coefficients of the equations.

The first form, Equation 3-49, is used when the clearness index parameter is the only indicator to describe the diffuse index *k*, whereas, the second form, Equation 3-50, utilises an extra parameter (represented by the symbol *P*), besides the clearness index. The optical air mass, the sine of the solar altitude angle and the ambient temperature are the indicators that could be used as the second parameter. Consequently, four potential models are obtained, one from Equation 3-49 and three from Equation 3-50. Curve fitting toolbox in MATLAB (2012) was used to find the values of the coefficients of these models, and Table 3-3 shows these values.

Table 3-3 Fitting values of the coefficients found through utilising the curve fitting toolbox in MATLAB.

Model	Equation	Indicators	a0	a1	a2	a3	a4	a5	a6
M1	49	k_t	0.158	-0.822	-5.042	9.125			
M2	50	k_t & m'	0.828	1.388	3.013	-7.676	4.227	0.12	-.0142
M3	50	k_t & sin(β)	1.332	1.298	0.840	-2.500	-1.726	0.376	-0.508
M4	50	k_t & T_{amb}	0.1764	-0.752	-6.664	9.263	-0.443	0.122	-0.002

To analyse the performance of the models M1, M2, M3 & M4, the same statistical indicators (MABE, RMSE and MAPE) were used in order to choose the best model. The scores of these indicators are reported and plotted in Table 3-4 and Figure 3-4, respectively.

Table 3-4 Results of MABE, RMSE & MAPE tests for four potential models.

Models	MABE (W/m^2)	RMSE (W/m^2)	MAPE (%)
M1	10.88	13.69	7.41
M2	16.68	21.59	12.17
M3	16.28	21.10	11.66
M4	11.96	16.56	8.29

As can be seen from the results, the M1 model (Equation 3-51), got the lowest values in all tests; 10.88W/m^2 in MABE, 13.69W/m^2 in RMSE and 7.41% in MAPE. Furthermore, the M4 model (Equation 3-52), was the second best model and its results were slightly different from M1 model results, however, M1 was considered the better one it does need only one parameter. Moreover, as inferred from M2 & M3 results, it is evident that using air mass or solar altitude angle did not lead to the desired improvement.

$$k = 0.1584 + 0.8218e^{-e^{(-5.042+9.125k_t)}} \quad \text{Equation 3-51}$$

$$k = 0.176 + 0.752e^{-e^{(-6.664+9.263k_t-0.443k_t^2+0.122T_{amb}-0.002T_{amb}^2)}} \quad \text{Equation 3-52}$$

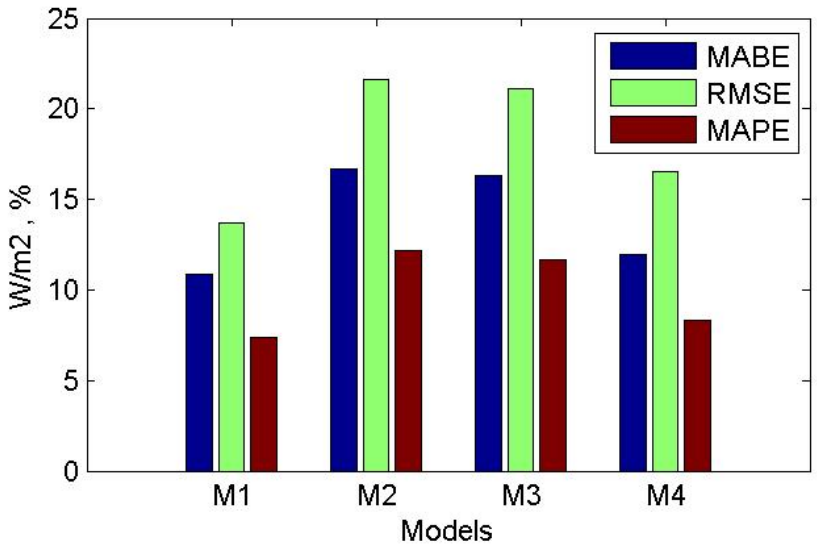

Figure 3-4 Results of the evaluation of the potential models.

In addition to these statistical tests, a scatter figure (see Figure 3-5) for the estimated diffuse irradiance against its counterpart measured value for each model was plotted to demonstrate the behaviour of the proposed models, which clearly shows the good performance of M1 model.

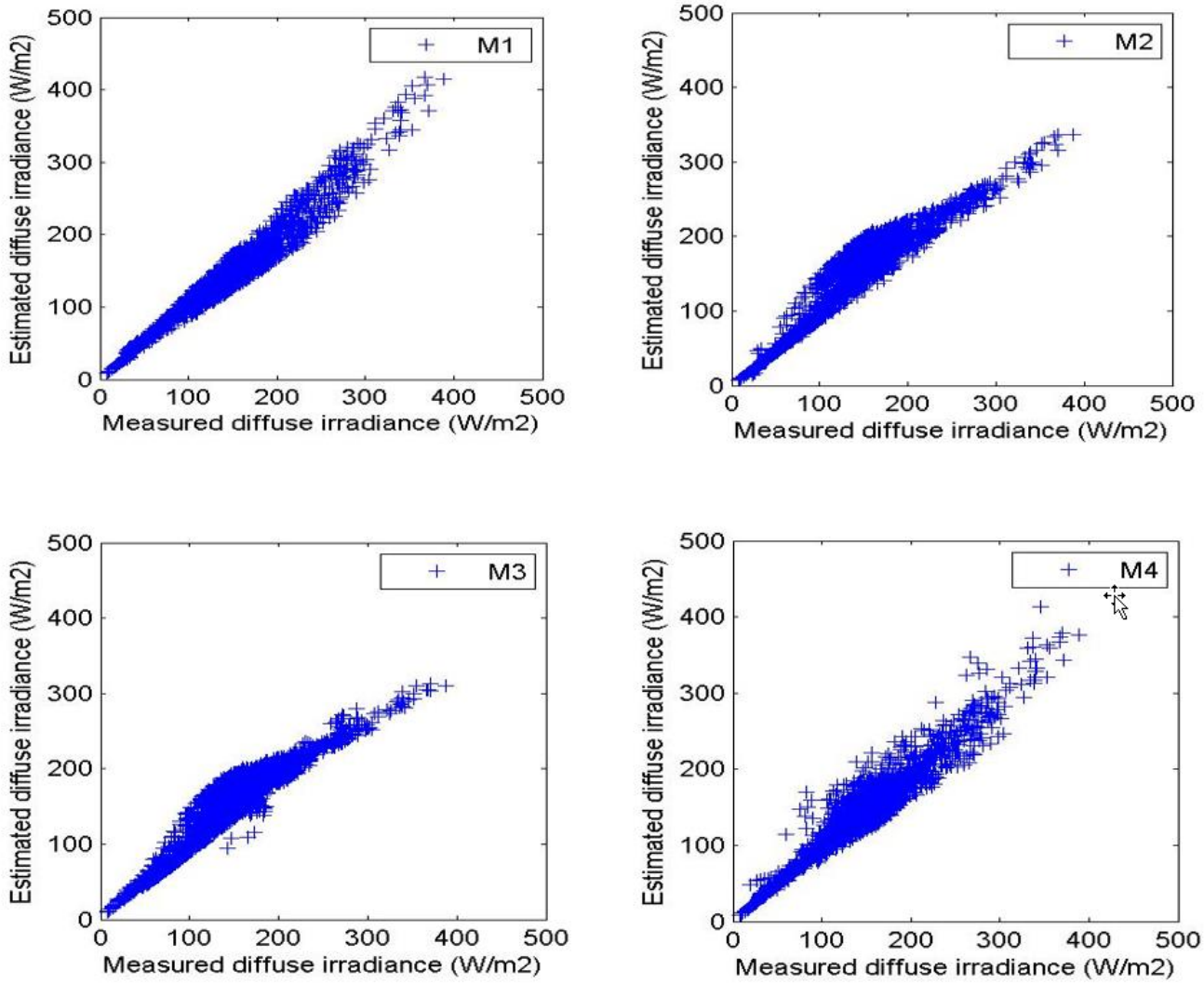

Figure 3-5 A scatter plot for the estimated diffuse irradiance against its counterpart measured value for M1, M2, M3 and M4 models.

3.1.5 Conclusion

Designing solar energy systems has become mainly reliant on the simulation software and these programs in turn depend directly on tools that describe the characteristics of the solar irradiation at the site of interest. Solar diffuse irradiance models can be used to predict the diffuse solar irradiance (as well as the direct irradiance) falling on horizontal surfaces by knowing the global solar irradiance. Therefore, the appropriate diffuse model is an important factor in the success of any designing or simulation process. An evaluation of the estimated diffuse solar irradiance falling on horizontal surfaces in Baghdad, Iraq based has been carried out, nine prediction models were used. MABE, RMSE and MAPE statistical indicators were used to determine the accuracy of the predictability of each model compared to a recently collected data. However, no one among these models obtained the best scores in all of these statistical tests. This gave us the motivation to propose a new model more suited to the climate of Baghdad. Two forms of logistic correlation were adopted for the potential models. The first form was based only on the clearness index, while in the second form, the optical air mass, the solar altitude angle and the ambient temperature were considered as the potential second parameter beside to the primary parameter (clearness index). Consequently, four new potential regressions (M1, M2, M3 and M4) have been proposed to estimate the diffuse index *k*. These proposed models were then analysed to choose the most suitable model. The statistical tests showed that the M1 model (based on the clearness index only) provides better prediction than the other models. Moreover, as inferred from M2 & M3 results, it is evident the using air mass or solar altitude angle did not lead to the desired improvement.

3.2 Feasibility of using of ASHRAE clear sky model in Baghdad

In this section, four clear sky models (ASHRAE new clear sky model, ASHRAE old clear sky model, AlRiahi model and AlSanea model) were used for computing the hourly average total solar irradiance on a horizontal surface in Baghdad. From measured data, eight days that represented the clearest sky days, one day for each month (from March to October 2012), were chosen in order to examine the applicability of those models for Baghdad's climate. The computed data from the aforementioned models have been plotted versus the observed data in these eight days.

3.2.1 Introduction

Most air-conditioning engineers use ASHRAE's clear sky model and climatic design data to select or design appropriate air conditioning systems, where clear sky condition means the "upper limit" of the solar irradiance used for calculating the buildings' cooling loads (Gueymard & Thevenard, 2009). Since the beginning of the last century, investigations have been conducted attempting to measure the solar radiation flux. Moon in 1940 (Stair & Ellis, 1968) proposed a model and diagrams to estimate clear sky solar radiation. In 1958, Threlkeld and Jordan proposed a model, which was considered a development of Moon's model (Amarananwatana & Sorapipatana, 2004). Gueymard & Thevenard (2009) reported that the first ASHRAE presented its official form of clear sky model in 1967, after the investigation had been carried out by Stephenson (1965). Many researchers had assessed this model, including Muneer et al. (1984), Nijegorodov (1996), Wong & Chow (2001), Al-Sanea et al. (2004), Amarananwatana & Sorapipatana (2004), Wessapan & Somsuk (2008) and Yildiz (2011), and their results revealed it needs further improvement. Some of these investigators have also offered their insights on how to modify the model. In addition, Western (1990) found this model not suitable to the New Zealand climate.

Furthermore, Galanis and Chatigny (1986) proved that it was not suitable for Canada, despite the fact that the ASHRAE clear sky model originally relied on an investigation focused on the climate of Toronto, Canada (work of Stephenson (1965)). Finally, Gueymard (2008) introduced a new clear sky model named REST2 model, and this model is characterised with ease of use, accuracy and the possibility of being used globally, in addition to requiring fewer parameters that depend on the sites. Thereafter, the REST2 model has been adopted as the new 2009 ASHRAE clear sky model (2009).

3.2.2 Numerical Model of AHRAE 2009 clear sky model

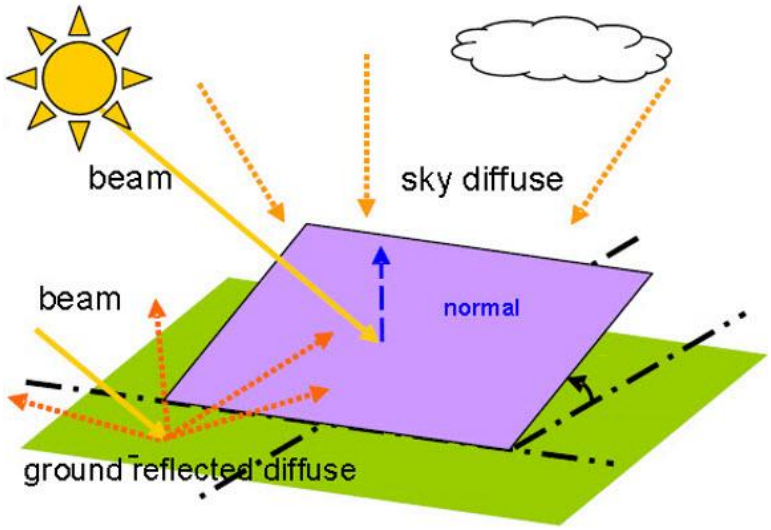

Figure 3-6 Components of solar irradiance incident on a tilted surface.

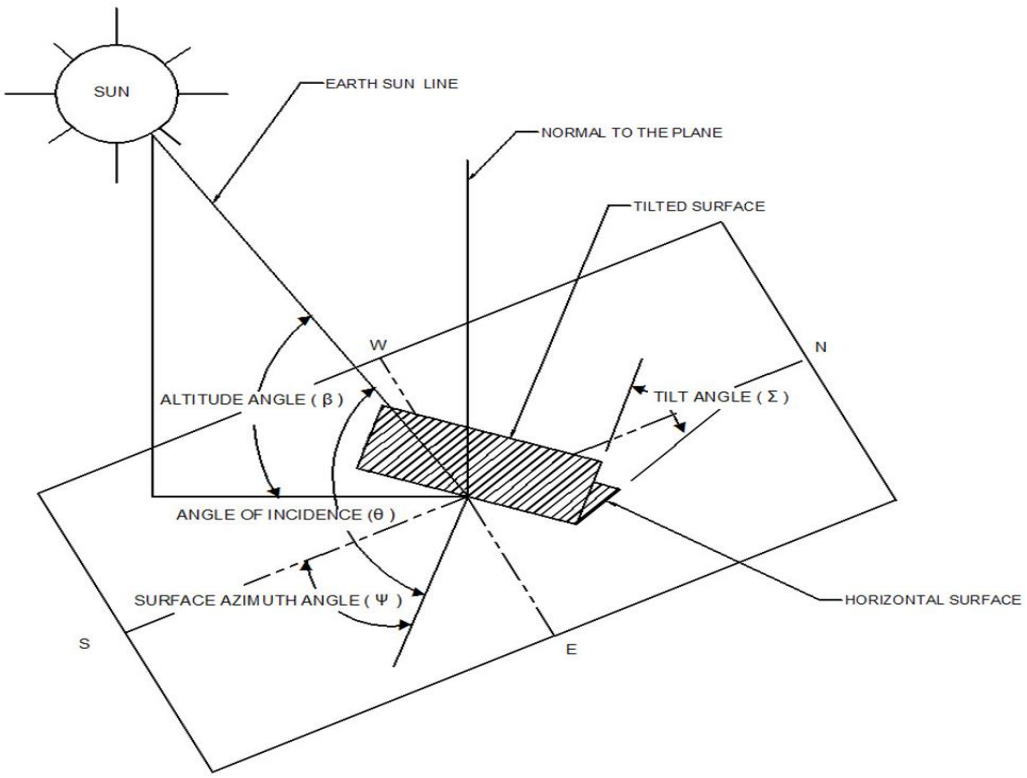

Figure 3-7 Solar angles for tilt and horizontal surfaces.

The intensity of the clear sky solar irradiance (E_t) fallen on tilted surfaces, see Figure 3-6, is equal to the sum of three components: the direct beam component (E_{th}), coming directly from the sun, the diffuse component (E_{td}), coming from the rest of the sky dome and the ground reflected component (E_{tr}), reflected from the surrounding environment. Figure 3-7 illustrates the solar angles for tilt and horizontal surfaces that will be used in the equations below:

$$E_t = E_{th} + E_{td} + E_{tr} \qquad \text{Equation 3-53}$$

$$E_{th} = E_b \cos\theta \qquad \text{Equation 3-54}$$

$$E_{td} = E_d\left(Y \sin\Sigma + \cos\Sigma\right) \qquad \text{Equation 3-55}$$

$$E_{tr} = E_b\left(\sin\beta + E_d\right)\rho_g \frac{\left(1-\cos\Sigma\right)}{2} \qquad \text{Equation 3-56}$$

where θ, β, Σ and ρ_g are the angle of incidence, solar altitude angle, tilt angle, and the angle of ground reflectance, respectively. The ratio Y is a function of the incidence angle.

$$Y = maximum\ of\ [0.45\ ,\ 0.55 + 0.437\cos\theta + 0.313\cos^2\theta] \qquad \text{Equation 3-57}$$

E_b and E_d are the beam (direct or normal) and diffuse components of clear sky solar radiation fallen on a horizontal surface, and they are calculated from the following equations, respectively:

$$E_b = I_o \exp\left(-\tau_b m^{ab}\right) \qquad \text{Equation 3-58}$$

$$E_b = I_o \exp\left(-\tau_d m^{ad}\right) \qquad \text{Equation 3-59}$$

where τ_b and τ_d are the beam and the diffuse pseudo optical depths, which are found from Table 3-5, interpolation is used to find values for the other days of the year. *ab* and *ad* can be calculated by the following equations, respectively:

$$ab = 1.219 - 0.043\ \tau_b - 0.151\ \tau_d - 0.204\ \tau_b\tau_d \qquad \text{Equation 3-60}$$

$$ad = 0.202 - 0.852\ \tau_b - 0.007\ \tau_d - 0.357\ \tau_b\tau_d \qquad \text{Equation 3-61}$$

Table 3-5 Solar clear sky irradiance and related data for Baghdad, Iraq (Thevenard, 2012).

Month	**Jan**	**Feb**	**Mar**	**Apr**	**May**	**Jun**	**Jul**	**Aug**	**Sep**	**Oct**	**Nov**	**Dec**
Day of year	21	52	80	111	141	172	202	233	264	294	325	355
τ_b	0.418	0.469	0.694	0.841	0.953	0.819	1.026	0.860	0.745	0.841	0.483	0.414
τ_d	1.909	1.753	1.345	1.210	1.133	1.245	1.100	1.224	1.325	1.224	1.745	1.929
$E_{b,noon}$	762	761	617	555	504	578	465	538	575	457	681	738
$E_{d,\ noon}$	159	201	320	384	422	377	432	374	320	315	182	149

It should be mentioned here that Equations 3-58 to 3-61 can be used even for the unclear sky (ASHRAE, 2009).

3.2.3 Verification

To validate the ASHRAE 2009 new model, three clear sky models were implemented. ASHRAE old model (2005) was selected, as it was found suitable for the climate of Turkey (Bakirci, 2009). AlRiahi model (Al-Riahi, Al-Jumaily & Ali, 1998) was chosen because it was proposed from measured data in Baghdad, Iraq. Finally, AlSanea model (Al-Sanea, Zedan & Al-Ajlan, 2004) was used, as it was a modification of the ASHRAE 2005 old model to make it suitable to the climate of Riyadh, Saudi Arabia. Three statistical indicators (MABE, RMSE and MAPE) were used to evaluate the accuracy and validity of the models.

3.2.4 Discussion

In the present study, MATLAB source codes were written to describe all aforementioned clear sky models as well as the statistical tests. Through available observed global solar irradiance during eight months (from March to October 2012), eight clear sky days were chosen (one day for each month) as follows: 15 March, 4 April, 7 May, 6 June, 17 July, 20 August, 9 September, and 13 October. The criteria for choosing these days are based on the recommendations of Amarananwatana & Sorapipatana (2004). Thereafter, each of these eight days was modelled with the four clear sky models. The calculated and measured data were then plotted in Figures 3-8, 3-9, 3-10, 3-11, 3-12, 3-13, 3-14, and 3-15. It is clear from those figures that the ASHRAE 2009 clear sky model agrees better with the observed data than the other three models.

In addition, the results of MABE, RMSE, and MAPE were tabulated in Tables 3-6, 3-7, 3-8, 3-9, 3-10, 3-11, 3-12 and 3-13. The comparisons showed that the ASHRAE 2009 clear sky model was more accurate than the other models.

As mentioned before, ASHRAE clear sky model will be used as one of the ways to evaluate the results of the proposed methodology of the solar irradiance fallen on a tilted surface (the next section).

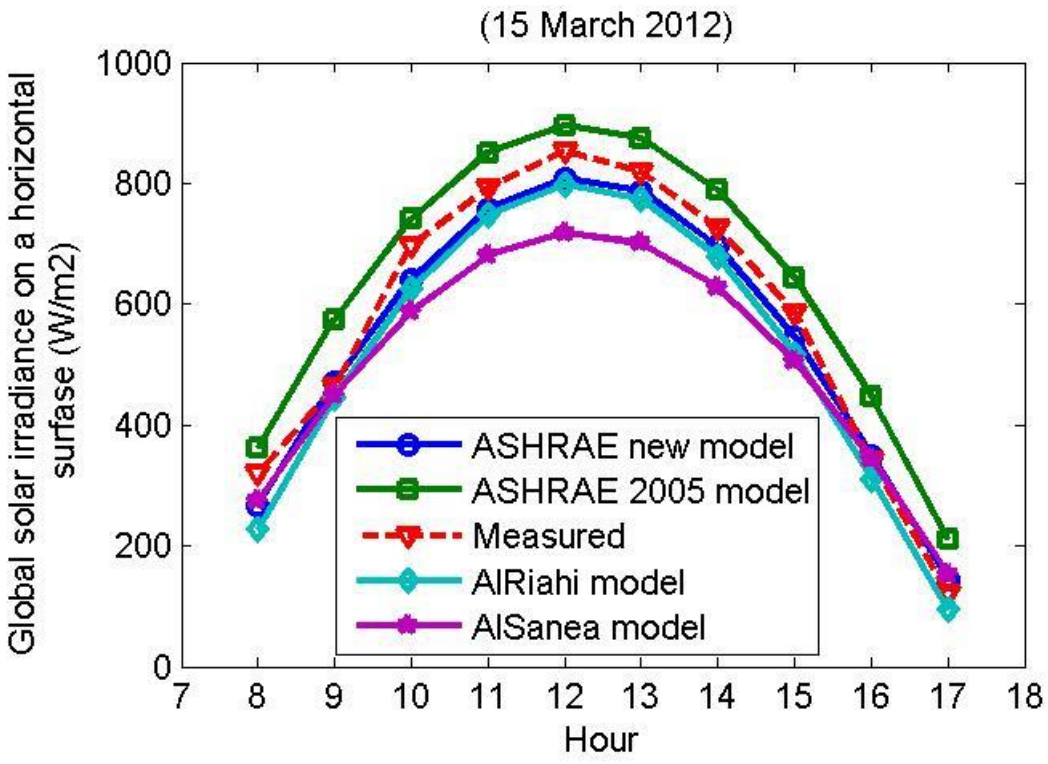

Figure 3-8 Hourly variation of global solar irradiance on March 15.

Table 3-6 Statistical results for March 15.

Model	MABE (W/m2)	RMSE (W/m2)	MAPE (%)
ASHRAE new	32.78	36.28	7.16
ASHRAE 2005	67.26	71.51	18.62
AlRiahi	49.89	54.16	10.94
AlSanea	74.37	86.91	13.06

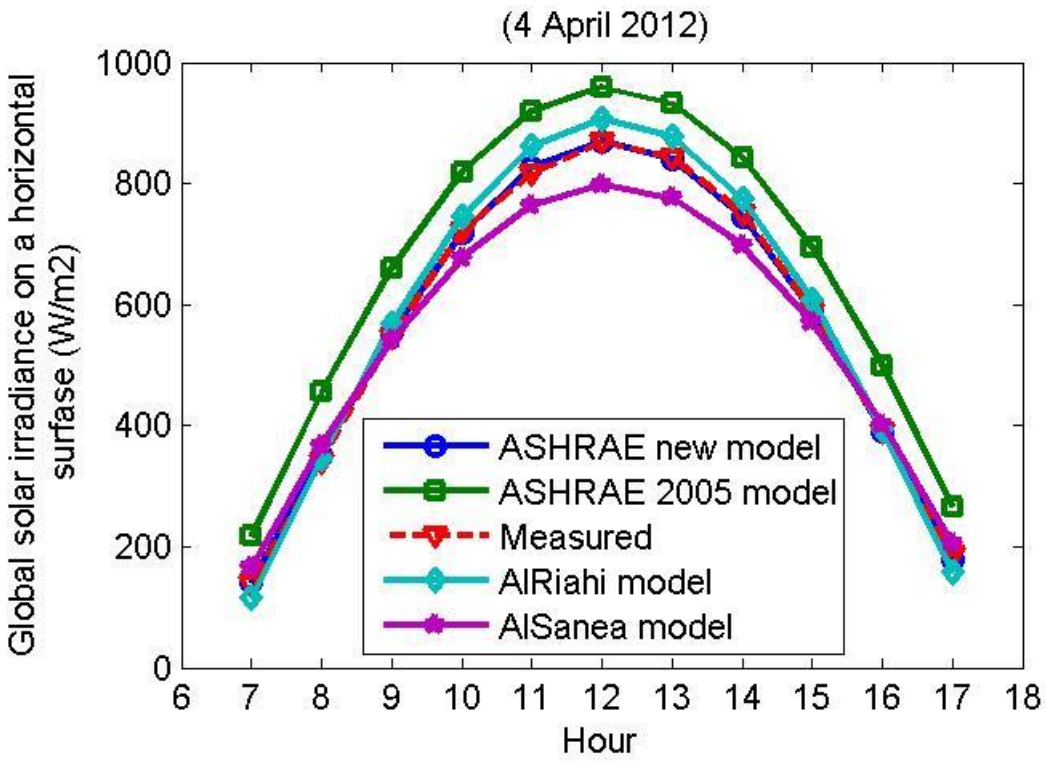

Figure 3-9 Hourly variation of global solar irradiance on April 4.

Table 3-7 Statistical results for April 4.

Model	MABE (W/m2)	RMSE (W/m2)	MAPE (%)
ASHRAE new	4.59	5.82	1.19
ASHRAE 2005	97.68	98.39	23.72
AlRiahi	23.83	26.77	5.51
AlSanea	36.11	41.9	7.37

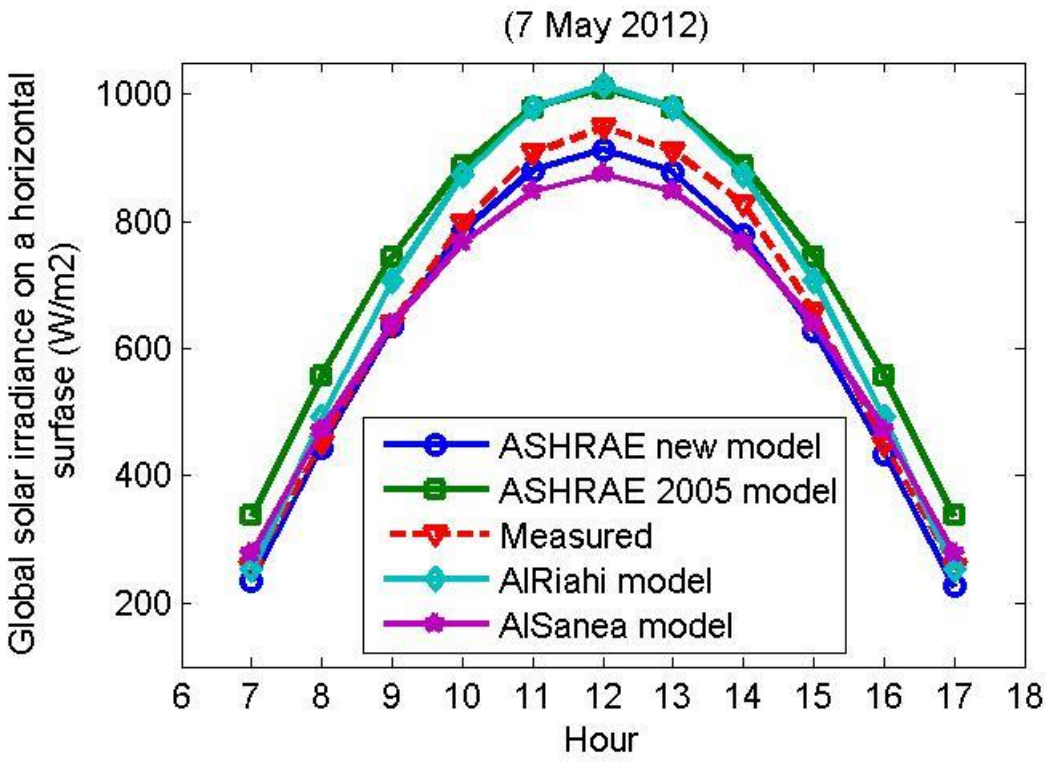

Figure 3-10 Hourly variation of global solar irradiance on May 7.

Table 3-8 Statistical results for May 7.

Model	MABE (W/m2)	RMSE (W/m2)	MAPE (%)
ASHRAE new	23.58	26.75	4.22
ASHRAE 2005	83.84	85.41	16.54
AlRiahi	47.39	53.19	6.75
AlSanea	36.06	42.65	5.74

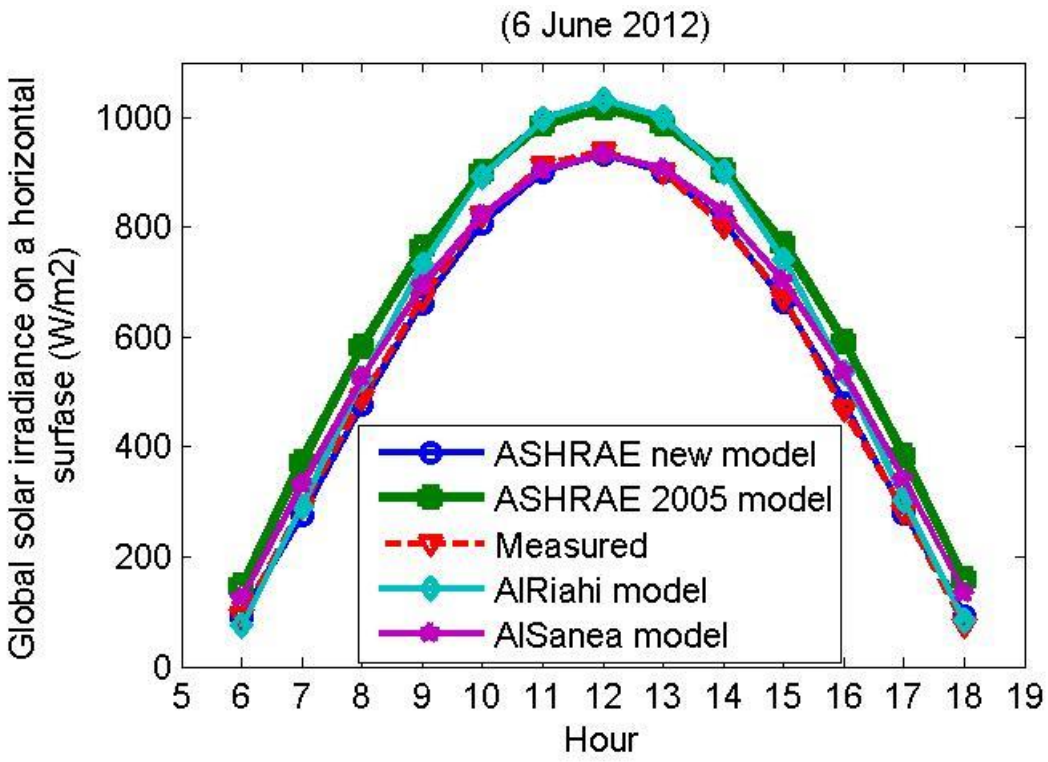

Figure 3-11 Hourly variation of global solar irradiance on June 6.

Table 3-9 Statistical results for June 6.

Model	MABE (W/m2)	RMSE (W/m2)	MAPE (%)
ASHRAE new	9.18	10.53	3.51
ASHRAE 2005	88.81	90.25	27.77
AlRiahi	55.96	65.20	10.10
AlSanea	30.43	36.89	14.18

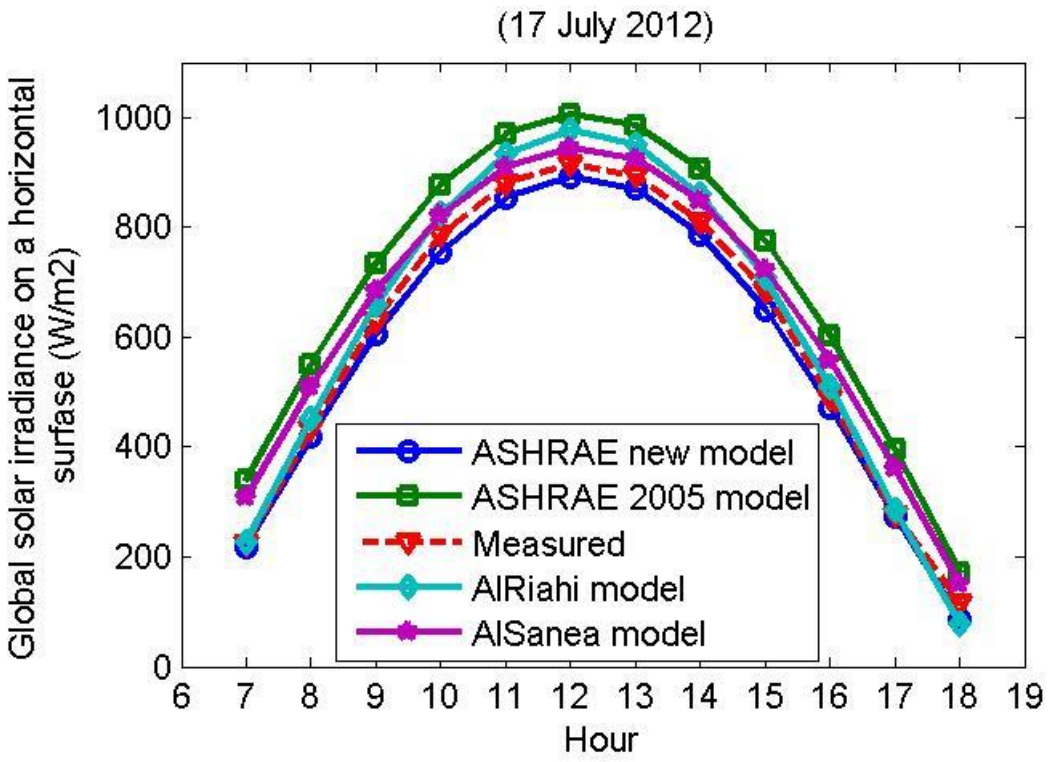

Figure 3-12 Hourly variation of global solar irradiance on July 6.

Table 3-10 Statistical results for July 6.

Model	MABE (W/m2)	RMSE (W/m2)	MAPE (%)
ASHRAE new	21.03	23.04	4.86
ASHRAE 2005	98.66	100.10	23.34
AlRiahi	33.41	38.28	7.05
AlSanea	50.19	54.43	13.60

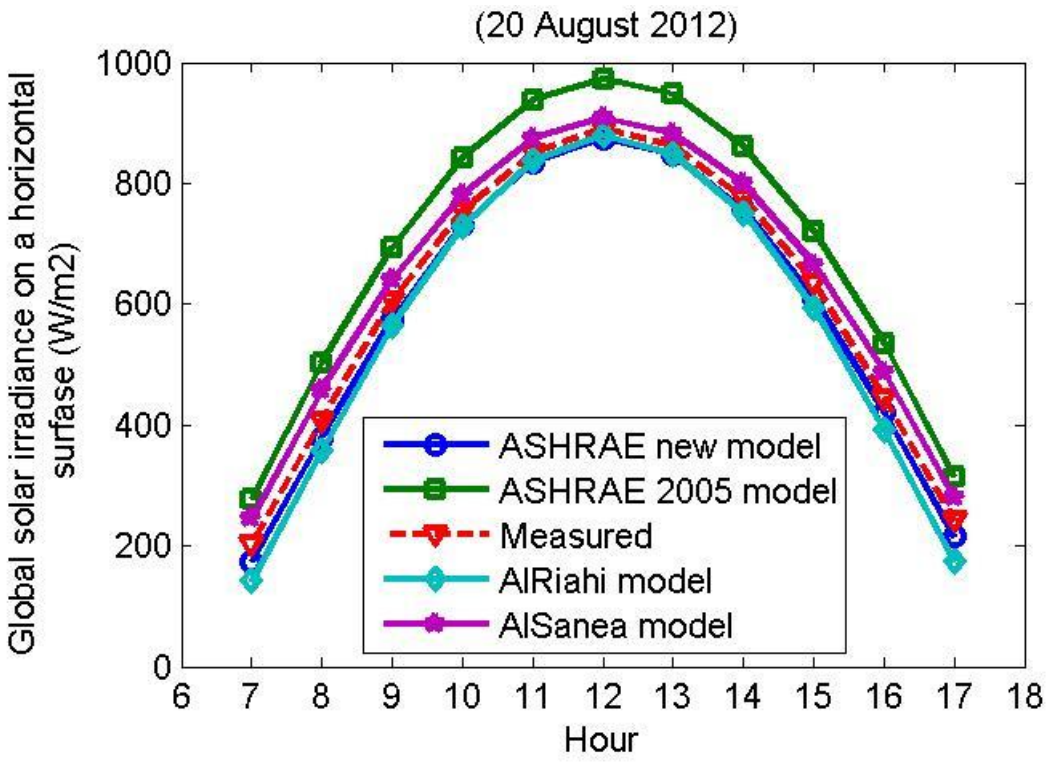

Figure 3-13 Hourly variation of global solar irradiance on August 20.

Table 3-11 Statistical results for March 21.

Model	MABE (W/m2)	RMSE (W/m2)	MAPE (%)
ASHRAE new	23.46	24.11	5.32
ASHRAE 2005	84.92	85.13	17.25
AlRiahi	37.07	41.91	9.80
AlSanea	31.59	33.01	7.41

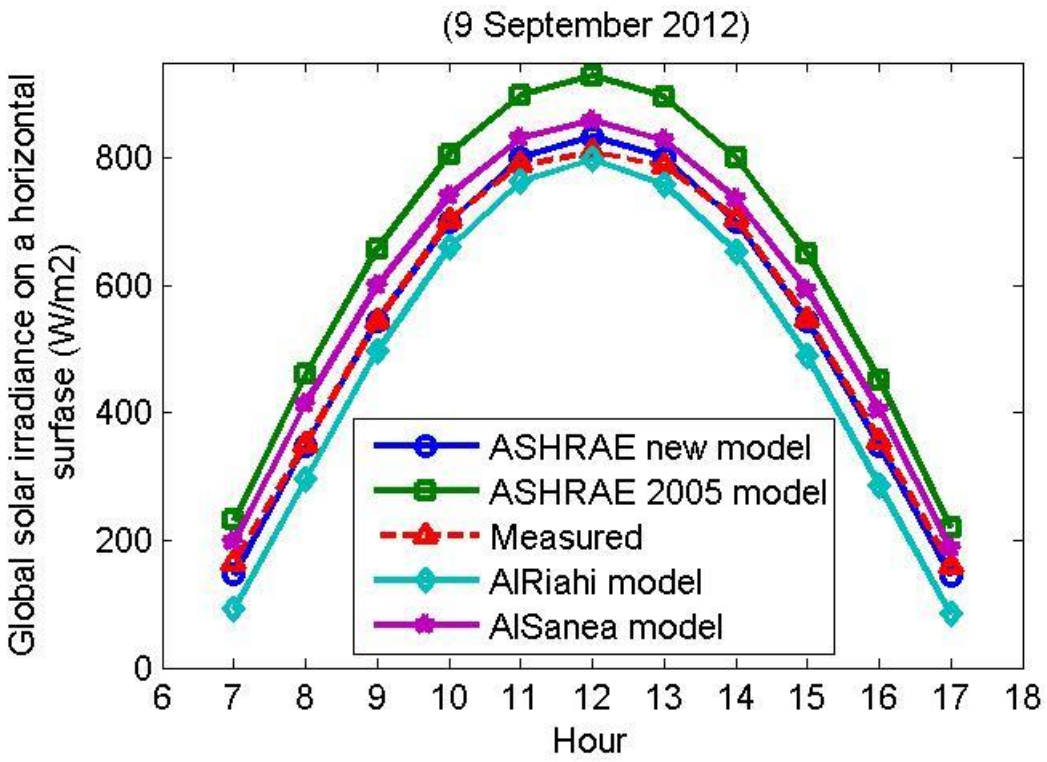

Figure 3-14 Hourly variation of global solar irradiance on September 9.

Table 3-12 Statistical results for September 9.

Model	MABE (W/m2)	RMSE (W/m2)	MAPE (%)
ASHRAE new	9.12	11.67	2.77
ASHRAE 2005	98.34	99.94	22.42
AlRiahi	49.44	53.01	15.28
AlSanea	42.90	44.05	10.41

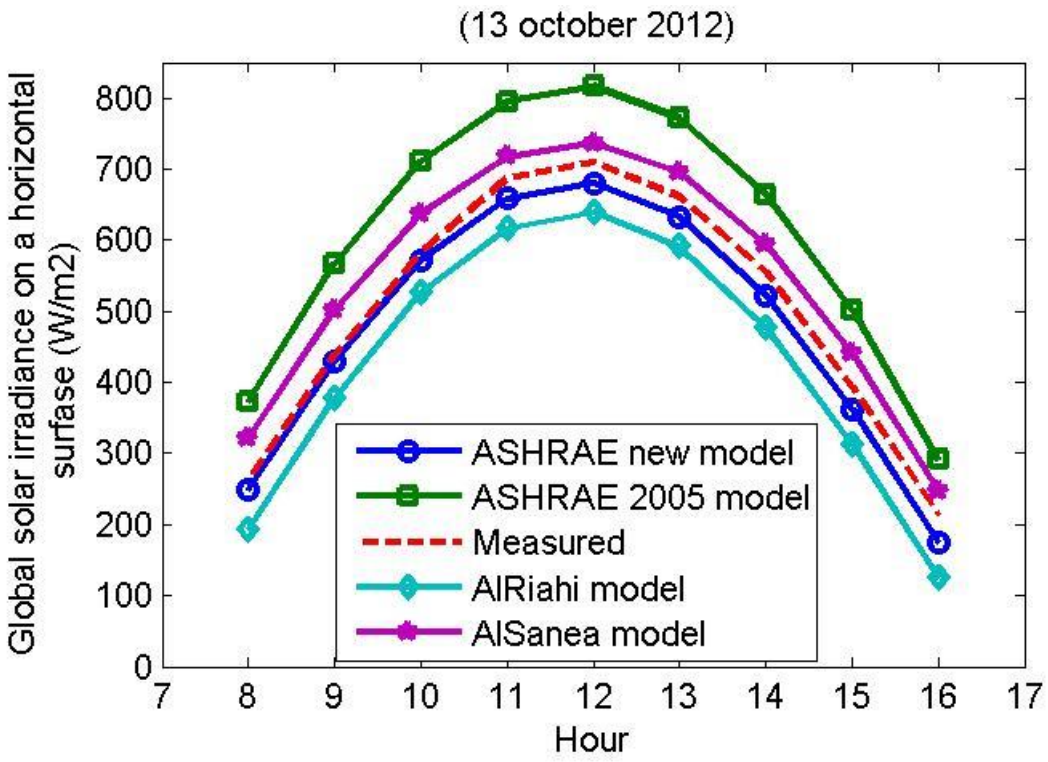

Figure 3-15 Hourly variation of global solar irradiance on October 13.

Table 3-13 Statistical results for October 13.

Model	MABE (W/m2)	RMSE (W/m2)	MAPE (%)
ASHRAE new	24.62	26.62	5.94
ASHRAE 2005	109.82	110.69	24.96
AlRiahi	71.86	72.43	17.45
AlSanea	42.81	44.68	10.42

3.3 The optimal tilt angles for solar collectors in Baghdad

This section addresses how to choose the tilt angle of the solar collectors used in Baghdad, Iraq, and makes recommendations for optimal tilt angles that could increase the energy that is collected. Investigation was made to find the most accurate and suitable model to describe the characteristics of solar irradiance on a tilted surface under Baghdad climate conditions. A methodology was proposed to obtain the optimal tilt angles and three methods were used to verify the results of the proposed methodology.

3.3.1 Introduction

Iraq represents an excellent location for solar energy projects where it has a high amount of solar radiation 6.5-7 kWh/m² (Alasady, 2011), and there are more than 3000 sunshine hours in Baghdad. Additionally, solar energy could meet all the energy needs of Iraq, as reported by AL-Jumaily et al. (2010).

The appropriate design, installation and exploitation of all available sources will lead to achieving the maximum possible performance of any system, including solar powered systems. Solar energy can be exploited directly through a variety of means, such as solar collectors and photovoltaic PV cells. It is an established fact that the intensity of solar radiation incident upon any surface is increased when a slope (tilt) is given to the surface from the horizon. Consequently, most solar energy applications used tilted solar panels. The sun tracking systems are the most efficient way to collect the maximum daily solar energy (Lave & Kleissl, 2011). However, these systems are expensive, required maintenance and are more complicated, particularly the Dual-Axis tracking systems (Lubitz, 2011). Therefore collectors are often fixed on the basis of optimal angles for collecting solar energy (Elminir et al., 2006). Solar angles for a tilted and horizontal surface can be seen in Figure 3-7.

Solar collector's orientation (surface azimuth angle ψ); measured from the south, and tilt angle $\sum$ with the horizontal are the important factors affecting the performance of the fixed solar collector (Chang, 2008; Ertekin, Evrendilek & Kulcu, 2008). Generally, the optimal orientation of a solar collector in the northern hemisphere is facing the equator; due south, which several studies have proved for different locations, such as Elsayed (1989), and Jafarkazemi & Saadabadi (2012). With regards to Iraq, Mahdi et al. (2011) experimentally showed that the optimal orientation for a solar panel is due south in Baghdad, through measuring the amount of energy output from five solar panels facing East, Southeast, South, Southwest and West.

Practical experience has also shown that the tilt angle is generally equal to the latitude angle (L) of the site. However, several studies have shown that the tilt angle of solar collectors depends on the latitude angle of the site, but is not necessarily equal to it; it may be preferable to add or subtract a number to/from L. Additionally, some of these studies have suggested the adoption of two tilt angles is better than using a year round tilt angle, this is done by adding a certain amount to the tilt angle in the summer and subtracting another amount from the tilt angle in the winter, when the year is divided into summer (May to September) and winter (October to March). Consequently, several empirical formulas and recommended equations have been proposed to estimate the best (optimal) tilt angle $\sum_{opt}$. Table 3-14 shows a summary of some recommendations for the value of the optimal tilt angle in terms of the latitude angle L.

Table 3-14 A summary of some recommendations for the value of tilt angle in terms of Latitude angle *L*.

Authors	Location	Recommended tilt angle (°)
Hottel (Elsayed, 1989)	Eastern side of the USA	*L + 20*
Chinney (Tang & Wu, 2004)	South Africa	*L + 10*
Lewis (1987)	Alabama, USA	*L ± 8*
Qiu & Riffat (2003)	Worldwide	*L ± 10*
Elminir et al.(2006)	Helwan, Egypt	*L ± 15*
Ulgen (2006)	Izmir, Turkey	*L + 34* *L - 19*
Chang (2009)	For latitudes below 65°, otherwise	*0.9 L* *56 + 0.4 (L - 65)*
Lave & Kleissl (2011)	Several regions of USA	*L - (0 to 10)*

Ultimately, despite the fact that these relationships that predict the tilt angle solely from just the latitude angle are simple and direct, the existence of differences and contradictions led to the equation being only approximate (Armstrong & Hurley, 2010).

A number of studies suggested correlations assuming that the optimal tilt angle depends on the declination angle of the sun δ; the angle between the rays of the Sun and the plane of the Earth's equator. However, as the declination angle changes daily, the tilt angle must be changed every day. That was not practical, so these correlations were modified to estimate optimal tilt angle every month or every season, as in Tiris & Tiris (1998). Kacira et al. (2004) revealed that changing the tilt angle each month maintains nearly the total amount of solar energy that would be collected when the collectors are mounted according to its daily optimum angle. EL-Kassaby (1988) presented four recommended equations, where the year was divided into four seasons, to predict the optimal tilt angle. Soulayman (1991) examined El-Kassaby's method and suggested corrections to make it more

accurate. Bakirci (2012b) established general models for Turkey to determine the optimal tilt angle based on the declination angle. Sunderan et al. (2011) revealed that the monthly average optimal tilt angle for Malaysia is $\sum_{opt} = L - \delta$, however, Rakovec et al. (2011) found this kind of correlation was not valid in the Slovenia.

Nowadays, however, the major approach to finding the optimal tilt angle is to maximise the intensity of solar irradiance falling on surfaces (Armstrong & Hurley, 2010). This approach is broadly done in two ways:

- The first method measures the amount of solar irradiance (monthly or seasonally or yearly averages) at different tilt angles and identifies the highest value as well as the counterpart tilt angle (which represents the optimal tilt angle), as done by Armstrong & Hurley (2010), and Bakirci (2012a). Additionally, one study attempted to maximise the extraterrestrial solar radiation instead of the global solar irradiance (Gunerhan & Hepbasli, 2007).
- The second method finds the tilt angle directly, as in El-Kassaby (1988), Skeiker (2009) and Benghanem (2011). This method relies on the mathematical approach that is used to find the maximum values of a continuous function (e.g. the global solar irradiance I_g) through differentiation of the function with respect to an independent variable (which is here the tilt angle) and then makes the derivation results equal to zero to find the amount of the independent variable that makes the function achieve the maximum value. The disadvantage of this method is that the main function may be a very complicated equation, in addition to, potentially depending on many independent variables; thus the differentiation process could be difficult.

Ultimately, the basis of both methods is to propose an analytical model to measure the amount of solar irradiance on an inclined surface.

With regard to Iraq, investigations that relate to choosing the optimal angles are unsatisfactory and contradictory. Al-Riahi & Al-Kayssi (1998) revealed from measuring the intensity of solar irradiance on a horizontal, a 30° tilted surface (due south) and a vertical surface in Baghdad, that the 30° tilted surface was the better for collecting solar energy. Hamad (1988) found the yearly average optimal angle was L+8° in Basra, southern Iraq. Almousawi (2010) asserted that the solar collectors will receive maximum solar irradiance when the surface azimuth angle (orientation of the surface) is equal to the latitude angle for Baghdad; i.e. 33.3° Southwest, and this recommendation is contradicted by all the studies presented in the literature.

This section addresses how to choose the tilt angle of the solar collectors in Baghdad, Iraq, and make recommendations for optimal tilt angles that could increase the energy that is collected. This has been done by the following process:

- First, an investigation was made to find the most accurate and suitable model to describe the characteristics of solar irradiance on a tilted surface at Baghdad.
- Next, the optimal tilt angles for collectors were calculated for eight months (from March to October) by searching for the values of which the monthly average daily global solar irradiance on a tilted surface was a maximum.
- Then, the results were verified by using three methods: the ASHRAE clear sky model (2009), Elsayed's correlation (1989) and the TRNSYS software (Klein *et al.*, 2012).
- Finally, the yearly average optimal tilt angle was presented.

The outcomes of the study can be considered as a guide in the designing of the solar powered systems for Baghdad's climate, which in turn could increase the exploitation of solar energy and hopefully accelerate Iraq's transformation to an eco-friendly country.

3.3.2 Models of the solar irradiance falling on a tilted surface

Because the data for solar irradiance falling on a tilted surface are infrequently available, researchers have proposed various models to estimate it by knowing the characteristics of the solar irradiance on a horizontal surface; global solar irradiance and its diffuse and direct normal components are transposed and projected on a tilted surface (El-Sebaii *et al.*, 2010), the components of solar radiation incident on a tilted surface can be seen in Figure 3-6. The main difference among these models is how to describe the diffuse irradiance.

Tilted surface models can be classified into isotropic and anisotropic models. "The isotropic models assume that the intensity of diffuse sky radiation is uniform over the sky dome. Hence, the diffuse radiation incident on a tilted surface depends on the fraction of the sky dome seen by it. The anisotropic models assume the anisotropy of the diffuse sky radiation in the circumsolar region (sky near the solar disk) plus an isotropically distributed diffuse component from the rest of the sky dome" (Noorian, Moradi & Kamali, 2008).

The amount of solar irradiance falling on a horizontal surface can be taken either:

- directly from the meteorological stations and meteosat (satellite) data, such as Hammer et al. (2003) and Benghanem (2011).
- Or, indirectly by using models to estimate of global solar irradiance and its direct and diffuse components. Al-Rawahi et al. (2011) classified these models into two categories: parametric, as in the ASHREA clear model, and decomposition models that use the known global solar irradiance to find its components.

3.3.3 Proposal of a method to obtain the solar irradiance on a tilted surface in Baghdad

Because of the lack of data and research on models of solar radiation on inclined surfaces in Iraq, we have focused on the studies that have dealt with this subject in the neighbouring countries to Iraq. As mentioned before, the only difference between the models is the way of processing the diffuse irradiance component.

Kacira et al. (2004) used the isotropic model of Liu and Jordan (1962) to find the monthly average optimal tilt angle for a PV panel in Sanliurfa, Turkey. Likewise, the isotropic model of Liu and Jordan was implemented to calculate the optimal tilt angles in Erzurum, Turkey (Bakirci, 2012a). Nijmeh and Mamlook (2000) compared the isotropic model of Liu and Jordan (1962) and the anisotropic model of Hay (1979) with measured solar radiation data on a tilted surface in Amman, Jordan. They concluded that both models are almost equally accurate, and suitable to estimate the solar radiation on tilted surfaces in Amman. Noorian et al. (2008) carried out a comparison between twelve models and measured hourly diffuse solar irradiance data on a tilted surface in Tehran, Iran. They found that the Skartveit and Olseth model (1986) was very compatible with the measured data for the south-facing surfaces. It should be added here that Skartveit and Olseth's model (1986) is a modified version of Hay`s model (1979). Instead of assessing and adopting a specific model, Benghanem (2011) used results of eight diffuse models to develop a best-fit polynomial equation to estimate the solar radiation incident on tilted surfaces in Madinah, Saudi Arabia. The derivation of this equation with respect to tilt angle was equal to zero to find the optimal tilt angles. Khalil and Shaffie (2013) found that the Skartveit and Olseth model (1986) was among the most accurate models for calculation of the solar irradiance on south-facing tilted surfaces in Cairo, Egypt. Consequently, the Skartveit and Olseth model (1986) was chosen in this study to convert the hourly horizontal

solar irradiance to that over tilted surfaces in Baghdad, Iraq. The Mathematical procedure is demonstrated in the following steps:

The model that has been proposed in Section 3.1 was used to estimate the hourly diffuse solar irradiance on horizontal surfaces I_d from the hourly global solar irradiance I_g (hourly global irradiance measured data from March to October 2012 was used).

Direct beam solar irradiance falling on a horizontal surface (I_b) is the difference between the global solar irradiance and its diffuse component.

$$I_b = I_g - I_d \qquad \text{Equation 3-62}$$

The total hourly solar irradiance on a tilted surface I_t is the summation of its direct beam I_{bt}, diffuse I_{dt} and ground reflected I_r components, as written below:

$$I_t = I_{bt} + I_{dt} + I_r \qquad \text{Equation 3-63}$$

The hourly direct beam irradiance on a tilted angle can be expressed as:

$$I_{bt} = I_b \; r_b \qquad \text{Equation 3-64}$$

where r_b is the geometric factor in terms of the incident angle θ and the zenith angle Z, and is given by:

$$r_b = \frac{\cos(\theta)}{\cos(Z)} \qquad \text{Equation 3-65}$$

The hourly ground reflected irradiance can be expressed by:

$$I_r = I_g \rho_g \frac{(1-\cos(\Sigma))}{2} \qquad \text{Equation 3-66}$$

where ρ_g and Σ are ground reflectance and the tilt angle of the surface.

As mentioned before, the Skartveit and Olseth model (1986) will be used to calculate the diffuse irradiance on a tilted surface, and this model can be expressed as:

$$I_{dt} = I_d \left[\frac{I_b}{I_o \cos(Z)} r_b + \Omega \cos(\Sigma) + \left(1 - \frac{I_b}{I_o \cos(Z)} - \Omega \right) \left(\frac{1 + \cos(\Sigma)}{2} \right) \right] \quad \text{Equation 3-67}$$

where

$$\Omega = \max \left[0, \left(0.3 - 2 \frac{I_b}{I_o \cos(Z)} \right) \right] \quad \text{Equation 3-68}$$

Then, the main objective equation for finding the optimal tilt angle is:

$$\max imise \ (I_t) \qquad 0 < \Sigma < 90^\circ \quad \text{Equation 3-69}$$

3.3.4 Validation of the proposed method

The proposed methodology was conducted to find the optimal tilt angles for eight months, from March to April 2012. Three methods were implemented to validate the proposed model: ASHRAE Clear sky model (2009), Elsayed's correlation (1989) and TRNSYS software (Klein *et al.*, 2012).

3.3.4.1 Optimal tilt angle based on ASHRAE clear sky model

The new clear sky model of ASHRAE (2009) was used in this study to obtain the optimal tilt and surface azimuth angles for inclined surfaces in Baghdad (this model has been proved applicable for the Baghdad climate in Section 3.2). The following steps clarify how this was done:

- First, the tilt and surface azimuth angles were imposed.
- Second, the monthly average daily global solar irradiance was measured for each month.

- Third, the processes were repeated for different tilt and surface azimuth angles.
- Fourth and finally, searching in the results for the highest value of solar irradiance for each month and its counterpart tilt and surface azimuth angles, the values of these two angles represented the monthly average optimal values $\sum_{opt}$ & ψ_{opt}.

This process has been repeated to maximise the amount of the yearly average daily global solar irradiance and also in order to identify the yearly average optimal tilt and surface azimuth angles. In both cases, the tilt angle was varied from 0° to 90° and the azimuth surface angle was varied from 45° Southeast to 45° Southwest; in steps of 1°. The flow chart of using ASHRAE clear sky model to calculate the yearly average optimal tilt and surface azimuth angles is shown in Figure 3-16. For the monthly optimal angles case, the monthly average daily solar irradiance was calculated instead of yearly average daily solar irradiance in the flow chart.

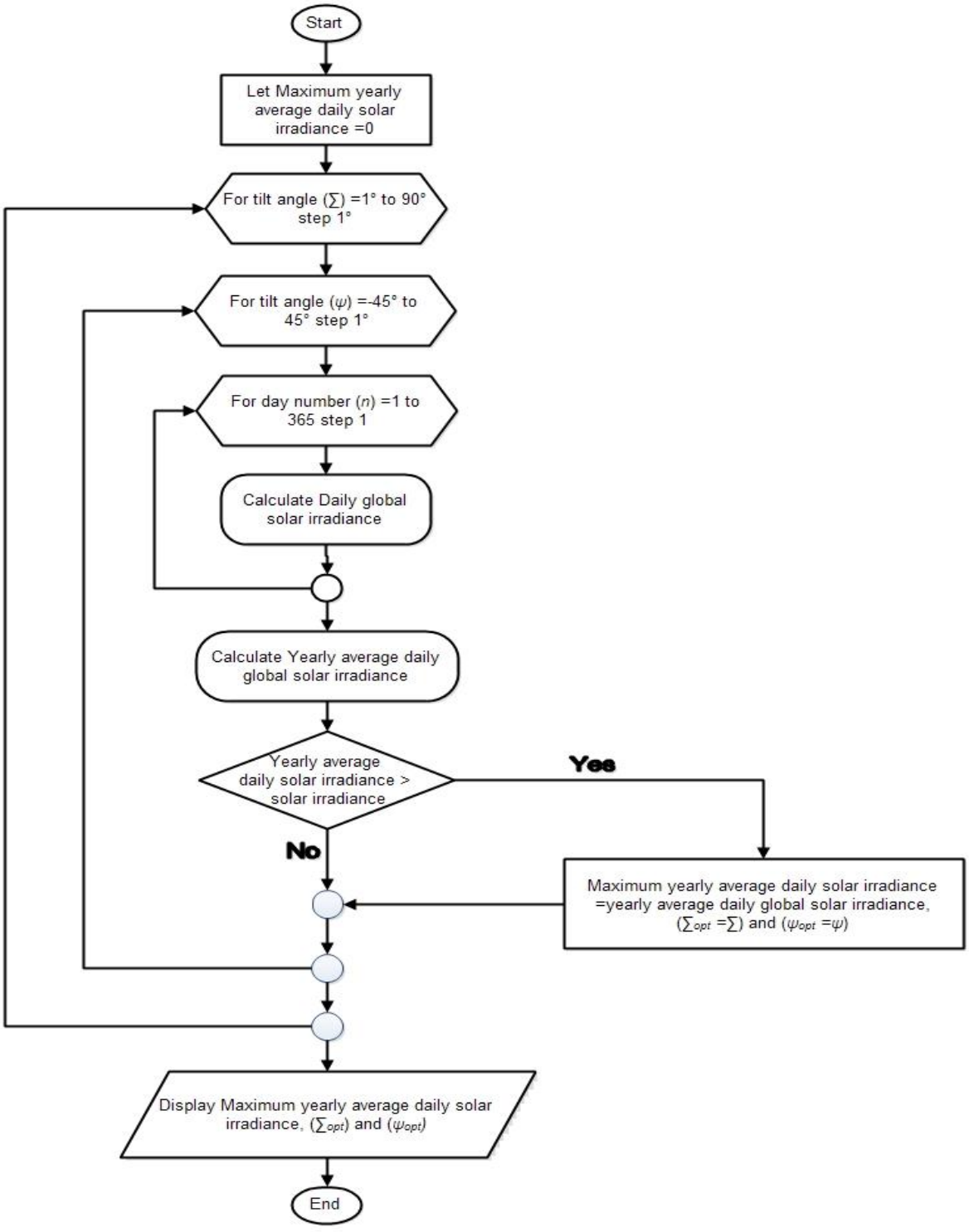

Figure 3-16 The flowchart of using ASHRAE clear sky model for calculating the yearly average optimal tilt and surface azimuth angles.

It should be noted that the optimum tilted angle for the surfaces under un-clear sky circumstances would be less (a flatter angle) than the recommended angles by clear sky

model in order to collect more energy from the (sky) diffuse irradiance. In other words, the recommended angles by ASHRAE clear sky model represent the upper range (limit) for the values of the optimal tilt angle.

3.3.4.2 Optimal tilt angle based on Elsayed's correlation

Elsayed's correlation (1989) was selected to compare the results of the proposed model, because it is simple and straightforward. Additionally, it has been examined in several investigations, for example: Elminir et al. (2006) proposed a geometrical base model for estimation of the optimal tilt angles in Helwan, Egypt. They found that their results totally agreed with the results that have been obtained by using Elsayed's correlation. However, later, Elsayed's correlation was used with a geometrical model to verify a methodology proposed by Armstrong & Hurley (2010) to determine the solar irradiance and optimal tilt angle for Galway, Ireland. The results showed that Elsayed's correlation was more applicable for cloudy skies such as Ireland. Therefore, the recommended tilt angles by Elsayed's correlation were considered the optimal tilt angles for cloudy conditions, which is flatter (less) than for clear and part cloudy skies such as in Baghdad's climate. In other words, the recommendations of Elsayed's correlation represent the lower range (limit) for the values of the optimal tilt angle. Elsayed's correlation for finding the monthly average tilt angle of surfaces facing south can be expressed as:

$$\Sigma_{opt} = \left(6 - 4.8K_T + 0.86K_T^{0.27}L + 0.0021L^2\right) + \left(31K_T^{0.37} + 0.094K_T^{0.49}L + 0.00063K_T^{-0.17}L^2\right)\cos\left(360\frac{n' + 11.5}{360}\right) \quad \text{Equation 3-70}$$

where K_T is the monthly average clearness index and n', proposed by Klein (1977), is a specific day in each month that could represent the main characteristic of that month. The monthly clearness index K_T in Baghdad is illustrated in Figure 3-17 (Al-Riahi & Al-Kayssi, 1998).

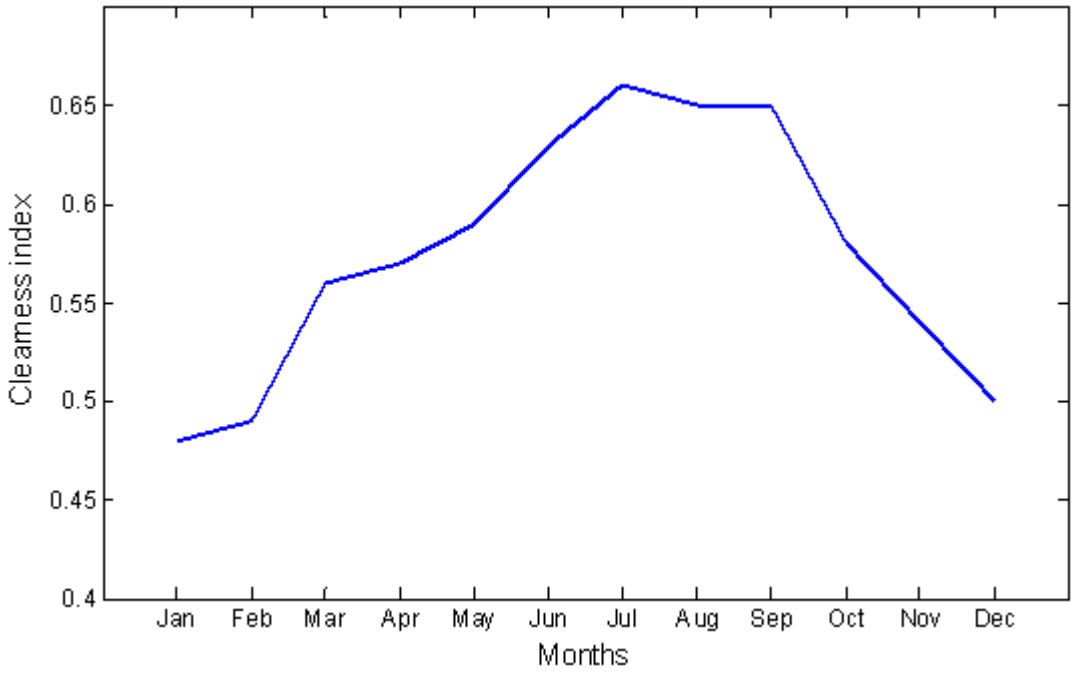

Figure 3-17 Monthly average clearness index K_T in Baghdad.

Elsayed (1989) also suggested an equation to estimate the yearly average optimal tilt angle in terms of monthly average of both the clearance index and the global solar irradiance I_G, as indicated below:

$$\Sigma_{opt} yearly = \frac{Sum\ \left(\Sigma_{opt} I_g\right)}{Sum\ \left(I_G\right)} \qquad \text{Equation 3-71}$$

Figure 3-18 shows the observed monthly average global solar irradiance in Baghdad, Iraq (AL-Salihi, Kadum & Mohammed, 2010).

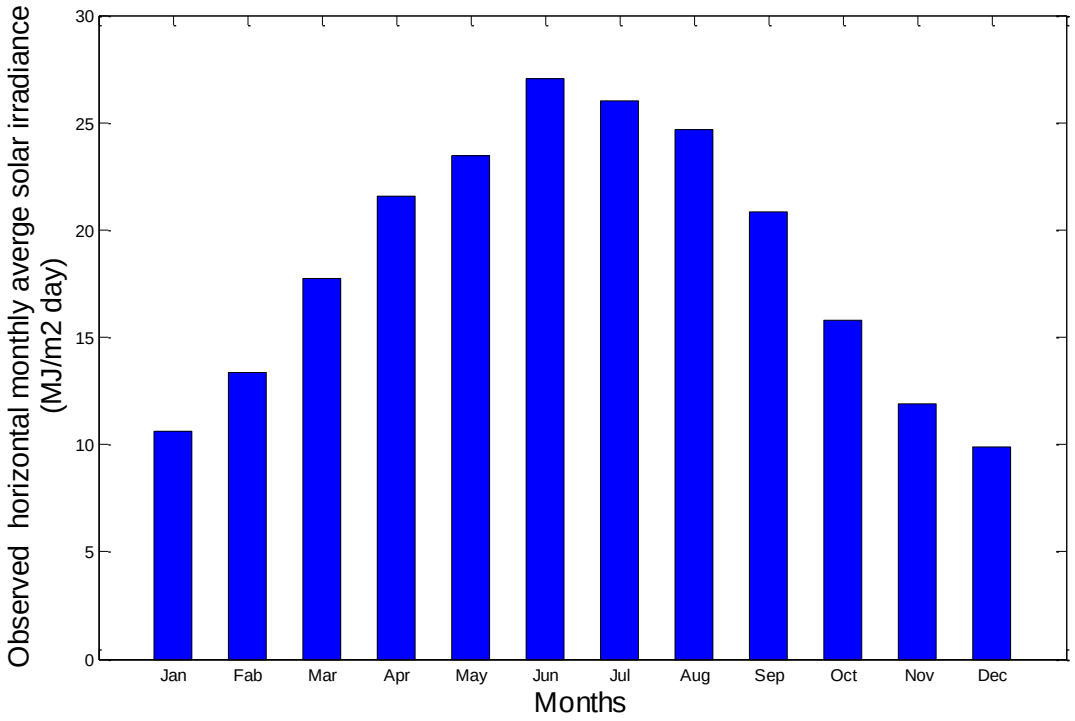

Figure 3-18 The observed monthly average global solar irradiance in Baghdad, Iraq.

3.3.4.3 Optimal tilt angle based on TRNSYS software

TRNSYS version 17.1 software was used to evaluate the results of the proposed model, where the monthly average daily useful energy gain from a solar collector is used as an indication for the assessment of the results through modelling a flat solar collector (TRNSYS software will be explained in the next chapter). A daily operation schedule for the collector was assumed from sunrise to sunset, and the Typical Meteorological Year 2 (TMY2) data file of Baghdad; available with the TRNSYS program package, was used. Several studies had used TRNSYS directly to find the optimum tilt angle; such as Shariah et al. (2002), which used a TRNSYS model for a thermos-syphon system to find the yearly average optimal tilt angle for two cities in Jordon, or indirectly to obtain the optimum design variables, including the optimum tilt of the collector, for solar powered systems, such as Al-Alili et al. (2010) and Hang et al. (2011).

In this method, the tilt angle was varied from 0° to 90° in steps of 1° and the optimal tilt angle (monthly or yearly average) was identified when the maximum useful gain was reached.

3.3.5 Results and Discussion

It should be noted that MATLAB (2012) source codes were written to describe the proposed method, ASHRAE clear sky model and Elsayed's correlation. Figures 3-19 & 3-20 are samples of MATLAB results; Figure 3-19 represents the optimal angles for the January using ASHRAE clear sky model, and Figure 3-20 represents the yearly average of the optimal angle using ASHRAE clear sky model. The results of the proposed method, ASHRAE clear sky model, Elsayed's correlation and TRNSYS program were tabulated in Table 3-15.

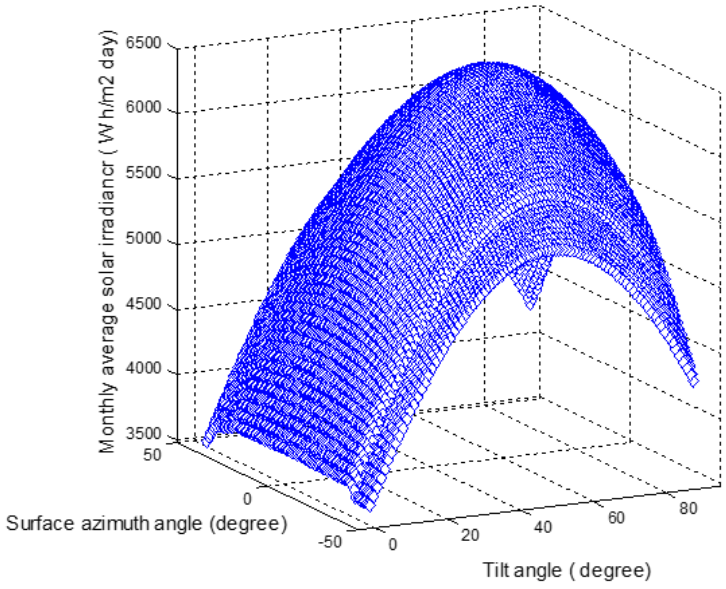

Figure 3-19 The variation of monthly average solar irradiance with variation of both surface azimuth and tilt angles for January.

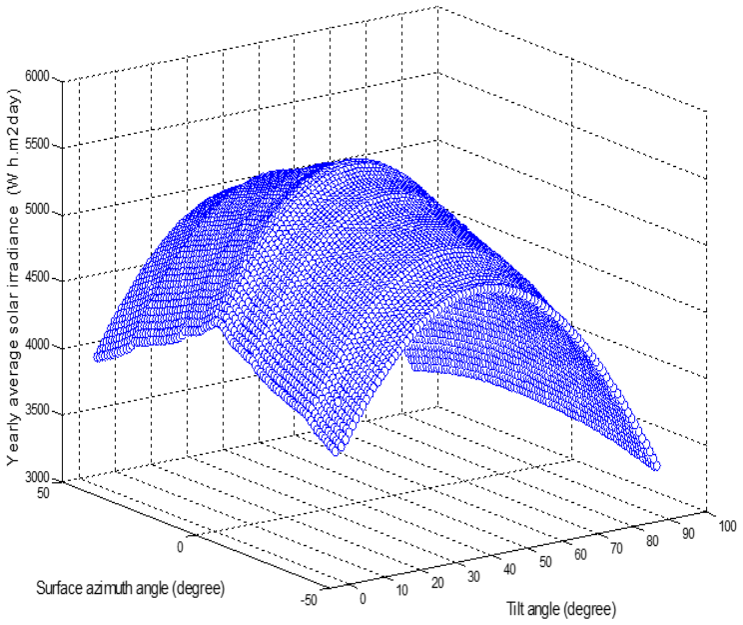

Figure 3-20 The variation of yearly average solar irradiance with variation of both surface azimuth and tilt angles.

Table 3-15 Optimal tilt angles $\sum_{opt}$ obtained by several models for Baghdad.

Tilt angle $\sum_{opt}$ °	**Model**	**Jan**	**Feb**	**Mar**	**Apr**	**May**	**Jun**	**Jul**	**Aug**	**Sep**	**Oct**	**Nov**	**Dec**	**Yearly**
	ASHRAE model	58	50	40	31	25	23	25	29	37	47	55	59	37
	The proposed model	-	-	37	21	10	5	7	18	32	43	-	-	-
	TRNSYS program	57	49	36	21	9	4	6	16	30	44	55	58	35
	Elsayed correlation	55	46	33	18	6	1	3	14	29	43	54	58	24
	Latitude angle	-	-	-	-	-	-	-	-	-	-	-	-	33.3

It was found that the proposed model was in good agreement with the TRNSYS results and the maximum angle difference did not exceed 2°. Which was within the upper (ASHRAE clear sky model) and lower (Elsayed's correlation) limits of the optimal tilt

angles. Consequently, it can be claimed with confidence that the proposed methodology is suitable for modelling the solar irradiance flux on a tilted surface in Baghdad, Iraq.

In order to assess the results, the monthly average daily useful energy gain from TRNSYS model of the solar collector was calculated at the optimal tilt angles obtained from each method, as well as when the tilt angle is equal to the latitude angle of Baghdad: 33.3°, see Figure 3-21. As mentioned earlier, latitude angle is used commonly as a rule of thumb in collector installation. Therefore, the percentage change of monthly average daily useful energy gain for each method compared to monthly average daily useful energy gain when the solar collector tilts at latitude angle, was calculated and drawn in Figure 3-22. The negative sign means a reduction in the monthly average daily useful energy gain, while the positive sign means the opposite.

With regard to the yearly average tilt angle, the monthly average daily useful energy gain was insignificantly changed when all yearly average tilt angles were obtained from all methods. That means that the best choice for yearly average tilt angle in Baghdad is equal to the latitude angle.

With regard to monthly average tilt angle, the monthly average daily useful energy gain was increased by an average of 6.1% when the tilt angles were equal to the optimal tilt angles obtained from ASHRAE clear sky model. The monthly average daily useful energy gain was increased by an average of 7.6% when the tilt angles were equal the optimal tilt angles obtained from Elsayed's correlation. The monthly average daily useful energy gain was increased by an average of 8.1% when the tilt angles were equal to the optimal tilt angle obtained by using TRNSYS model. Consequently, through the results, all methods used to obtain the monthly average optimal tilt angles led to a noticeable increase in the

amount of useful energy, gaining nearly 9%, which is similar to the result of Benghanem (2011).

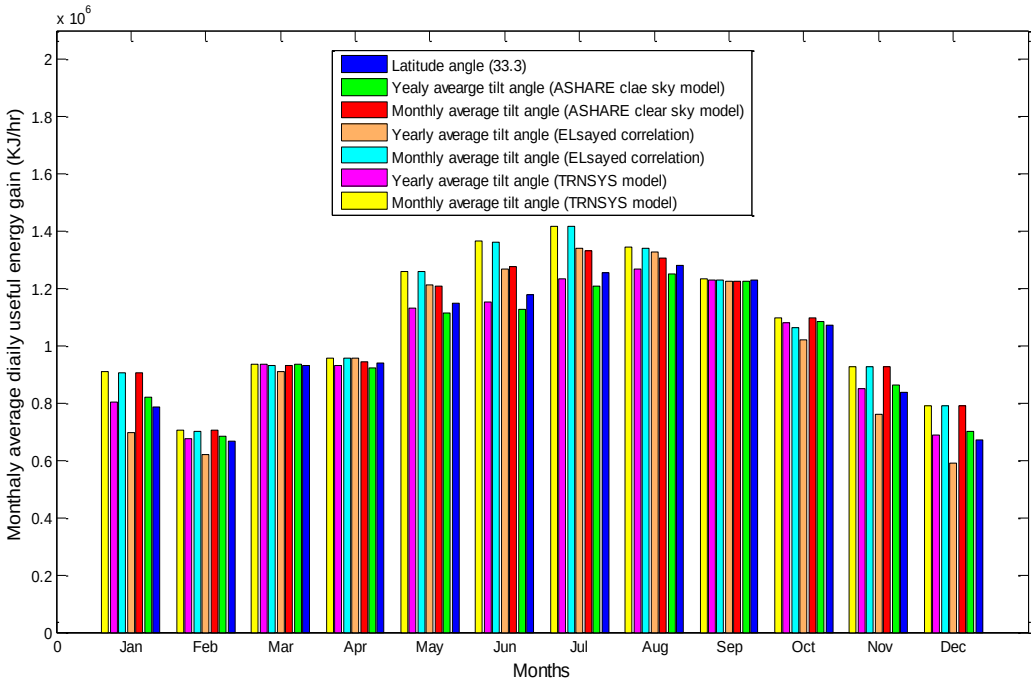

Figure 3-21 Monthly average daily useful energy gain from the solar collector at different tilt angles.

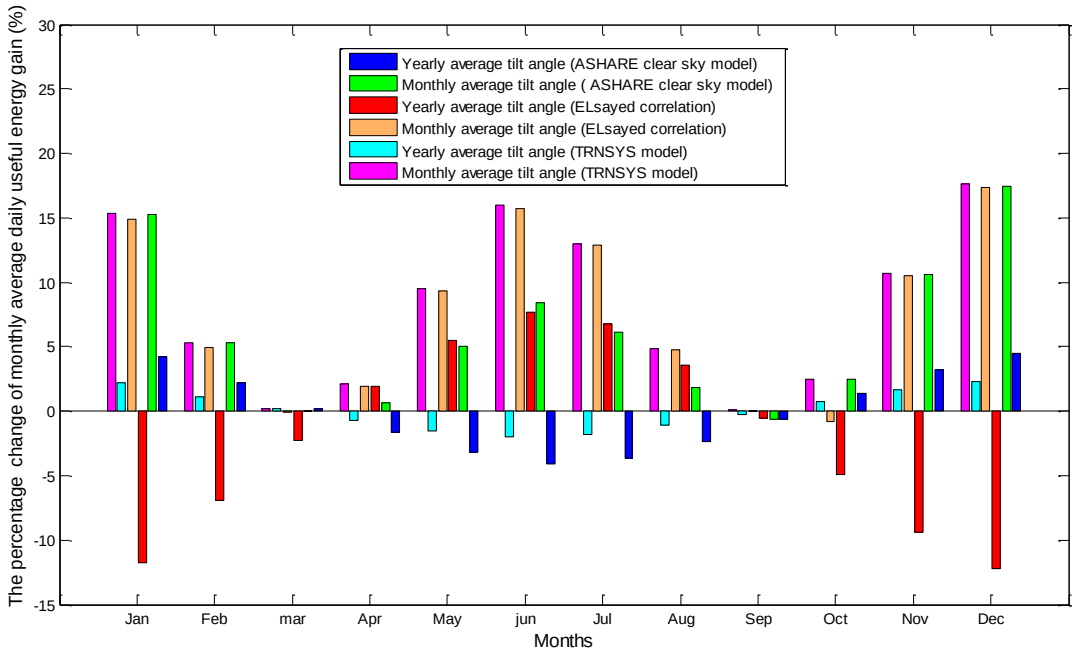

Figure 3-22 Percentage change of monthly average daily useful energy gain in comparison to monthly average daily useful energy gain when the solar collector inclines at latitude angle of Baghdad.

3.3.6 Conclusion

This study addresses how to choose the tilt angle of the solar collectors used in Baghdad, Iraq, and makes recommendations for optimal tilt angles that will lead to an increase in collected solar energy. First, an investigation was made to find the most accurate and suitable model to describe the characteristics of solar irradiance on a tilted surface. Second, a method to obtain the solar irradiance on a tilted surface in Baghdad was proposed. Next, the optimal tilt angles for collectors were calculated using the proposed method for eight months (from March to October) by searching for the highest values of the monthly average daily global solar irradiance on a tilted surface. Three methods; the ASHRAE 2009 clear sky model, Elsayed's correlation and TRNSYS software, were used to find the optimal tilt angles in order to verify the results of the proposed method. From the results, it can be claimed with confidence that the proposed method is suitable for modelling the solar irradiance flux on a tilted surface in Baghdad, Iraq. Additionally, adopting these monthly average optimal tilt angles led to a noticeable increase in the amount of useful solar energy gaining nearly 9%, representing a possibility of obtaining more energy without harming the environment, through a simple change in the tilt angle of solar panels and at no greater cost than the cost of this change. In addition, this report revealed that the best choice for yearly average tilt angle in Baghdad is equal to the latitude angle. The outcomes of the study can be considered as a guide in the designing of solar powered systems for Baghdad's climate, which in turn could increase the exploitation of solar energy and hopefully accelerate Iraq's transformation to an eco-friendly country.

Chapter Four

Optimisation of a solar cooling absorption system based on exergic, economic and environmental aspects

This chapter presents an exergic, economic and environmental analysis of a solar cooling absorption system in Baghdad, Iraq that is used for a domestic application. A multi-objective optimisation using genetic algorithm technique was used to obtain optimal potential designs. A decision-making tool called TOPSIS was then implemented to select the most suitable design. Furthermore, the performances of the individual components of the selected design were analysed comprehensively. A cold thermal energy storage unit with the solar absorption cooling system was suggested in order to store the cold energy produced by the system at times when the solar energy is available (at daytime) and use (discharge) it at times when there is no solar energy available (at night).

4.1 System description

Figure 4-1 illustrates the configuration of the solar cooling system used in this report. The solar absorption cooling system produces a cooling effect by using solar energy, where the solar collectors collect and transfer the solar thermal energy to the system. The system includes solar collector (evacuates tube collectors are used here), hot storage tank, auxiliary heater, absorption chiller, cooling tower and pumps. The absorption chiller is the core of the system and the solar absorption cooling system can be divided into four loops (subsystems); solar loop, heating loop, cooling tower loop, and chilled loop.

- In the first loop (solar loop) the evacuated tube solar collectors absorb the solar radiation and convert it into thermal energy that is used to heat up the water (point

1) coming from the hot storage tank by pump 1, the hot water (point 2) is returned back to the top of the hot storage tank.

- In the second loop (heat loop), the hot water (point 3) from the top of the tank passes through the auxiliary heater (used to boost the temperature of the fluid when it drops below the required temperature in the absorption chiller) to the absorption chiller (point 5), then the warm water (point 6) is pumped back from the chiller to the hot storage tank (point 8) by pump 2. The bypass (tempering valve and three-way valve) is used when the returned water (point 7) is warmer than the water in the top of the hot storage.
- In the third loop (cooling tower loop) the warm water from the chiller (point 9) is pumped by pump 3 to the cooling tower to cool down and then return to the chiller (point 11).
- In the fourth loop (chilled loop), pump 4 pumps the chilled water (point 12) from the chiller to the building that required the cold effects (point 13), and the water from the building is returned to the chiller again (point 14).

The controller C1 is the main controller that turns the whole system ON and OFF, which is based upon the needs of the building for cooling; the controller C2 activates the auxiliary heater when needed; and the controller C3 controls the flow of the fluid in the solar loop based on the availability of the solar irradiance.

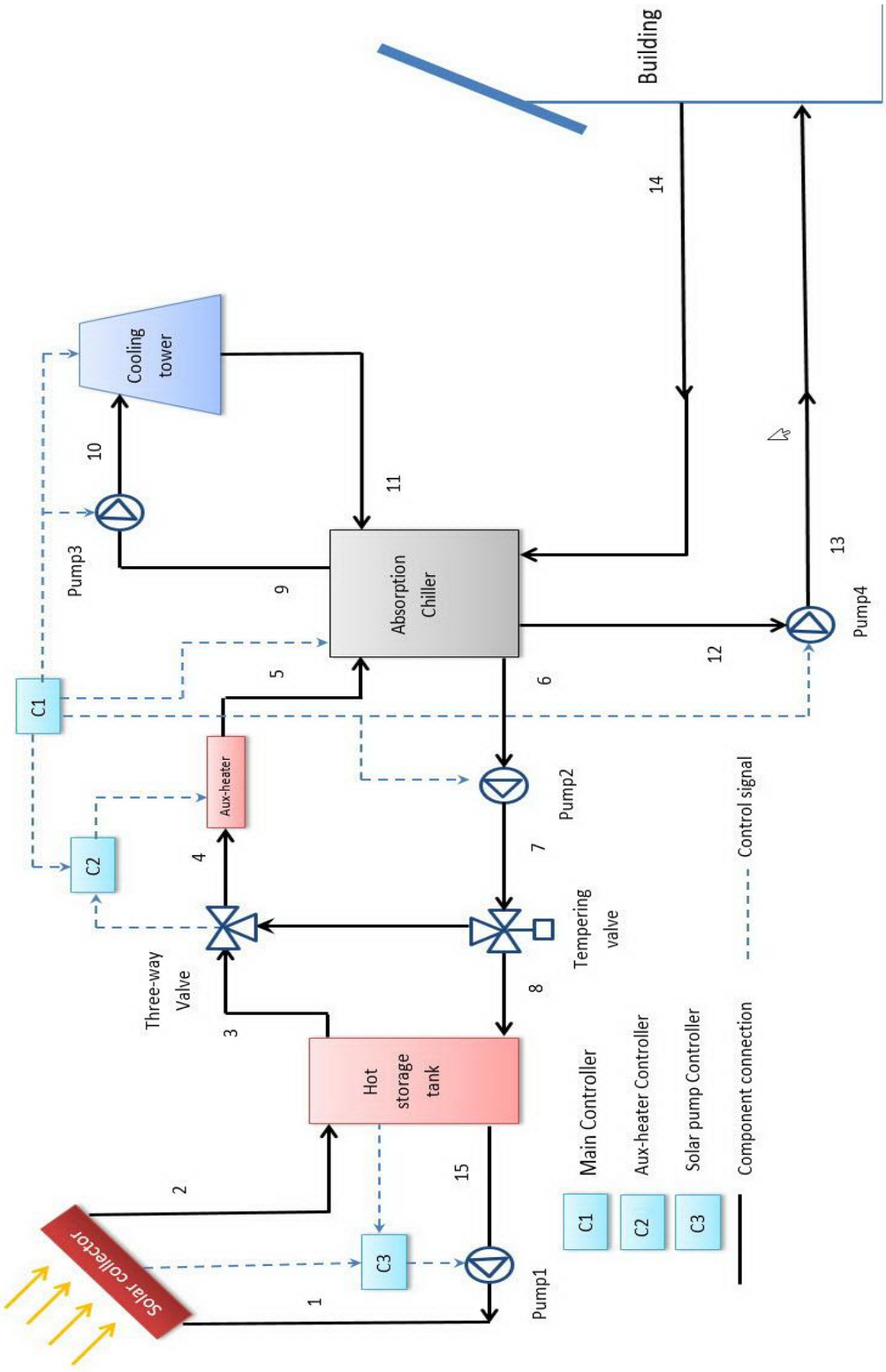

Figure 4-1 Schematic of the solar absorption cooling system used in this study.

4.2 System modelling

The solar absorption cooling system was modelled using TRNSYS software. TRNSYS is an extremely flexible graphically based software environment used to simulate the dynamic behaviour of transient systems; it is also used to solve the problems of modelling and analysing the complex energy systems (*TRNSYS*). The "simulation studio" is the main graphical interface of the programme; the system (to be modelled) is divided into individual components described as a "Units" (TRNSYS has an extensive library of verified components). Each unit in the TRNSYS is regarded as a "Type" (for example, Type 71 in Figure 4-2 represents an evacuated tube solar collector). The project can be built by connecting these types with each other as required. Individually, each "Type" has a "proforma" (black box) that defines the inputs, outputs, and parameters of the component. Thus, the main task after the use of TRNSYS has been reduced and confined to identifying and selecting the proper components for the parts of the system, in addition to understanding the mathematical description of the components and finding their required input parameters (which are often obtained from the manufacturer's data). Figure 4-2 shows a model of the solar absorption cooling system on the simulation studio of the TRNSYS. The coloured lines, such as red and yellow, are used to connect between the types (components) of the model (different colours are used to distinguish between the loops of the system). Solar loop components are connected by the yellow line, hot loop is connected by red lines, cooling tower loop components are connected by dark blue, and the light blue is used to connect the components of the chilled loop. The black, brown and orange lines are used for components such as printer, plotter, equation and text reader. The green lines are used for the controlling. The descriptions and the mathematical equations of the main components of the systems are presented briefly in the following subsections

(mostly based on the TRNSYS documentation (Klein *et al.*, 2012), where more details can be found):

4.2.1 Solar collector

Collectors can be defined as a special type of heat exchange that converts the solar radiation to useful thermal energy. In this report an evacuated tube collector is used, Type 71 represents heat pipe evacuated tube collector in the TRNSYS library. The thermal efficiency of the collector can be written as:

$$\eta = a_o + a_1 \frac{\Delta T}{I_T} - a_2 \frac{(\Delta T)^2}{I_T} \qquad \text{Equation 4-1}$$

where: a_o is the optical efficiency, a_1 is the first order coefficient, a_2 is the second order coefficient, ΔT is temperature difference between the inlet temperature of the collector and the ambient temperature and I_T is total irradiance of solar radiation. Type 71 needs a text file that includes a list of data of longitudinal and transverse incidence angle modifiers (IAM); this information can be obtained from the manufacturer.

4.2.2 Hot storage tank

Due to the intermittent nature of the solar energy, hot thermal energy storage plays a vital role in decreasing and eliminating the non-uniform heat intensity that is supplied to the chiller. Moreover, it is essential to make the system operate continuously. Type 4a in the library of the TRNSYS is used to model the hot stratified storage tank; this type consists of N nodes (sections) of full-mixed and equal volumes. Each section "interacts thermally" with the sections above and below by the fluid movement. Equation 4-2 shows the energy balance in node *i* (Shirazi *et al.*, 2016b):

$$M_i Cp \frac{dT_i}{dt} = \dot{m}_{Source}\, Cp\left(T_{i-1} - T_i\right) - \dot{m}_{Load}\, Cp\left(T_{i+1} - T_i\right) - UA_i\left(T_i - T_o\right) \qquad \text{Equation 4-2}$$

where: M_i is mass of the fluid in the node, Cp is the specific heat of the fluid, $\dot{m}_{Source}$ and $\dot{m}_{Load}$ are the mass flow rate from the heat source and the load sides, U is the overall heat losses of the tank to the environment, A_i is the heat transfer surface area, T_i is the temperature of the node, and the ambient temperature is T_o.

4.2.3 Absorption chiller

In TRNSYS, Type 107 is used to model the hot water fired absorption chiller; this type uses a catalogue data lookup approach to predict the performance of the chiller. The data file (text file) contains values of normalised fraction of full load capacity and fraction of design energy input for various values of fraction of design load, chilled water set point temperature, entering temperature of the hot water and entering cooling water temperature; these data can be obtained from the manufacturer. Type 107 first determines the amount of energy that must be removed from the chilled water stream in order to bring it from its entering temperature to the set point temperature by Equation 4-3. After obtaining the energy removed from the chilled water, the fraction of design load can be calculated by dividing the required energy removal by the chiller's capacity, as shown in Equation 4-4.

$$Q_{remove} = \dot{m}_{chw}\, cp_{chw}\left(T_{chw,in} - T_{chw,set}\right) \qquad \text{Equation 4-3}$$

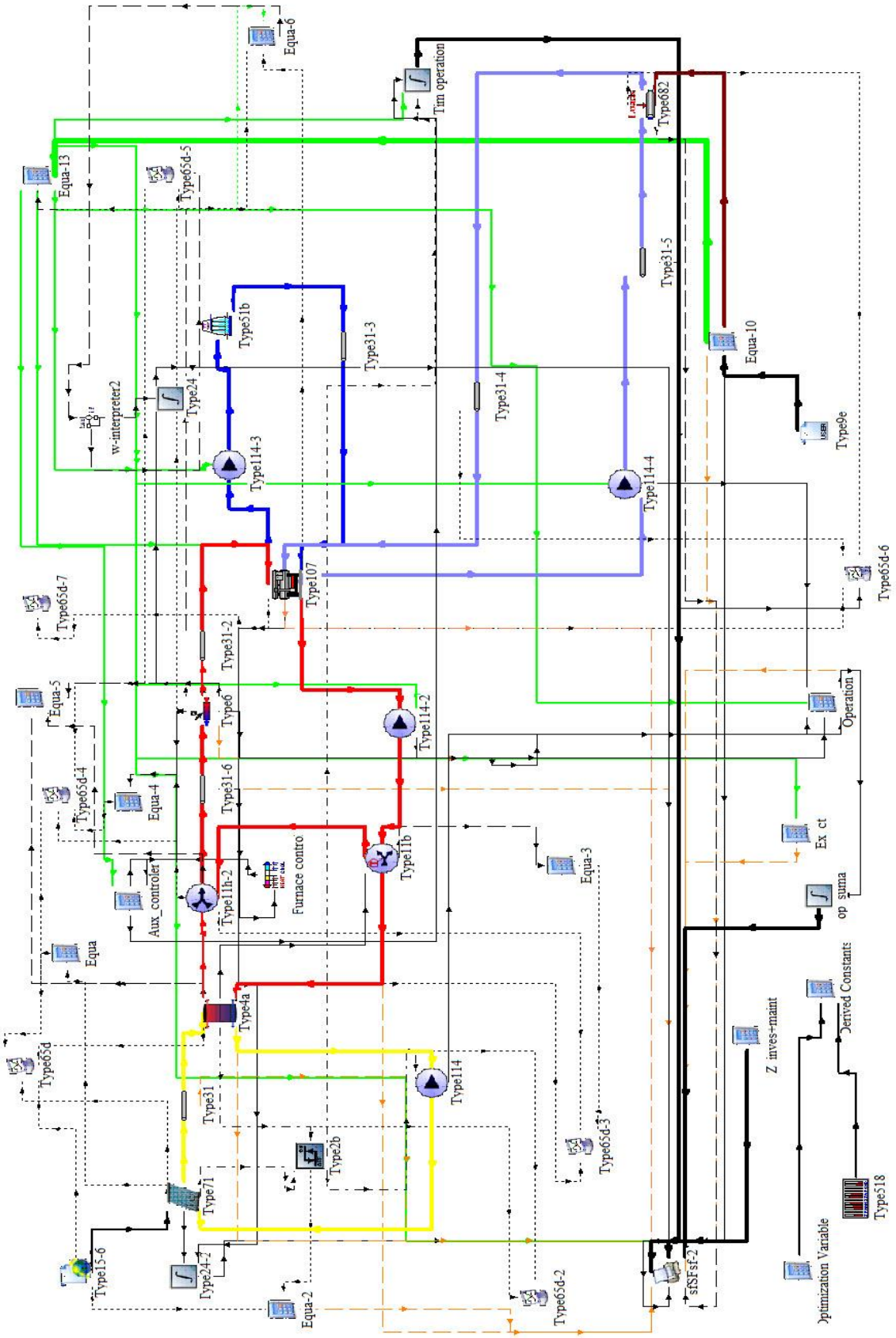

Figure 4-2 TRNSYS Scheme of the solar absorption cooling system.

$$f_{DesignLoad} = \frac{\dot{Q}_{remove}}{Capacity_{Rated}}$$ Equation 4-4

where: $\dot{m}_{chw}$ is the mass flow rate of the chilled water stream, cp_{chw} is the specific heat of the chilled water stream, $T_{chw,in}, T_{chw,set}$ is the chilled water inlet temperature and chilled water stream set point, $\dot{Q}_{removed}$ (or $\dot{Q}_{chw}$) is the amount of energy that must be removed from the chilled water stream, $f_{DesignLoad}$ is the fraction of design load, and $Capacity_{Rated}$ is the rated cooling capacity of the chiller.

The capacity of the chiller $Capacity$ at any given time can be calculated by Equation 4-5:

$$Capacity = f_{FullLoadCapacity} * f_{No\min alCapacity} Capacity_{Rated}$$ Equation 4-5

Where: $f_{FullLoadCapacity}$ is the fraction of the chiller's full load capacity during the operation under current conditions, $f_{No\min alCapacity}$ is the fraction of the chiller's nominal capacity during the operation under current conditions.

The energy that is delivered to the chiller by the hot water stream Q_{hw} can be calculated by using Equation 4-6:

$$Q_{hw} = \frac{Capacity_{Rated}}{COP_{Rated}} f_{DesignEnergyInput}$$ Equation 4-6

where: $f_{DesignEnergyInput}$ is the fraction of design energy Input currently required by the chiller and COP_{Rated} is the chiller's rated Coefficient of Performance.

The hot water outlet stream temperature $T_{hw,out}$ can be estimated by Equation 4-7

$$T_{hw,out} = T_{hw,in} - \frac{\dot{Q}_{hw}}{\dot{m}_{hw}\, cp_{hw}}$$ Equation 4-7

where: $T_{hw,in}$ is the inlet temperature of the hot water, $\dot{m}_{hw}$ is the mass flow rate of the hot water stream and cp_{hw} is the specific heat of the hot water stream.

The chilled water outlet temperature is then calculated from:

$$T_{chw,out} = T_{hw,in} - \frac{\text{minimum } of\left(\dot{Q}_{remove}, Capacity\right)}{\dot{m}_{chw}\, cp_{chw}}$$ Equation 4-8

The amount of energy rejection to the cooling water stream $\dot{Q}_{cw}$ is estimated by Equation 4-9:

$$\dot{Q}_{cw} = \dot{Q}_{chw} + \dot{Q}_{hw} + \dot{Q}_{paras}$$ Equation 4-9

Where $\dot{Q}_{paras}$ is the parasitic energy of the absorption chiller, due to the pumps and controls.

Moreover, the exiting cooling water stream temperature $T_{cw,out}$ can be calculated by using Equation 4-10:

$$T_{cw,out} = T_{cw,in} + \frac{\dot{Q}_{cw}}{\dot{m}_{cw}\, cp_{cw}}$$ Equation 4-10

$\dot{m}_{cw}$ is the mass flow rate of the cold water stream, cp_{cw} is the specific heat of the cold water stream and $T_{cw,in}$ is the cold water inlet temperature and chilled water stream set point

Finally, the coefficient of performance of the chiller COP is calculated by Equation 4-11:

$$COP = \frac{\dot{Q}_{chw}}{\dot{Q}_{paras} + \dot{Q}_{hw}} \qquad \text{Equation 4-11}$$

4.2.4 Auxiliary heater

When the solar radiation is insufficient and the hot storage tank is exhausted, the auxiliary heater is essential to maintain the system fluid at a desired temperature level. In TRNSYS, Type 6 represents the auxiliary. The thermal energy $\dot{Q}_{aux\ heater}$ that is provided by the auxiliary heater to the system fluid can be estimated by Equation 4-12:

$$\dot{Q}_{aux\ heater} = \frac{\dot{m}\,Cp\left(T_{set} - T_{in}\right) + UA_{aux\ heater}\left(T_{aux\ heater\ avg} - T_{o}\right)}{\eta_{aux\ heater}} \qquad \text{Equation 4-12}$$

where: T_{set} is the set temperature of heater internal thermostat, T_{in} here is the fluid inlet temperature, $UA_{aux\ heater}$ is the overall loss coefficient between the heater and its surroundings during operation and $\eta_{aux\ heater}$ is the efficiency of the auxiliary heater, and the average temperature $T_{aux\ heater\ avg}$ can be calculated by Equation 4-13:

$$T_{aux\ heater\ avg} = \frac{\left(T_{set} + T_{in}\right)}{2} \qquad \text{Equation 4-13}$$

4.2.5 Cooling Tower

A heat-reject subsystem is connected to the absorption chiller in order to cool down the condenser and the absorber of the chiller. In this report, a counter flow wet cooling tower type is used to eject the energy from a warm working fluid that returns from the chiller to the ambient air. In TRNSYS, the counter flow forced-draft cooling tower is represented by

using Type 51b. The type 51b is based on the effectiveness-number of transfer units (NTU) method (ASHRAE, 2012).

$$NTU = c\left(\frac{\dot{m}_{air}}{\dot{m}_{water}}\right)^{(1+n)} \quad \text{Equation 4-14}$$

where: $\dot{m}_{air}$ & $\dot{m}_{water}$ are the mass flow rates of the air and the water, respectively, and the constants c & n are the mass transfer constant and the mass transfer exponent, respectively; their values can be obtained by curve fitting of the manufacturer's data.

4.3 System analysing

This section presents the thermo-economic-environmental analysis of a solar absorption cooling system.

4.3.1 Exergy analysis

Exergy can be defined as the maximum useful work of the system in a given state when reaches equilibrium with the environment. The total exergy $\dot{E}$ of any system consists of physical exergy $\dot{E}^{PH}$, potential exergy $\dot{E}^{PT}$, kinetic exergy $\dot{E}^{KN}$ and chemical exergy $\dot{E}^{CH}$.

$$\dot{E} = \dot{E}^{PH} + \dot{E}^{PT} - \dot{E}^{KN} + \dot{E}^{CH} \quad \text{Equation 4-15}$$

Since there is no chemical reaction occurring in the system, chemical exergy is not used in the exergy analysis; additionally, the potential and kinetic exergy can be ignored (Sanaye & Shirazi, 2013). The exergy balance equation for each component in the system can be written as:

$$\sum \dot{E}_{in} = \sum \dot{E}_{out} + \dot{E}_{D} \quad \text{Equation 4-16}$$

Or

$$\dot{E}_{heat} - \dot{E}_{work} + \dot{E}_{mass,i} - \dot{E}_{mass,o} = \dot{E}_D$$ Equation 4-17

where the exergy destruction or irreversibility $\dot{E}_D$ is the potential wasted work in each component, $\dot{E}_{heat}$ and $\dot{E}_{work}$ are the exergy of heat transfer and exergy of useful work, respectively.

Equation 4-17 can be simplified and written as:

$$\sum\left(1-\frac{T_o}{T_K}\right)\dot{Q}+\dot{W}+\sum\dot{m}_i * \Psi - \sum\dot{m}_o * \Psi = \dot{E}_D$$ Equation 4-18

where:

$\dot{m}_i, \dot{m}_o$ are inlet and outlet mass flow rate

$\dot{Q}$ is a rate of heat transfer at boundary temperature

$\dot{W}$ is the work rate

T_o is the ambient temperature

T_K is thermodynamic average temperature (boundary temperature).

Ψ' is the specific unit exergy, which can be expressed in Equation 4-19:

$$\Psi' = (h - h_o) - T_o(s - s_o)$$ Equation 4-19

where h is the enthalpy [$\Delta h = cp(T_2 - T_1)$] and s is the entropy [$\Delta s \cong cp \ln\frac{T_2}{T_1}$], cp is the specific heat capacity.

Substitution Equations Δh and Δs in equation 4-19, specific unit exergy equation can be rewritten as:

$$\Psi' = cpT_o\left(\frac{T}{T_o} - 1 - \ln\frac{T}{T_o}\right) \qquad \text{Equation 4-20}$$

By multiplying the specific unit exergy by the mass flow rate, the general form of the exergy destruction can be defined as:

$$\dot{E}_D = \dot{m}\,cpT_o\left(\frac{T}{T_o} - 1 - \ln\left(\frac{T}{T_o}\right)\right) \qquad \text{Equation 4-21}$$

The exegetic efficiency (second law efficiency) is an indicator of how much exergy is transformed into useful work, and can be calculated according to the following equation:

$$\varepsilon = \frac{\dot{E}_{out}}{\dot{E}_{in}} = 1 - \frac{\dot{E}_D}{\dot{E}_{in}} \qquad \text{Equation 4-22}$$

The exergy efficiency for the whole system is calculated according to the following equation:

$$\varepsilon_{total} = 1 - \frac{\dot{E}_{D,total}}{\dot{E}_{in}} \qquad \text{Equation 4-23}$$

where: $\dot{E}_{D,total}$ is the summation of the exergy destruction of the main component (can be found in Table 4-1), and $\dot{E}_{in}$ is the summation of the power consumption for all pumps in the system plus the exergy of solar radiation (exergy of the sun) plus the exergy of the auxiliary heater.

Table 4-1 The exergy destruction equations used for the solar absorption cooling system*.

Component	Exergy destruction equations
Solar collector	$\dot{E}_{D,coll} = \dot{m}_1(\Psi'_1 - \Psi'_2) + \dot{Q}_{solar}\left(1 - \frac{T_o}{T_{coll}}\right)$ $\dot{Q}_{solar}$ is solar radiation exergy, T_{coll} is thermodynamic average temperature of the collector
Hot storage tank	$\dot{E}_{D,HTES} = \left[\dot{m}_2(\Psi'_2 - \Psi'_{15}) + \dot{m}_3(\Psi'_8 - \Psi'_3)\right]$
Auxiliary heater	$\dot{E}_{D,aux} = \dot{m}_4(\Psi'_4 - \Psi'_5) + \dot{Q}_{aux\ heater}\left(1 - \frac{T_o}{T_{aux\ heater\ avg}}\right)$
Absorption chiller	$\dot{E}_{D,chill} = \left[\dot{m}_5(\Psi'_5 - \Psi'_6) + \dot{m}_9(\Psi'_{11} - \Psi'_9) + \dot{m}_{12}(\Psi'_{14} - \Psi'_{12})\right]$
Cooling tower	$\dot{E}_{D,ct} = \dot{m}_{10}(\Psi'_{10} - \Psi'_{11}) + \dot{W}_{fan,ct}$ $\dot{W}_{fan,ct}$ is the amount power consumption by the cooling tower fan.

*These equations are based on Figure 4-1 of the solar absorption cooling system.

4.3.2 Economic analysis

Total cost rate $C^{\bullet}_{total}$ function of the system is equal to the summation of the investment cost rate and operation cost rate, and it is defined by the following equation:

$$C^{\bullet}_{total} = \sum Z^{\bullet}_{K} + C^{\bullet}_{OP} \qquad \text{Equation 4-24}$$

Where $Z^{\bullet}_{k}$ is the investment and maintenance cost rate and $C^{\bullet}_{op}$ is the operational cost rate of the system.

4.3.2.1 Investment and maintenance cost rate

The investment and maintenance cost rate $Z^{\bullet}_{k}$ (hourly cost rate US$/hr) for the main components in the system (solar collector, absorption chiller, hot and cold storage tank, cooling tower and auxiliary heater) is estimated. The following Equation converts the capital cost in US$ to a cost per unit of time.

$$Z^{\bullet}_{k} = \frac{PW_k * crf * \Omega'}{N}$$ Equation 4-25

where: PW_k is the present worth of the component k, crf is a capital recovery factor, Ω' is the maintenance factor and N is the operation hours of the system.

The capital recovery factor is based on the interest rate *ir* and the system life span *n*, and it can be determined by the Equation below:

$$crf = \frac{ir(ir+1)^n}{(ir+1)^n - 1}$$ Equation 4-26

The present worth of the component *k* can be calculated by:

$$PW_k = C_k - sv\ (pwf)$$ Equation 4-27

where: C_k is the capital cost of the component *k*, Table 4-2 illustrates the initial cost of the main components of the system and pwf is the present worth factor, which is estimated by the following equation:

$$pwf = \frac{1}{(1+ir)^n}$$ Equation 4-27a

sv is the salvage value and is equal to:

$$sv = C_k\ \mu$$ Equation 4-27b

where: μ is the salvage value percentage.

Table 4-2 Initial cost of the main component in the system.

Components	Cost	Unit
Evacuated tube solar collector (Al-Alili *et al.*, 2012)	256.9	US$/m^2
Absorption chiller -YAZAKI WFC-SC5 (Kohlenbach & Jakob, 2014)	24641	US$
Cooling Tower (Al-Alili *et al.*, 2012)	67.6	US$/kW$_{th}$
Storage Tank (Al-Alili *et al.*, 2012)*	811.2	US$/m^3
Auxiliary heater (Tsoutsos *et al.*, 2010)	50	US$/kW$_{th}$
Pumps (Gebreslassie *et al.*, 2009)	$630(w)^{0.4}$	US$

*The initial cost of hot and cold storage tanks are assumed equal.

4.3.2.2 Operation cost rate

The operational cost of the system $C^{\bullet}_{op}$ is determined by multiplying the summation of the power consumption in all pumps and fans by the cost of the electricity C_{elec} (US$/kW.hr)

$$C^{\bullet}_{op} = \left(op_{aux} + \dot{W}_{pu1} + \dot{W}_{pu2} + \dot{W}_{pu3} + \dot{W}_{pu4} + \dot{W}_{fan,ct} \right) * C_{elec} \qquad \text{Equation 4-28}$$

where: op_{aux} is the required heating rate in the auxiliary heater, $\dot{W}_{pu1}$ is the amount of power consumption in pump 1, $\dot{W}_{pu2}$ is the amount of power consumption in pump 2, $\dot{W}_{pu3}$ is the amount power consumption in pump 3, $\dot{W}_{pu4}$ is the amount of power consumption in pump 4 and $\dot{W}_{fan,ct}$ is the amount power consumption by the cooling tower fan.

4.3.3 Environmental analysis

Environmental assessment has become vital in modelling thermal systems, due to global warming problems. Generally, carbon footprint (CO_2 emissions) is used to evaluate the

environmental impacts of the system (Hang *et al.*, 2013). The CO_2 emissions include indirect emissions embedded in upstream production of the system (the manufacturing stage) $CO_{2emission,manufactor}$, and direct emissions embedded in on-site emissions of the system (the operating stage) $CO_{2emission,operation}$. Therefore, the total annual CO_2 emission equation is:

$$CO_{2emission,total} = CO_{2emission,manufactor} + CO_{2emission,operation} \quad \text{Equation 4-29}$$

The carbon emission of the manufacturing stage is equal to the summation of emissions in the manufacturing stage for all components of the system divided by the system life span; the values of the carbon emissions of the manufacturing stage for each component can be found in Table 4-3.

Table 4-3 The carbon emissions of the manufacturing stage.

Component	CO_2 emissions	Unit
Absorption chiller (Single effect) (Hang, Qu & Zhao, 2011)	217.3	Kg/kW
Evacuated tube solar collector (Hang, Qu & Zhao, 2011)	101.39	Kg/m^2
Storage tank (Hang *et al.*, 2013)*	821.28	Kg/m^3
Auxiliary heater (Hang *et al.*, 2013)	38.9	Kg/kW
Cooling tower (Genchi, Kikegawa & Inaba, 2002)	4.418	Kg/kW
Pump (Hang, Qu & Zhao, 2011)	191.5	Kg/kW

*The carbon emissions of the manufacturing stage of hot and cold storage tanks are assumed equal.

The Equation of CO_2 emissions in the operation stage is equal to:

$$CO_{2emission,operation} = \left(op_{aux} + \dot{W}_{pu1} + \dot{W}_{pu2} + \dot{W}_{pu3} + \dot{W}_{pu4} + \dot{W}_{pu5} + \dot{W}_{fan,ct} \right) * \mu_{Co_2} \quad \text{Equation 4-30}$$

Where μ_{CO_2} is the CO_2 emission factor in Kg of CO_2/kW.hr .

4.3.4 Payback period

A preliminary judgment of economic feasibility can be providing by calculating a simple payback of the system. Payback period means how long it will take to get the investment cost back by saving energy. It is calculated by dividing the initial cost of the major components of the system by the cost saving per year.

$$SP = \frac{C_{inv}}{C_{Saving\ per\ year}} \qquad \text{Equation 4-31}$$

where: SP is the simple payback in years, C_{inv} is the investment cost and $C_{Saving\ per\ year}$ is the cost saving per a year.

4.4 Multi-objective optimisation and decision-making process

Optimisation process generally means finding the best feasible design for the system by minimising or maximising items (objects) such as efficiency, cost and energy. Instead of having a single unique solution by using a single-objective optimisation, many possible solutions can be produced from a multi-objective optimisation. Multi-objective solutions can be expressed by Pareto fronts. In general, system optimisation can be classified into classical and evolutionary methods. Genetic algorithm (GA) is one of the types of the evolutionary method. GA is based on Darwin's laws and it is able to solve multi-objective optimisation functions. In GA, the design parametric vector is called a chromosome; each chromosome is made of discrete units known as genes. Those genes that control the feature of the chromosome, can be modified. In each iteration, a new generation of candidate solutions (populations) will be generated, and the fitness of each solution is evaluated (the fitness is the values of the objective functions). The best fit solutions are selected, modified (crossover) and altered (mutated) to form the next generation. The optimisation process is

terminated when the objectives are satisfied or a certain number of generations is reached (the maximum limit of generations); more details about genetic algorithm optimisation can be found in Goldberg (1989) and Mitchell (1998). Figure 4-3 represents the flow chart of working principles for the genetic algorithm.

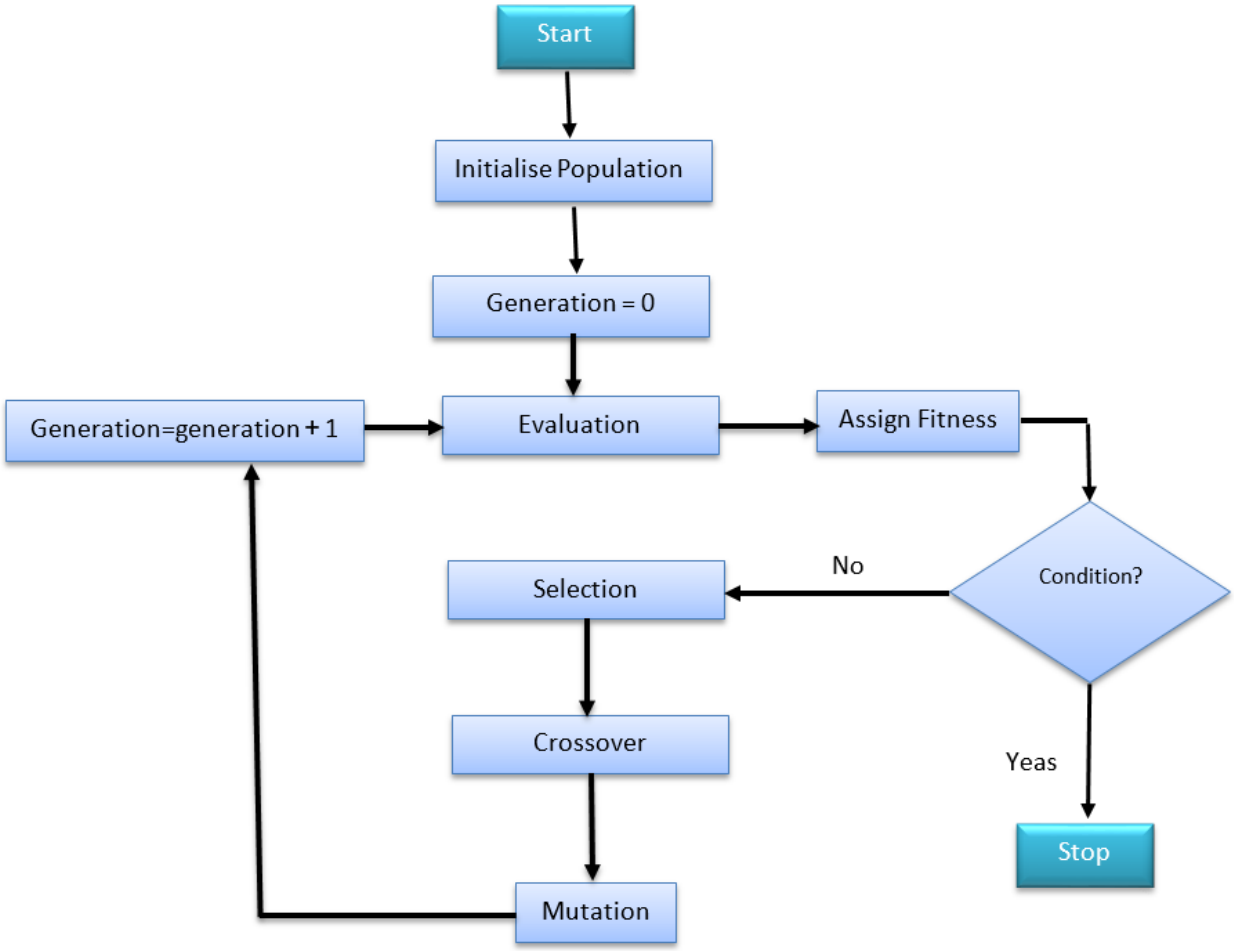

Figure 4-3 A flow chart of working principles of the genetic algorithm.

Mathematically, multi-objective optimisation can be charicaterised by maximising or minimising the vector function below, which has (m) objectives and (n) variables

$$F(x) = F(f_1(x), f_2(x), \ldots\ldots\ldots\ldots\ldots f_m(x))$$

Where $F(x)$ is the function of the variable $(x = x_1, x_2, x_2, \ldots\ldots, x_n)$

The objective function in the optimisation process might be maximising or minimising.

Minimise or maximise $(f_1(x), f_2(x), \ldots\ldots\ldots\ldots, f_m(x))$

Subject to $g_j(x) \geq 0 \qquad j = 1,2,\ldots\ldots\ldots\ldots, j$

$h_k(x) = 0 \qquad k = 1,2,\ldots\ldots\ldots\ldots, k$

$x_i(lower) \leq x_i \leq x_i(upper) \qquad i = 1,2,\ldots\ldots\ldots\ldots, n$

In the present study, three objective functions are used to optimise the system. These are Equation exergy efficiency (Equation 4-23), total cost rate (Equation 4-24) and total annual CO_2 emissions (Equation 4-29), which are used with equal importance (equal weight) in the optimisation approach; the optimisation process aims to maximise the exergy efficiency and minimise the cost rate and the total annual CO_2 emissions. In this study, the MATLAB genetic algorithm multi-objective tool (MathWorks, 2014) is used for optimisation and the default values of the tool are kept without any change.

4.4.1 Coupling TRNSYS with MATLAB

TRNSYS does not have a multi-objective optimisation tool, which led the implementation of the MATLAB genetic algorithm multi-objective tool. Therefore, a connection (coupling) between TRNSYS and MATLAB is needed. The coupling procedure can be simplified using the following steps: First, MATLAB reads TRNSYS input files and changes the design variables. Second, MATLAB calls TRNSYS to simulate the model along with the updated input files. Third, MATLAB reads the output files of the simulation and assesses the values of the objective functions. Finally, the previous three steps will be repeated till the criteria of the objective function are fulfilled. Figure 4-4 shows the flow diagram of coupling TRNSYS with MATLAB.

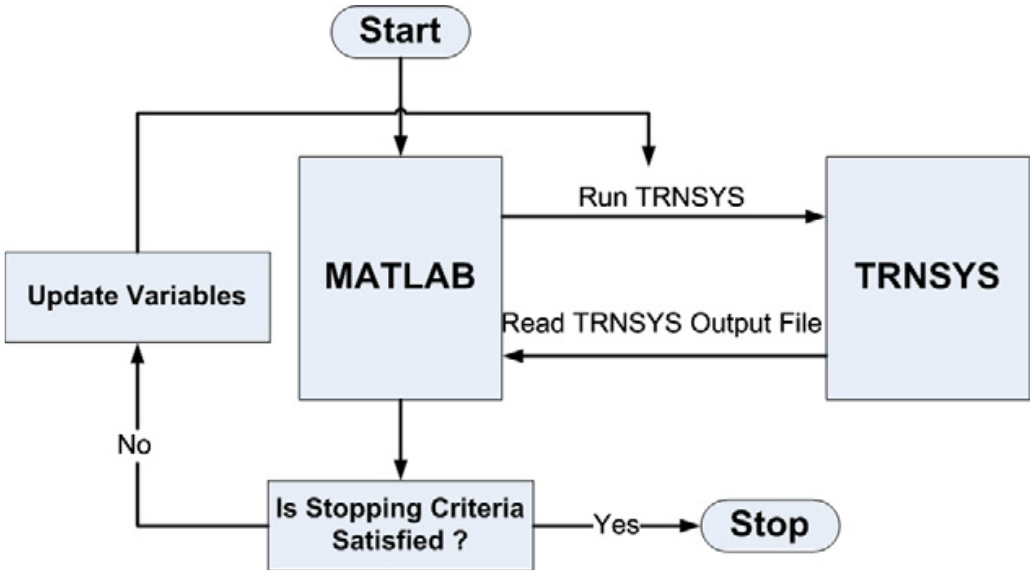

Figure 4-4 A flow diagram of coupling TRNSYS with MATLAB (Al-Alili *et al.*, 2010).

4.4.2 The decision-making process

As mentioned before, a multi-objective optimisation produces many solutions that can all satisfy the purpose of the optimisation mathematically. However, for practical reasons a single optimal solution should be selected. Therefore, a decision-making tool should be utilised. There are many approaches that can be used to find the optimum solution from Pareto front. TOPSIS (Technique for Order Performance by Similarity to Ideal Solution) is one of the decision making methods, which is characterised by simplicity to deal with multiple objectives problems. Ahmadi et al. (2013) have implemented several decision-making methods to find the optimal solution of a multi-objective optimisation process, and they found that TOPSIS "has superiority" over other approaches. Additionally, TOPSIS has been used frequently in many studies that addressed multi-objective optimisation, such as Shirazi et al. (2014) and Abdullah (2016). For the sake of presenting the TOPSIS approach in an easier way, the tool will be demonstrated in the results and discussion section.

4.5 Case study

The proposed methodology was applied to a residential house, and the Iraqi solar house was selected, shown in Figure 4-5, due to the availability of adequate information and data (Al-Karaghouli et al. (1989), and Joudi & Abdul-Ghafour (2003)). The Iraqi solar house is located in Baghdad, Iraq. The house has a solar absorption cooling system with 243m^2 flat plate solar collectors and 20m^3 of hot storage tank; it consists of four bedrooms, two bathrooms, a living and dining room, a kitchen and a machine room.

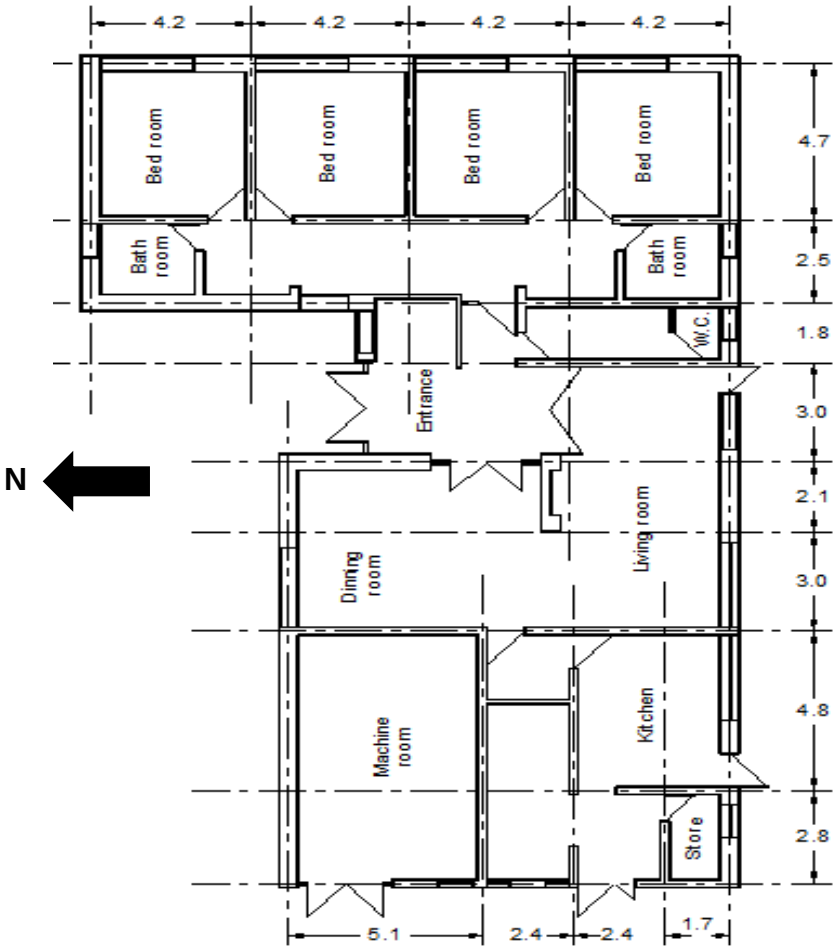

Figure 4-5 Iraqi Solar House.

Figure 4-6 shows the annual cooling load required by the house, the white space beneath the curve means that cooling effects are required 24 hours per day.

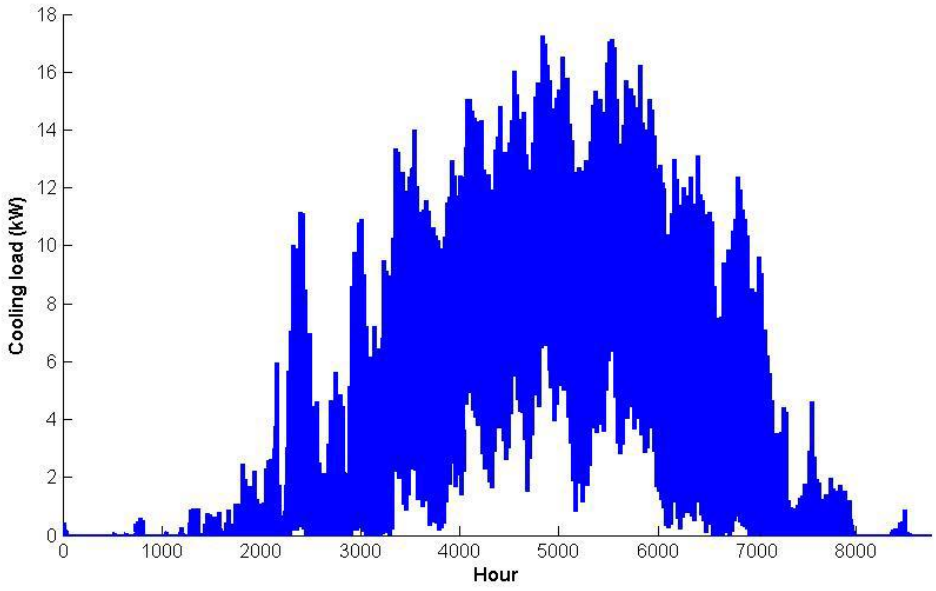

Figure 4-6 The annual cooling load of the Iraqi solar house.

Figure 4-7 shows the daily solar global radiation as well as the daily temperature in Baghdad (Figure 4-7 is based on the Typical Meteorological Year 2 (TMY2) data file of Baghdad, available with the TRNSYS program package).

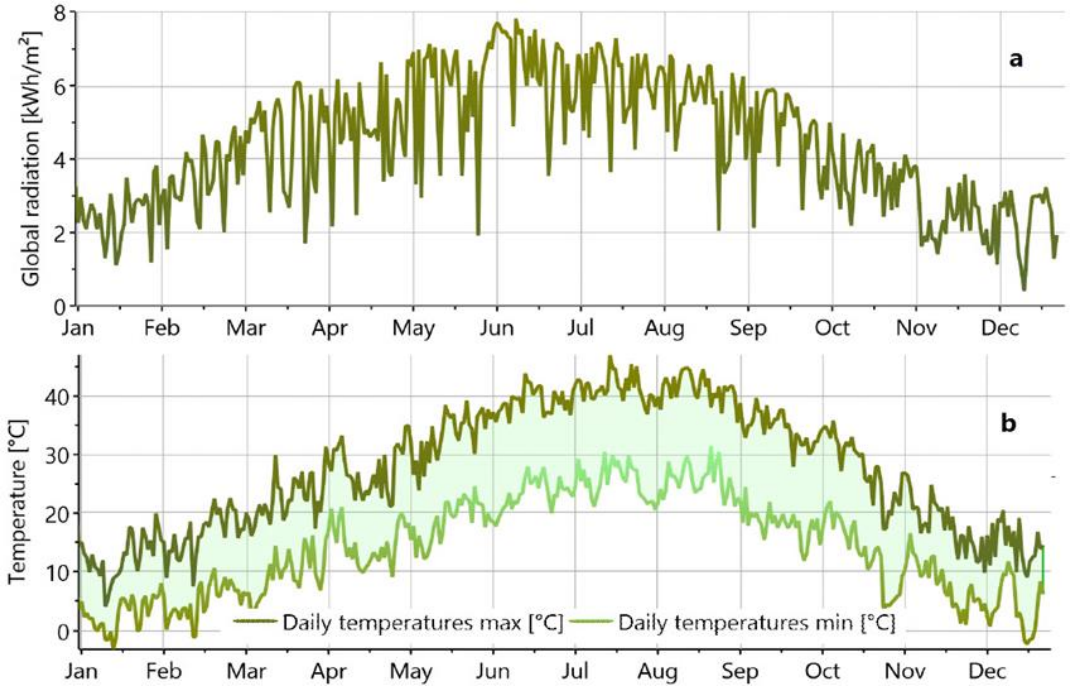

Figure 4-7 shows a) daily solar global radiation and b) daily temperature in Baghdad.

The highest daily globe solar irradiance is nearly 8kWh/m^2 and the highest daily temperature exceeds 45°C (sometimes the temperatures exceed 50°C). There are seven months with a need for cooling effects (April to October). The average daily sunshine hours within these months are 10hrs from an average daylight of 13hrs per day (*ClimaTemps: Baghdad*).

As can be seen from Figure 4-6, a 5 Ton Refrigeration (17.6 $kW_{refrigeration}$) chiller is required to provide the cooling demand in the house; to meet this the YAZAKI WFC-SC5 absorption chiller was selected. Modelling of YAZAKI WFC-SC5 absorption chiller by the TRNSYS component of type 107 has been validated in Martínez et al. (2012). Table 4-3 lists the general Specification of the YAZAKI WFC-SC5 absorption chiller.

Table 4-3 Specifications of the YAZAKI WFC-SC5 absorption chiller (Yazaki-airconditioning, 2007).

Cooling Capacity			17.6	kW
Chilled water	Chilled Water Temperature	Inlet	12.5	°C
		Outlet	7.0	°C
	Rated Water Flow		0.77	L/sec
			2.77	m^3/hr
Cooling Water	Heat Rejection		42.7	kW
	Cooling Water Temperature	Inlet	31.0	°C
		Outlet	35.0	°C
	Rated Water Flow		2.55	l/sec
			9.18	m^3/hr
Heat Medium	Heat Input		25.1	kW
	Heat Medium Temperature	Inlet	88	°C
		Outlet	83	°C
		Inlet Limit	70-95	°C
	Rated Water Flow		1.2	l/sec
			4.32	m^3/hr

Additionally, an evacuated tube solar collector made by APRICUS (*APRICUS*) was selected to provide the solar energy to the absorption chiller. Modelling of APRICUS evacuated tube collectors by the TRNSYS component of type 71 has been validated in Shirazi et al. (2016a). The characteristics of the solar collector are given in Table 4-4.

Table 4-4 Characteristics of the APRICUS evacuated tube solar collector (Davis, 2014).

Name	Value
Optical efficiency (a_0)	71%
First order IAM* (a_1)	1.737 W/m².K
Second order IAM* (a_2)	0.008 W/m².K

*Incident angle modifier

As mentioned before, since a similar absorption chiller was used in Martínez et al. (2012), a similar cooling tower was selected here. The cooling tower brand is TEVA TVA008, and the values of the mass transfer constant and mass transfer exponent are 0.5 and -0.856 (Martínez, 2014), respectively.

TRNSYS simulation period was seven months from the first of April (hour 2160) to the end of October (hour 7296), with a 1-minute simulation time step. Typical meteorological year 2 data file was used as the weather data for Baghdad.

4.6 Design variables and input parameters

Generally, there are the key variables that are frequently used in most of the research that deals with the optimisation process of the solar absorption cooling system, such as Hang et al. (2013). These design parameters are:

- Area of the solar collectors A_r
- Tilt or inclination angle of the solar collectors from the horizontal surface (usually the solar collectors in the northern hemisphere face south).
- Volume of the hot storage tank V

This study assumes that the tilt angle of the solar collectors can be changed on a monthly basis, as in Arsalis & Alexandrou (2015). From Chapter Three, monthly average optimal tilt angles for solar collectors under Baghdad climate have been obtained, and these optimal tilt angles are listed in Table 4-5. In addition, the same work explains also that the best direction to install a solar collector in the northern hemisphere (as is the case of Baghdad) is south.

Table 4-5 Monthly average tilt angle for solar collectors in Baghdad, Iraq.

Month	Apr	May	Jun	Jul	Aug	Sept	Oct
Optimal tilt angle	21	10	5	7	18	32	43

Thus, only two key design parameters are considered in this report, and their ranges are listed in Table 4-6.

Table 4-6 Design parameters and their ranges.

Key Parameters	Ranges
Collector area A_r	45 -200 m^2
Hot storage tank volume V	0.5 - 20 m^3

In addition to the design variables, there were other input parameters required in the exergic, economic and environmental analyses. Table 4-7 lists all the inputs that have been used in this study.

Table 4-7 Input parameters used in the analysis.

Description	Value
Dead state temperature T_o	298.15K (25°C)
Maintenance factor Ω' (Kwak, Kim & Jeon, 2003)	1.06
Interest rate in IRAQ *ir* (*Trading Economics: Iraq Interest Rate*)	6%
System life span *n* (Hang *et al.*, 2013)	20year
Salvage value percentage μ (Caliskan, Dincer & Hepbasli, 2013)	20%
Electricity cost in Iraq C_{elec} (*Iraqi Electricity Ministry*)	0.18US$/kW.hr
CO_2 emission factor in Iraq μ_{CO_2} (Brander et al., 2011)	0.821Kg $_{CO2}$/kW.hr

4.7 Results and discussion

4.7.1 Multi-optimisation results

The final results achieved by GA optimization of the solar absorption cooling system are illustrated in Table 4-8. Additionally, Figure 4-8a shows the points of Pareto Front in three-dimensional coordinates. If maximisation of the exergy efficiency and minimisation of CO_2 emissions are the only goals concerned, the solution could be point A (optimum point) 58.89% and 28744.31Kg, respectively. But this point will lead to the highest total cost rate 5.18US$/hr. Alternatively, if the total cost is taken as the only desired aim, point B could be chosen as the optimum point, which has a total cost rate 3.41US$/hr. But this point will lead to the lowest exergy efficiency 48.15% and highest CO_2 emissions 49313.31Kg.

Table 4-8 Final results of the GA optimisation and the corresponding design parameters.

No.	Exergy efficiency %	Total cost rate (US$/hr)	Annual CO_2 emissions (kg)	Collector area (m^2)	Tank volume (m^3)
1	51.60	3.71	39872.89	83.71	5.37
2	49.48	3.47	48286.81	44.91	1.00
3	49.52	3.47	47872.52	44.86	2.21
4	56.97	5.12	29352.68	192.18	10.44
5	53.18	3.90	36854.88	102.44	8.32
6	49.68	3.61	42247.29	69.90	2.79
7	52.02	3.82	38394.53	92.35	6.49
8	48.15	3.41	49313.31	45.13	1.01
9	58.58	4.71	29932.25	179.28	19.84
10	50.15	3.53	43271.01	65.39	2.82
11	58.89	5.18	28744.31	188.70	19.90
12	57.26	4.86	29000.33	192.48	11.55
13	54.55	4.03	34042.42	120.92	9.48
14	56.23	4.19	32199.70	137.18	13.18
15	54.54	4.03	34136.66	120.33	9.33
16	57.36	4.31	31822.60	147.22	17.48
17	56.64	4.27	32944.28	139.75	16.75
18	48.96	3.51	46295.54	53.02	2.04

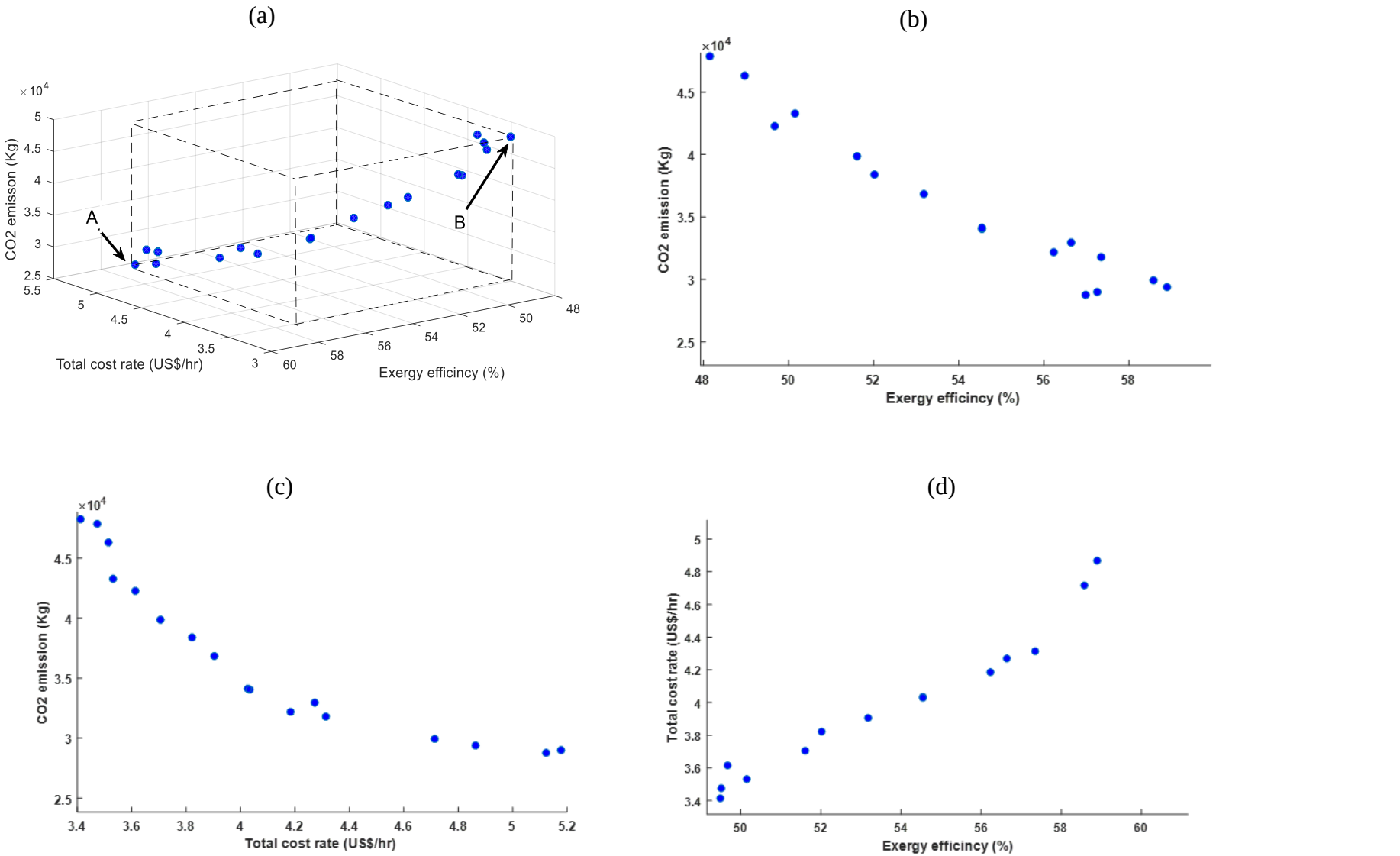

Figure 4-8 Pareto front of the model. a) 3D dimension of the Pareto front; b) the project in the exergy efficiency-CO2 emission; c) the project in total cost rate-CO_2 emission and d) the project in the exergy efficiency –total cost rate plane.

From Figures 4-8b and 4-8c, it can be seen that annual CO_2 emissions decrease as both exergy efficiency and total cost rate increase. Figure 4-8d shows a direct correlation between exergy efficiency and total cost rate, because both are inversely proportional to the amount of annual CO_2 emissions. Similar relationships between exergy efficiency, total cost rate and annual CO_2 emission have been found in Ahmadi et al. (2011), Shirazi et al. (2014) and Abdullah (2016).

4.7.2 TOPSIS results

Figure 4-9 shows the Pareto front of the optimisation plus the guidelines and the points that are used in TOPSIS.

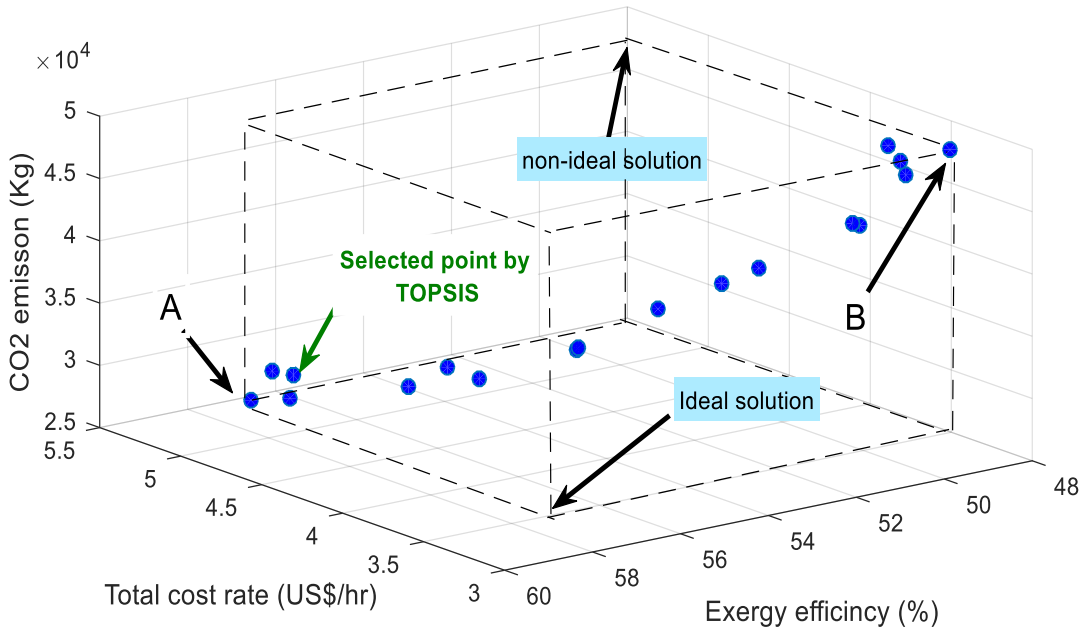

Figure 4-9 Pareto front of the optimisation plus the guidelines and the points that are used in TOPSIS.

In the TOPSIS method the first step is to obtain the weighted normalised decision matrix of the alternative optimal solutions. To doing that, the weight (importance) of each objective function has been assumed to be equal to 1/3; Table 4-9 shows the weight of each

objective and the optimisation results. Then, all objective functions must be non-dimensionalized; Equation 4-32 is used to obtain the normalised decision matrix.

$$r_{ij} = \frac{x_{ij}}{\sqrt{\sum_i x_{ij}^{\ 2}}} \qquad \text{Equation 4-32}$$

For $i = 1,\ldots\ldots\ldots, m$ and $j = 1,\ldots\ldots\ldots, n$

Table 4-9 Values of decision matrix.

		Exergy efficiency	Cost rate (US$/hr)	CO_2 emission
Weight		0.333333	0.333333	0.333333
Alternative solutions	A1	51.602	3.707	39872.892
	A2	49.485	3.472	48286.814
	A3	49.522	3.473	47872.522
	A4	56.974	5.124	29352.682
	A5	53.183	3.904	36854.880
	A6	49.678	3.613	42247.296
	A7	52.025	3.821	38394.532
	A8	48.150	3.412	49313.312
	A9	58.580	4.714	29932.248
	A10	50.149	3.531	43271.012
	A11	58.894	5.178	28744.314
	A12	57.260	4.865	29000.334
	A13	54.547	4.034	34042.418
	A14	56.228	4.185	32199.699
	A15	54.536	4.028	34136.665
	A16	57.359	4.314	31822.598
	A17	56.635	4.271	32944.285
	A18	48.964	3.514	46295.537

Next, by multiplying each column ‘objective’ with the corresponding weight, the weighted decision matrix can be obtained.

$$v_{ij} = w_i r_{ij}$$ Equation 4-33

The values of the normalised and weighted normalised decision matrix are shown in Tables 4-10a and 4-10b.

Table 4-10 The normalised (a) and weighted normalised (b) decision matrix.

a

Normalized matrix			
A1	0.226660152	0.212944225	0.246515539
A2	0.217358772	0.199437595	0.298534903
A3	0.217523478	0.199514095	0.295973528
A4	0.250253238	0.29437671	0.181473972
A5	0.233601624	0.224280378	0.227856574
A6	0.21820901	0.207555618	0.261195374
A7	0.228514315	0.219493597	0.237375524
A8	0.211495249	0.196001999	0.304881262
A9	0.2573073	0.270791518	0.18505716
A10	0.220273879	0.202827127	0.267524532
A11	0.258686694	0.297463933	0.177712719
A12	0.251509168	0.279453257	0.179295571
A13	0.239592826	0.231725285	0.210468427
A14	0.246976718	0.240405072	0.199075756
A15	0.239544399	0.231371168	0.211051113
A16	0.251943536	0.247845525	0.196744317
A17	0.248765773	0.245350042	0.203679182
A18	0.21507273	0.201858767	0.286223761

b

Weighted decision matrix.		
0.075553384	0.638832675	0.739546619
0.072452924	0.598312787	0.895604709
0.072507826	0.598542284	0.887920585
0.083417746	0.883130132	0.544421916
0.077867208	0.672841135	0.683569722
0.072736336	0.622666855	0.783586122
0.076171438	0.658480792	0.712126573
0.070498416	0.588005997	0.914643786
0.0857691	0.812374553	0.55517148
0.073424626	0.608481383	0.802573596
0.086228898	0.892391799	0.533138157
0.083836389	0.83835977	0.537886714
0.079864275	0.695175855	0.631405281
0.082325573	0.721215217	0.59722727
0.079848133	0.694113504	0.63315334
0.083981179	0.743536575	0.590232952
0.082921924	0.736050127	0.611037546
0.07169091	0.605576301	0.858671283

The second step, the best and the worst solutions (positive ideal B^+ and negative non ideal B^- solutions, respectively) should be identified in the weight normalised matrix. The best and worst values in a maximise objective function, such as exergy efficiency, are

represented the largest and smallest values, respectively; and vice versa for a minimise objective function, such as cost rate function. Table 4-10b shows the best (highlighted in green) and the worst (highlighted in red) solutions for each objective.

$$B^{+} = \left(v_1^{+}, \ldots\ldots\ldots v_n^{+}\right) \qquad \text{Equation 4-34}$$

$$B^{-} = \left(v_1^{-}, \ldots\ldots\ldots v_n^{-}\right) \qquad \text{Equation 4-35}$$

The third step is finding the separation of all solutions from the Ideal non-ideal solutions and these are done by using Equations 4-36 and 4-37, respectively. The results are then listed in Tables 4-11 and 4-12.

$$S_i^{+} = \sqrt{\sum_{j=1}^{n}\left(v_{ij} - B_j^{+}\right)^2} \qquad \text{Equation 4-36}$$

$$S_i^{-} = \sqrt{\sum_{j=1}^{n}\left(v_{ij} - B_j^{-}\right)^2} \qquad \text{Equation 4-37}$$

Table 4-11 Separation of each alternative from the positive ideal solution.

Objective1	Objective2	Objective3	Separation
0.000113967	0.002583351	0.042604453	0.212842127
0.000189777	0.00010623	0.131382001	0.362874646
0.000188268	0.000111013	0.125870572	0.35520396
7.90258E-06	0.087098255	0.000127323	0.295353146
6.99179E-05	0.007197001	0.022629656	0.172906259
0.000182049	0.001201375	0.062724183	0.253194802
0.000101152	0.004966697	0.032036853	0.192625809
0.000247448	0	0.145546545	0.381829796
2.11414E-07	0.050341249	0.000485467	0.225448282
0.000163949	0.000419241	0.072595456	0.27051552
0	0.092650717	0	0.304385802
5.7241E-06	0.062677012	2.25488E-05	0.250410233
4.05084E-05	0.011485379	0.009656428	0.145541454
1.52359E-05	0.017744696	0.004107414	0.14787612
4.07142E-05	0.011258803	0.010003037	0.145953946
5.05224E-06	0.024189761	0.003259816	0.165694384
1.09361E-05	0.021917064	0.006068315	0.167320995
0.000211353	0.000308716	0.105971816	0.326330944

Table 4-12 The separation of each alternative from the negative ideal solution.

Objective1	Objective2	Objective3	Separation
2.55527E-05	0.064292229	0.030659018	0.308183063
3.8201E-06	0.086482465	0.000362486	0.294701157
4.03773E-06	0.086347537	0.000714129	0.295068982
0.000166909	8.57785E-05	0.137064233	0.370562978
5.42991E-05	0.048202494	0.053395223	0.318829133
5.00829E-06	0.072751545	0.017176111	0.299887754
3.21832E-05	0.054714359	0.041013222	0.309450746
0	0.092650717	0	0.304385802
0.000233194	0.00640276	0.129220339	0.368586886
8.5627E-06	0.080605124	0.012559728	0.305243205
0.000247448	0	0.145546545	0.381829796
0.000177902	0.00291946	0.141945891	0.380845445
8.77193E-05	0.038894129	0.080224051	0.345262072
0.000139882	0.029301422	0.100753245	0.360824817
8.74172E-05	0.039314282	0.079236871	0.344439502
0.000181785	0.022157878	0.10524239	0.357186299
0.000154344	0.024442718	0.092176749	0.341721832
1.42204E-06	0.08226313	0.003132921	0.29222846

The final step, the relative closeness of each alternative to the ideal solution is computed by using Equation 4-38. The value of the relative closeness (TOPSIS scores) is a number between zero and one, and the value closer to one is the better solution.

$$C_i^+ = \frac{S_i^-}{\left(S_i^- + S_i^+\right)}$$ Equation 4-38

Table 4-13 and Figure 14-10 illustrate the final scores of the TOPSIS tool, and the alternative solution A14 is the closer score to one (0.709306374), thus this point can be set as the optimum solution.

Table 4-13 TOPSIS scores for each alternative solution.

Alternative	Scores
A1	0.591493595
A2	0.448163019
A3	0.453761741
A4	0.556470949
A5	0.648375404
A6	0.542211557
A7	0.616341756
A8	0.443571675
A9	0.620479907
A10	0.530158193
A11	0.556428325
A12	0.60331409
A13	0.703462901
A14	0.709306374
A15	0.702373784
A16	0.68311244
A17	0.671302715
A18	0.472433946

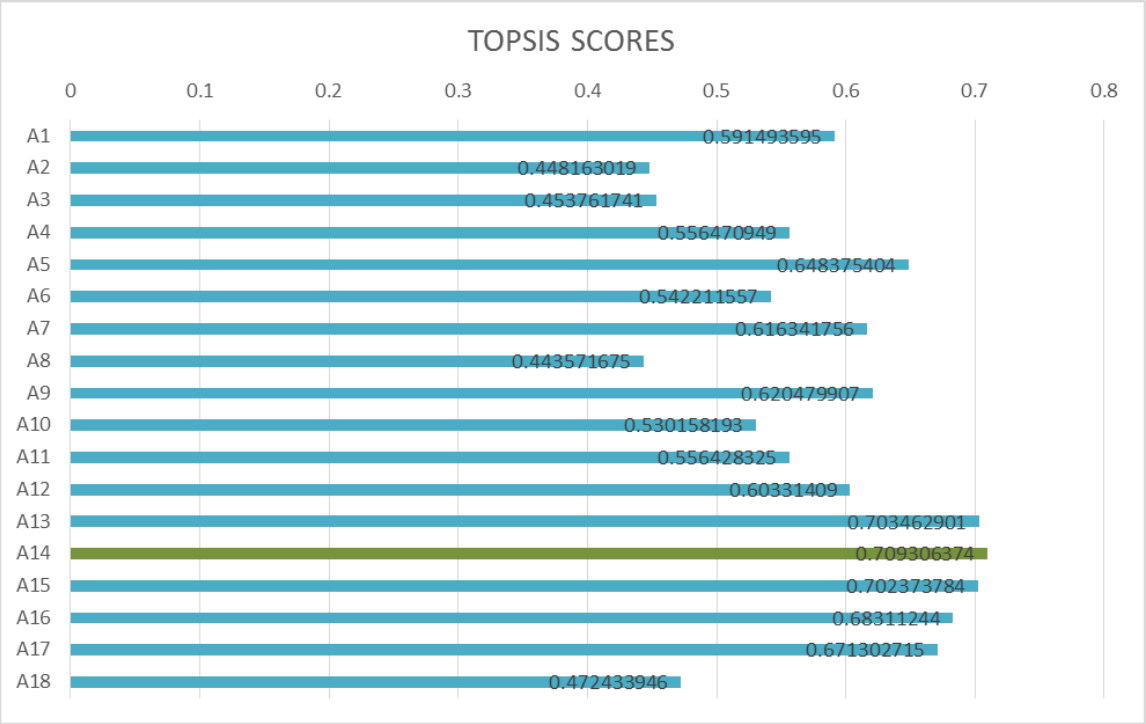

Figure 4-10 TOPSIS scores for each alternative solution.

4.7.3 Analysing the optimum solution

The final design parameters of the optimum solution that have been selected by TOPSIS are listed in Table 4-14.

Table 4-14 Design parameters of the optimum solution.

Key Parameters	Ranges
Collector area	137.18m^2
Hot storage tank volume	13.16m^3

The optimum solution will be analysed in this section to identify the exergy efficiency, exergy destruction, CO_2 emissions and cost rate of each individual component. Table 4-15 lists the specific characteristics (exergy destruction, exergy efficiency, total cost rate and the annual CO_2 emissions) of each component of the optimum system that have been achieved using the TOPSIS decision making method. In addition, the percentage distribution of the values in Table 4-15 has been drawn in Figure 4-11.

Table 4-15 Specific characteristics of the optimum system.

Components	Exergy destruction (kW)	Exergy efficiency (%)	Total cost rate (US$/hr)	Annual CO_2 emissions (Kg)
Solar collector	9.363	7.001	2.041	1252.16
Hot storage tank	0.652	13.702	0.195	540.420
Auxiliary heater	0.044	58.663	1.063	22840
Absorption chiller	1.670	22.415	0.451	249.475
Cooling tower	1.131	13.058	0.233	3952.432

Figure 4-11a shows the percentage distribution of the exergy destruction (irreversibility) of each component. The highest exergy destruction was found to be originating from the solar collector 73%, and lowest exergy destruction was in the auxiliary heater (1%). Similar results have been found in Onan et al. (2010).

Since the highest exergy destruction was located in the solar collector, the lowest exergy efficiency must be found in the same component. As shown in Figure 4-11b, the solar collector has the lowest value (6%) of exergy efficiency, and this small value means a poor exploitation of the available solar energy that could be absorbed in the solar collector, and similar results have been noted in Onan et al. (2010).

The Figure 4-11c illustrates the total cost rate of each component in the system. The highest percentage cost rate occurred in the solar collector: 51%; while the next highest was in the auxiliary heater: 27%. The high cost rate in the collector results from the large area of the collector, 137.18m^2, which in turn means a high investment cost rate (1.964US$/hr), while the cost rate in the auxiliary heater is high due to the high operational cost rate (1.04US$/hr, which represents an annual electricity consumption of 27795kW.hr). Table 4-16 lists the investment and operation cost rates for the solar collector and the auxiliary heater.

Table 4-16 Investment and operation cost rates of the solar collector and the auxiliary heater.

Components	Investment cost rate (US$/hr)	Operation cost rate (US$/hr)
Solar collector	1.964	0.0774
Auxiliary heater	0.023	1.040

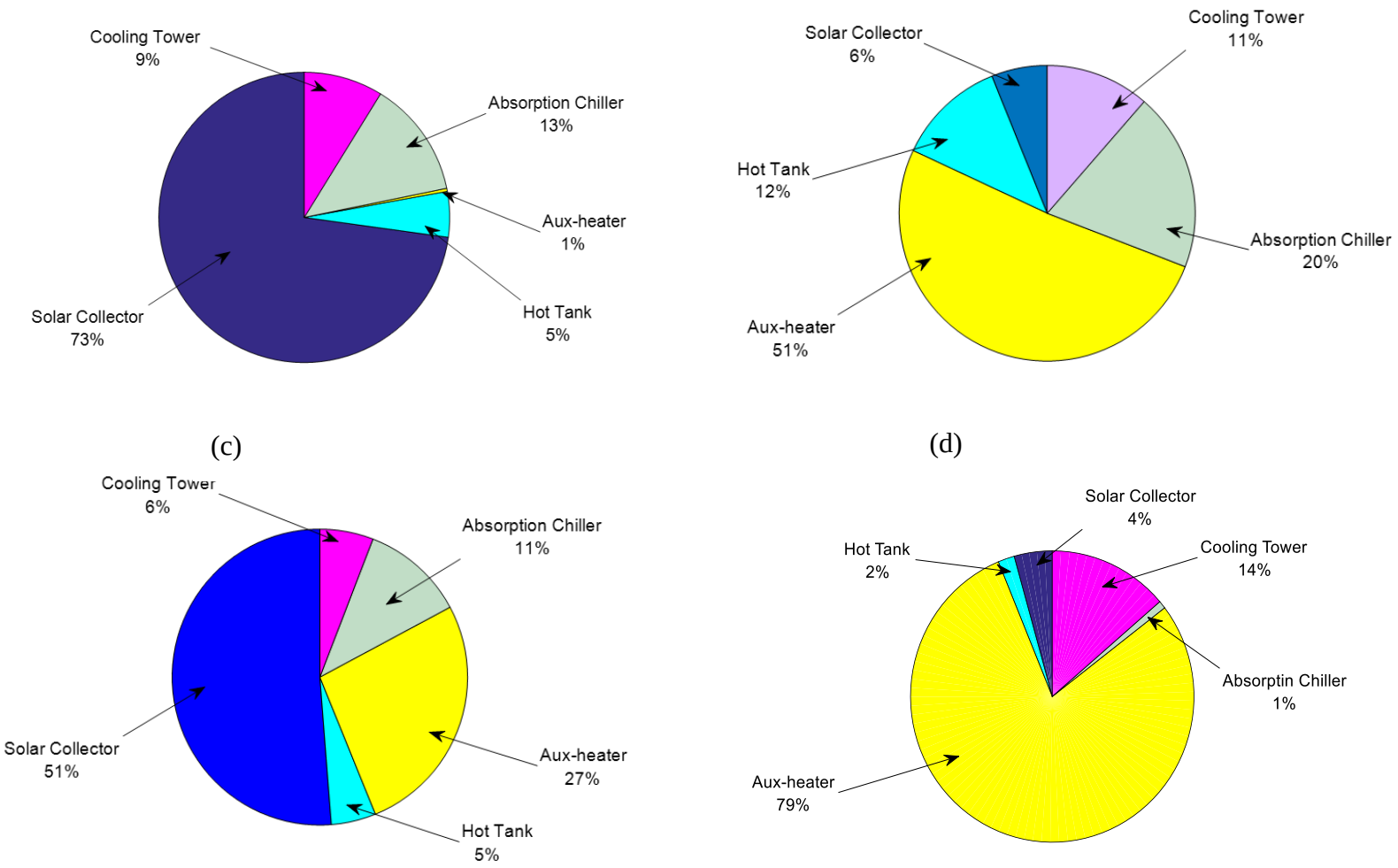

Figure 4-11 a) Percentage distribution of exergy destruction, b) Percentage distribution of exergy efficiency, c) percentage distribution of the total cost rate (US$/hr) and d) percentage distribution of the annual CO2 emission (kg).

Figure 4-11c and Table 4-16 reveal that although the investment cost rate of the auxiliary heater is 1% of the investment cost rate of the solar collector, the total cost rate of the auxiliary heater is half the total cost of the solar collector. The high cost rate in the auxiliary heater due to its operation at night, when the house needs the cooling effects and the solar energy is not available.

Figure 4-11d illustrates the annual amount of CO_2 emissions for each main component in the system. The lowest CO_2 emissions were in the absorption chiller and the highest CO_2 emissions were in the auxiliary heater. Although the collector has a large area (thus needing more materials for its manufacture), it did not emit as much CO_2 as the auxiliary heater.

Therefore, from the data listed in the last three paragraphs, the auxiliary heater operation should be reduced, and this might be done in two ways:

- Increasing the solar collector area, thus making more solar energy available. But this leads to increasing the cost of the system, as well as it would not eliminating or reducing the operation of the auxiliary heater at night.
- Or, introducing a cold storage tank with an appropriate control strategy to store cold thermal energy in the day in order to use it at night. Sanaye & Shirazi (2013) state that "Although utilising cold storage systems and their auxiliary equipment incur extra initial costs, these additional costs are paid back in a short time because of reduction in electricity consumption in comparison with conventional systems (systems without cold storage tank)". For example, installing a cold storage tank with the air-conditioning system has led to 63% energy savings (Cole, Powell & Edgar, 2012). Additionally, Rismanchi et al. (2012) wrote that using cold storage tank could reduce the CO_2 emissions by 14% to 46%.

A cold thermal energy tank can store the cold energy produced by the solar absorption cooling system at times when the solar energy is available (daytime) and use (discharge) it at times when there is no solar energy available (at night). It should be noted that since the absorption system is fully dependent on the auxiliary heater at night for producing the cooling effects, reduction in the operation of the auxiliary at night also means reduction of the operation of the whole solar absorption system.

With regard to the payback period of the proposed solar absorption cooling system, it was equal 18.7years and the annual solar energy gain was 22741.4kW.hr, which represents 4093.4US$ saving per year. It is worth mentioning here that the proposed solar absorption system has got payback period less than its life span (20years) without any kind of government incentives, which is better than the results of the studies of Hang et al. (2011) and Shirazi et al. (2016b).

4.7.4 Comparison with the original system

The optimised solar absorption cooling system obtained from the GA and TOPSIS process was compared with the original solar cooling that was installed in the building. Table 4-17 lists the specifications of the original system (taken from Al-Karaghouli et al. (1989) and Joudi & Abdul-Ghafour (2003)) and the optimised system.

Table 4-17 Specifications of the original system and the optimised system.

Main component		Original system	Proposed (obtained from GA)
Chiller size		10TR (35kW)	5TR (17.6kW)
Collector	Type	Flat plate	Evacuated tube
	Area	243m²	137m²
	Orientation	Southeast 22.5°	South
	Slope	15.6	Change monthly (see Table 4-5)
Hot tank volume		20m³	13.2m³
Solar fraction		0.51	0.45
Investment cost		-	76409US$
Coefficient of performance		0.443	0.57

As can be seen from the above table, the size of the absorption chiller, the area of the collectors and the volume of the hot tank are reduced, and this in turn means reducing the cost of the system (both investment and operational cost, which is one of the objectives of this work). The coefficient of the performance of the system is increased by 22%, but the solar fraction of the optimised system is lower than the original system by 12%.

4.8 Conclusion

In this chapter, a methodology to design and asses a solar cooling absorption system based on exergic, economic and environmental considerations was proposed. A case study of a domestic house located in Baghdad, Iraq has been used to demonstrate this approach. A multi-objective optimisation using the genetic algorithm technique was used to obtain potential optimised designs. Then, a decision-making tool called TOPSIS was implemented to select the most suitable design. The optimal proposed system has exergy efficiency of 56%, total cost rate of 4.19US$/hr, annual CO_2 emissions of 32199kg and payback period of 18.7years. The comparison of the optimised system with the original system in the building showed that the size of the absorption chiller, the area of the

collectors and the volume of the hot tank are reduced, and this in turn means reducing the cost of the system, which is one of the objectives of this work. The performances of the individual components of the selected design were analysed comprehensively. The results showed that although the auxiliary heater has the highest exergy efficiency 58.6%, it has the highest operation cost 1.04US$/hr and the highest annual CO_2 emissions 22840kg. Therefore, this study suggests using cold thermal energy storage with the solar absorption cooling system in order to store the cold energy produced by the system at times when the solar energy is available (daytime) and use (discharge) it at times when there is no solar energy available (at night).

Chapter Five

A generic control strategy for solar cooling systems with cold thermal energy storage for residential applications

In this chapter, a new generic and simple control strategy is proposed for charging and discharging the water cold thermal energy storage used in a solar absorption cooling system. Five scenarios were considered to manage the quantity of charging of the cold storage tank according to the splitting rate of the mass of the supplied chilled water by the chiller to the cold storage tank and the building. In order to assess the proposed approach, the solar absorption system is analysed based on exergy efficiency, cost rate and annual CO_2 emission aspects, as well as the payback period criteria. The genetic algorithm multi objective optimisation technique and the decision-making tool (TOPSIS) were used to find the optimal design. The proposed system was also compared with a non-storage (without cold storage tank) solar absorption system.

5.1 System description

Figure 5-1 illustrates the solar cooling system (before adding the proposed configuration and controlling of the CTES) used in this report. As mentioned before, the solar absorption cooling system produces a cooling effect by using solar energy, where the solar collectors collect and transfer the solar thermal energy to the system. The system includes a solar collector, hot storage tank or HTES, auxiliary heater, absorption chiller, cooling tower and cold storage tank. Solar absorption cooling system can be divided into five loops (subsystems): solar loop, heating loop, cooling tower loop, chilled loop and load loop.

- In the first loop (solar loop) the evacuated tube solar collectors absorb the solar radiation and convert it into thermal energy that is used to heat up the water (point

1) coming from the hot water through pump 1, the hot water (point 2) is returned back to the top of the hot storage tank.

- In the second loop (heating loop), the hot water (point 3) from the top of the tank passes through the auxiliary heater (used to boost the temperature of the fluid when it drops below the required temperature in the absorption chiller) to the absorption chiller (point 5), then the warm water (point 6) is pumped back from the chiller to the hot storage tank (point 8) by pump 2. The bypass (tempering valve and three-way valve) is used when the returned water (point 7) is warmer than the water in the top of the hot storage.
- In the third loop (cooling tower loop) the warm water from the chiller (point 9) is pumped by pump 3 to the cooling tower to cool down and then return to the chiller (point 11).
- In the fourth loop (chilled loop), pump 4 pumps the chilled water (point 12) that is produced by the chiller to the cold storage tank (point 13), and the water from the cold tank is returned to the chiller again (point 17).
- In the fifth loop (load loop), the chilled water (point 14) from the cold storage tank will be supplied to the building (point 15) by pump 5, and then after the cooling effects are delivered, the water is returned to the cold tank (point 16).

The controller C1 is the main controller that turns the whole system ON and OFF, which is based upon the need of the building for cooling; the controller C2 activates the auxiliary heater when needed; and the controller C3 controls the flow of the fluid in the solar loop based on the availability of the solar irradiance.

The last two loops (chilled and load loops) will be modified according to the proposed configuration and control regime that will be discussed in the following section.

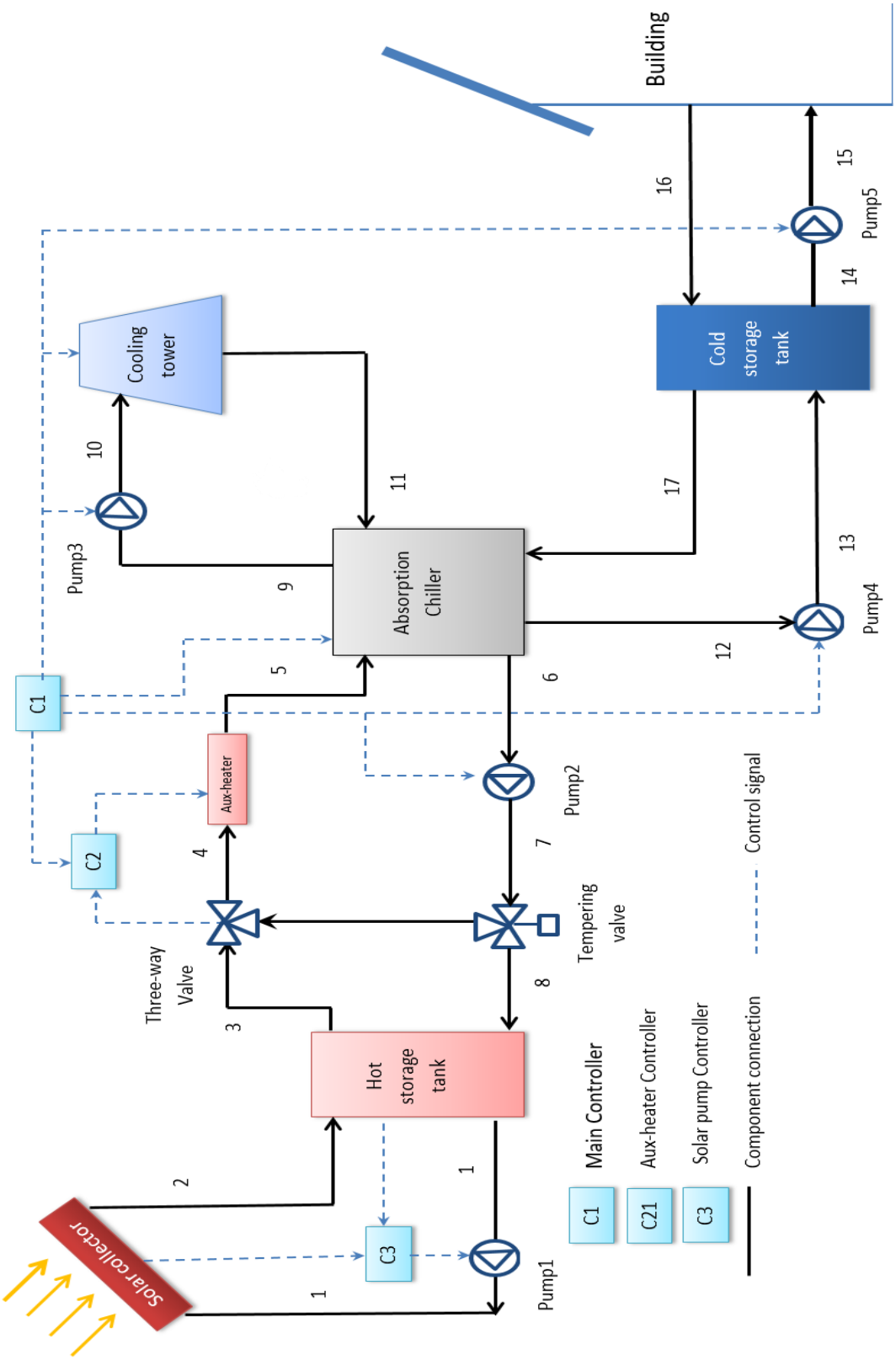

Figure 5-1 Schematic of the solar absorption cooling system used in this study (except the part of the CTES that will be modified by the proposed configuration and controlling regime).

5.2 The proposed control strategy

Instead of using sophisticated equations to determine the current state of the CTES that are used as guides for charging and discharging modes, simple and easy to apply equations that depend only on the water temperature on the top of the CTES (Tt_{CTES}) and the water temperature on the bottom of the CTES (Tb_{CTES}) are used as indicators for charging and discharging processes in this study. Figure 5-2 shows a schematic of the proposed CTES configuration as well as the charging and the discharging passages. Before presenting the control strategy of the CTES, the charging and discharging modes should be clarified:

- **Charging mode** is the mode when the chiller is ON and the chilled water is supplied by the primary pump (pump 4) to the bottom of the CTES (passage a-b) and to the building (passage a-d). Simultaneously, the water is returned back from the top of the CTES (passage g-h) and from the building (passage e-h) to the chiller. The conventional method of the quantity of charging of the CTES in the solar cooling systems depends on the surplus cold thermal energy remaining after providing the cooling loads required by the building. In this report, five scenarios will be considered to manage the quantity of charging of the CTES, these scenarios depend on the splitting rate of the mass of the supplied chilled water by the chiller to the CTES and the building. These scenarios are:
  - **a- Scenario I:** 10% of the mass of the supplied chilled water by the chiller flow to the CTES and the remaining 90% flows to the building.
  - **b- Scenario II:** 20% of the mass of the supplied chilled water by the chiller flows to the CTES and the remaining 80% flows to the building.
  - **c- Scenario III:** 30% of the mass of the supplied chilled water by the chiller flows to the CTES and the remaining 70% flows to the building.

d- **Scenario IV:** 40% of the mass of the supplied chilled water by the chiller flows to the CTES and the remaining 60% flows to the building.

e- **Scenario V:** 50% of the mass of the supplied chilled water by the chiller flows to the CTES and the remaining 50% flows to the building.

- **Discharging mode** when the chiller is OFF and the stored chilled water is pumped by the secondary pump (pump 5) from the bottom of the CTES to the building (passage c-d), and it is returned back to top of the CTES from the building (passage e-f).

The control strategy of the CTES consists of the following two periods:

5.2.1 Daytime period

The daytime period represents the inexpensive hours where the solar energy is available. This period starts one hour after sunrise and ends one hour after sunset in order to exploit the stored thermal energy in the hot storage tank (HTES) efficiently. At the beginning, the chiller starts to work and the CTES will be on charging mode where the chilled water is supplied to the bottom of the CTES (as well as to the building) until the water temperature at the top of the CTES drops to 8°C or below where the CTES will be fully charged.

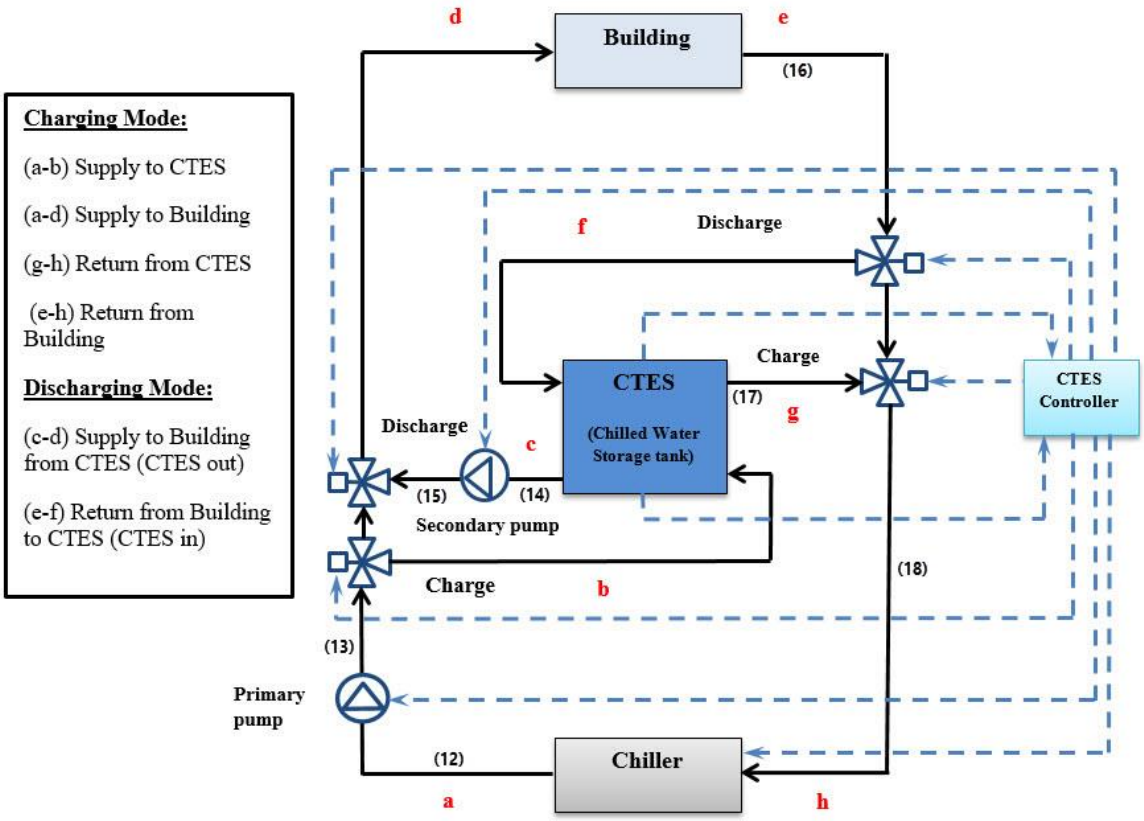

Figure 5-2 Schematic diagram of the proposed CTES configuration as well as the charging and discharging processes.

$Tt_{CTES} \leq 8^{\circ}C \Rightarrow CTES$ is fully charged, otherwise continue charging Equation 5-1

where Tt_{CTES} is the water temperature at the top of the CTES.

After the charging mode is stopped, the supplied chilled water (from the chiller) flows to the building only without splitting, and the chiller continues to operate until the end of the daytime period (the chiller stops only when there is no need for the cooling effect in the building); then it stops working. It must be mentioned here that there is no discharging mode in the inexpensive (cheap) hours.

5.2.2 Nighttime period

The nighttime period represents the expensive hours when the chiller depends only on the hot thermal energy produced by the auxiliary heater to activate (due to unavailability of the solar irradiance). This period starts one hour after sunset and ends one hour after

sunrise, i.e. after the daytime is finished and the chiller stops working. At the beginning, the CTES will be on discharging mode where the chilled water is supplied from the bottom of the CTES to the building (the water is returned back from the building to the top of the CTES) until the water temperature at the bottom of the CTES rises to 16°C, which means the whole stored cold thermal energy has been consumed and the CTES needs charging. The CTES will then be switched to charging mode, and the chiller turns ON to supply the chilled water to the CTES and to the building. As in the daytime period, charging the CTES will continue until the water temperature at the top of the CTES drops to 8°C. After that, the CTES will be switched back to discharging, and this process is repeated until the end of the nighttime period. It must be mentioned here that supplying the chilled water to the building will be stopped (whether from the CTES (discharging mode) or from the chiller (charging mode)) if there is no need for the cooling effect in the building. The controlling functions are illustrated in Figure 5-3.

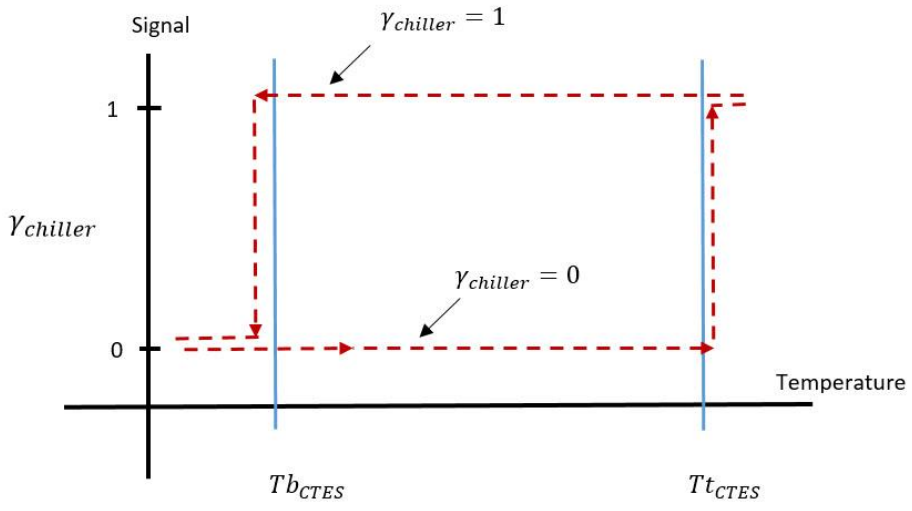

$\gamma_{Chiller}$ – *The control signal of the ciller*

Tb_{CTES} – *Water temperature at the bottom of the CTES*

Tt_{CTES} – *Water temperature at the top of the CTES*

Figure 5-3 Controller function of the CTES charging and discharging modes during the nighttime period.

Mathematically, the control function is expressed as follows:

$$If\ \gamma_{Chiller} = 0\ \ and\ \ Tb_{CTES} \geq 16^{\circ}C\ \ \Rightarrow \gamma_{Chiller} = 1\ ,otherwise\ \ \gamma_{Chiller} = 0 \qquad \text{Equation 5-2}$$

$$If\ \gamma_{Chiller} = 1\ \ and\ \ Tt_{CTES} \leq 8^{\circ}C\ \ \Rightarrow \gamma_{Chiller} = 0\ \ ,otherwise\ \ \gamma_{Chiller} = 1 \qquad \text{Equation 5-3}$$

where Tb_{CTES} is the water temperature at the bottom of the CTES.

After the system has been demonstrated in this section, the system analysing will be presented in the following section.

5.3 System analysis

The same of the thermo-economic-environmental analysis that has been presented in Chapter Four (Section 4.3) was used here to asses the proposed system, the exergy destruction of main components of the system can be found in Table 5-1.

Table 5-1 The exergy destruction equations used for the solar absorption cooling system*.

component	Exergy destruction equations	
Solar collector	$\dot{E}_{D,coll} = \dot{m}_1(\Psi'_1 - \Psi'_2) + \dot{Q}_{solar}\left(1 - \frac{T_o}{T_{coll}}\right)$	$\dot{Q}_{solar}$ is solar radiation incidence on the collector, T_{coll} is the thermodynamic average temperature of the collector
Hot storage tank	$\dot{E}_{D,HTES} = \left[\dot{m}_2(\Psi'_2 - \Psi'_{19}) + \dot{m}_3(\Psi'_8 - \Psi'_3)\right]$	
Auxiliary heater	$\dot{E}_{D,aux} = \dot{m}_4(\Psi'_4 - \Psi'_5) + \dot{Q}_{aux}\left(1 - \frac{T_o}{T_{aux}}\right)$	$\dot{Q}_{aux}$ is the amount of heating rate of the auxiliary heater, T_{aux} is the thermodynamic average temperature of the collector
Absorption chiller	$\dot{E}_{D,chill} = \left[\dot{m}_5(\Psi'_5 - \Psi'_6) + \dot{m}_9(\Psi'_{11} - \Psi'_9) + \dot{m}_{12}(\Psi'_{18} - \Psi'_{12})\right]$	
Cooling tower	$\dot{E}_{D,ct} = \dot{m}_{10}(\Psi'_{10} - \Psi'_{11}) + \dot{W}_{fan,ct}$	$\dot{W}_{fan,ct}$ is the amount power consumption by the cooling tower fan.
Cold storage tank	$\dot{E}_{D,CTES} = \dot{m}_{Ch\arg}(\Psi'_{17} - \Psi'_{13}) + \dot{m}_{DisCh\arg}(\Psi'_{14} - \Psi'_{16})$	$\dot{m}_{Ch\arg}$ is the charging mass flow rate (equals zero at discharge mode) and $\dot{m}_{DisCh\arg}$ is the discharging mass flow rate (equals zero at charging mode),

*These equations are based on Figure 5-1 and the proposed configuration in Figure 5-2.

5.4 Multi-objective optimisation

In order to assess the proposed approach, the solar absorption system is analysed based on exergy efficiency, cost rate and annual CO_2 emission aspects, as well as the payback period criteria. The genetic algorithm multi objective optimisation technique and the decision-

making tool (TOPSIS) were used to find the optimal design for each scenario. Additionally, in order to demonstrate the performances of the selected best solutions, a base system that is the same solar absorption cooling system but without CTES will be considered; the base system is the same optimised system that has been obtained in Chapter Four. The same case study that has been explained in Section 4.5 was used here.

5.5 Design variables and input parameters

Four key variables were used in the optimisation process of the solar absorption cooling system.

- Area of the solar collectors A_r
- Tilt or inclination angle of the solar collectors from the horizontal surface.
- Volume of the HTES V_h
- Volume of the CTES V_c (not used if the system does not have a CTES, as in the base system).

Monthly average optimal tilt angles for solar collectors under Baghdad climate have been obtained in Chapter Three. Thus, only three key design parameters are considered in this chapter, and their ranges are listed in Table 5-2.

Table 5-2 Design parameters and their ranges

Key Parameters	Ranges
Collector area A_r	45 -200 m^2
HTES volume V_h	0.5 - 20 m^3
CTES volume V_c*	0.5 - 20 m^3

*Not used in the non-storage base system.

5.6 Results and discussion

After obtaining Pareto Front potential solutions and using the decision making tool TOPSIS for each case, six optimal solutions have been chosen. Table 5-3 lists the optimal values of the design parameter with their corresponding performances for each case.

Table 5-3 the optimal values of the design parameter with their corresponding performances for each case.

Case	Collector area A_r m^2	HTES volume V_h m^3	CTES volume V_c m^3	Exergy efficiency %	Total cost rate US$/hr	CO2 emissions Kg/year	Operation hour hr	Solar fraction -	Payback Period year
Base	137.18	13.6	-	56.23	4.19	32199.7	4809	0.45	18.7
I	127.11	11.28	1.29	63	3.85	23559.27	4151	0.56	15.8
II	117.33	4.95	1.49	69.42	4.25	21282.24	2981	0.67	9.3
III	124.22	5.25	3.72	70.22	4.32	19094.15	2931	0.72	9.3
IV	128.26	9.32	2.63	71.49	4.2	17973.48	2929	0.73	9.9
V	162.67	15.3	8.89	71.58	4.61	15057.5	2932	0.8	11.8

5.6.1 Exergy efficiency

Figure 5-4 shows the exergy efficiency for each case and their corresponding amount of change compared with the base system.

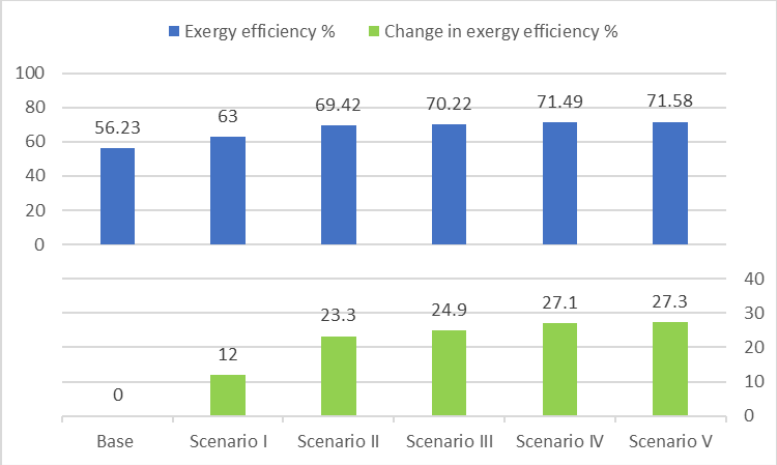

Figure 5-4 Exergy efficiency for each case and their corresponding amount of change compared with the base system.

As can be seen from Figure 5-4, the lowest and highest exergy efficiency are in base system 56.23% and the scenario V system 71.58% (an increase of 27.3% compared to the base system), respectively. However, there is relatively little difference between scenarios II, III, IV (69.4-71.5% exergy efficiency) and scenario V.

5.6.2 Cost rate

Since the cost performances used here are in time rate, the operation hours of the absorption chiller should be presented. Figure 5-5 shows the operation hours of the chiller for each case and their corresponding amount of change compared with the base system, the shortest and longest hours of the operation are in the scenario IV base system 2929hr (decreasing at a rate of 39.1% from the base system) and the base system 4809hr, respectively. However, there is relatively little difference between scenarios III (2931hr), IV and V (2931hr).

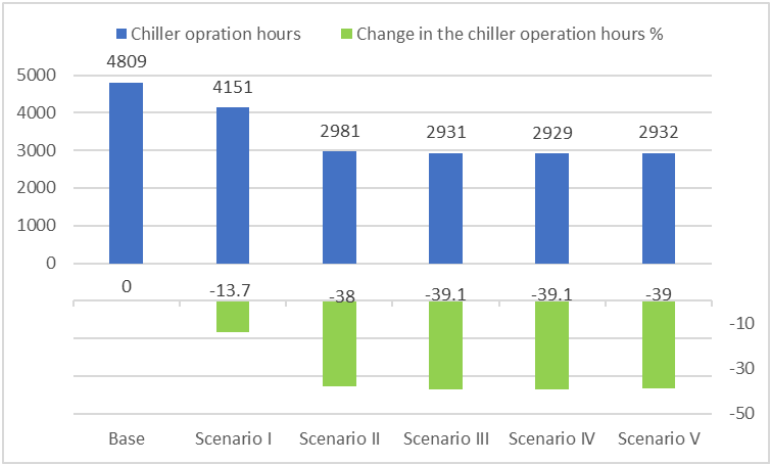

Figure 5-5 The operation hours of the chiller for each case and their corresponding amount of change compared with the base system.

Figure 5-6 shows the total cost rate for each case and their corresponding amount of change compared with the base system. The minimum and maximum cost rate are in scenario I 3.85US$/hr (decreasing at rate 8.1% from base system) and scenario V 4.61US$/hr (increasing at rate 9.1% from the base system), respectively.

As explained in the economic analysis section, cost rate is the summation of investment and operation cost rates. Thus, both investment and operation cost rates should be presented. Figures 5-7 and 5-8 demonstrate the investment cost rate and the operation cost rate for each case and their corresponding amount of change compared with the base system. As can be seen from Figure 5-7, the lowest and highest investment cost rate are in scenario I 2.63US$/hr (decreasing at rate 3.7% from base system) and scenario V 3.61US$/hr (increasing at rate 32.2% from base system), respectively. From Figure 5-8, the lowest and highest operation cost rates are in scenario V 1US$/hr (decreasing at rate 31% from base system) and scenario II 1.52US$/hr (increasing at rate 4.8% from base system), respectively.

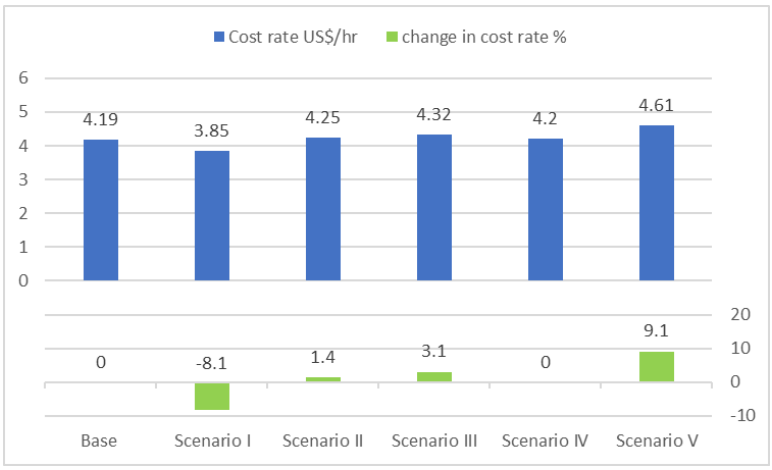

Figure 5-6 The total cost rate for each case and their corresponding amount of change compared with the base system.

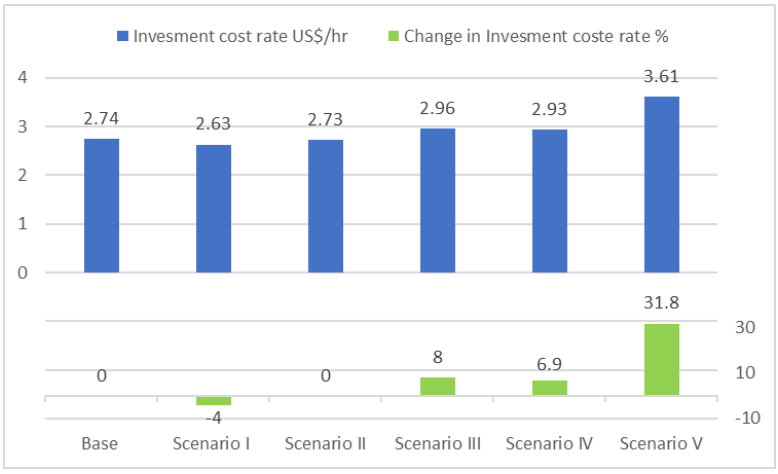

Figure 5-7 The investment cost rate for each case and their corresponding amount of change compared with the base system.

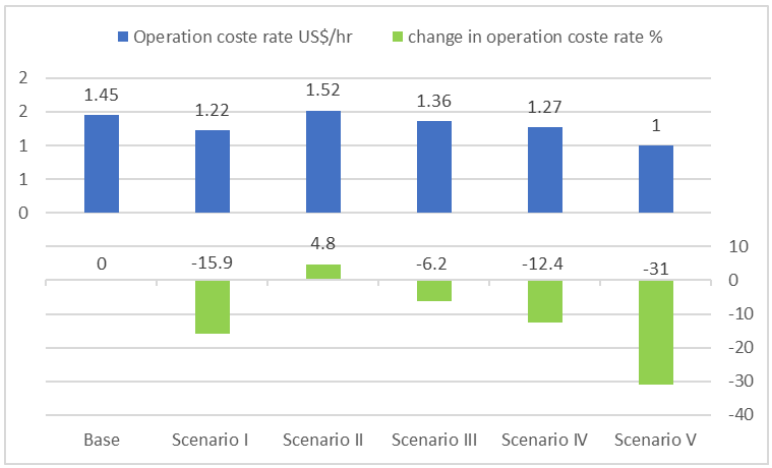

Figure 5-8 The operation cost rate for each case and their corresponding amount of change compared with the base system.

For further interpretation of the cost, Table 5-4 lists the total investment in US$ and the annual operation cost rate in US$/year (multiplying the operation cost in US$/hr by its corresponding annual operation hours) for each case, as well as their corresponding amount of change compared with the base system. With regard to the investment cost, the lowest and highest investment costs are in scenario II, shaded in green colour, 66256US$ (decreasing at a rate of 13.3% from the base system) and the scenario V 92289US$ (increasing at a rate of 20.8% from the base system), respectively. With regard to the annual operation cost rate, the lowest and highest cost rates are in scenario V, shaded in green, 2932US$/year (decreasing at rate 58% from base system) and the base system 6973US$, respectively. However, although scenario V is the best choice in terms of the annual operation cost rate, it is the worst case in terms of investment cost (20.8% more expensive than the base system) due to having larger components (collector, HTES and CTES, as can be seen from Table 5-3) compared to other cases. On the other hand, the best choice in terms of the investment cost (scenario II) is 35% less expensive than the base system in terms of the operation cost. Thus, it seems that scenario II is the best choice economically.

Table 5-4 Investment and annual operation cost rate and their corresponding amount of change compared with the base system.

Case	Investment		Operation	
	Cost US$	Change from base %	Annual cost rate US$/year	Change from base %
Base	76409	-	6973	-
I	73716	-3.5	5064	-27.4
II	66256	-13.3	4531	-35.0
III	72071	-5.7	3986	-42.8
IV	73525	-3.8	3720	-46.7
V	92289	20.8	2932	-58.0

5.6.3 CO_2 emissions

Figure 5-9 shows the total annual CO_2 emissions for each case and their corresponding amount of change compared with the base system.

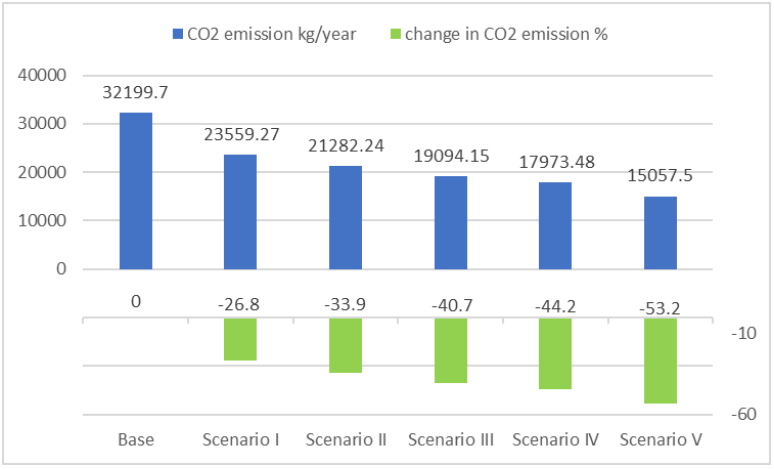

Figure 5-9 Total annual CO2 emissions for each case and their corresponding amount of change compared with the base system.

As can be seen from Figure 5-9, the highest and lowest total annual CO_2 emissions are in base system 32199.7kgCO_2/year and the scenario V system 15057.5kgCO_2/year (a decrease of 53.2% compared to the base system), respectively. As explained in the

environmental analysis section, total annual CO_2 emissions is the summation of manufacturing stage and operating stage emissions. Thus, both manufacturing stage and operating stage emissions should be presented. Table 5-5 lists the annual CO_2 emission of both manufacturing stage and operating stage for each case and their corresponding amount of change compared with the base system.

Table 5-5 The annual CO_2 emissions of both manufacturing stage and operating stage for each case and their corresponding amount of avoided CO_2 emissions compared with the base system.

Case	Manufacturing stage		Operating stage	
	CO_2 emissions $kgCO_2$/year	Change from base %	CO_2 emissions $kgCO_2$/year	Change from base %
Base	1555.4	-	30644.3	-
I	1482.1	-4.7	22077.1	-28.0
II	1182.2	-24.0	20100.0	-34.4
III	1421.8	-8.6	17672.3	-42.3
IV	1463.4	-5.9	16510.1	-46.1
V	2140.2	37.6	12917.3	-57.8

With regard to the annual manufacturing stage CO_2 emissions, the lowest and highest emissions rate is in scenario II, shaded in green, 1182.2$kgCO_2$/year (decreasing at rate 24% from base system) and scenario V 2140.2$kgCO_2$/year (increasing at rate 37.6% from base system), respectively. With regard to the annual operating stage CO_2 emissions, the lowest and highest emissions rates are in scenario V, shaded in green, 12917.3$kgCO_2$/year (decreasing at rate 57.8% from base system) and the base system 30644.3$kgCO_2$/year, respectively. However, although scenario V is the best choice in terms of the annual operating stage emissions, it is the worst case in terms of manufacturing stage due to having larger components compared to other cases. On the other hand, the best choice in terms of

the manufacturing stage (scenario II) has 34.4% less operating stage CO_2 emissions than the base system. Thus, it seems that scenario II is the best choice environmentally.

5.6.4 Simple payback

Table 5-6 lists the solar fraction and the annual cost saving due to using solar energy for each case, and their corresponding amount of change compared with the base system.

Table 5-6 The solar fraction and the annual cost saving for each case and their corresponding amount of change compared with the base system.

Case	Solar fraction		Annual cost saving	
	Value -	Change from base %	Value US$/year	Change from base %
Base	0.45	-	4093.4	-
I	0.56	24.4	4672.3	14.1
II	0.67	48.9	7150.8	74.7
III	0.72	60.0	7718.6	88.6
IV	0.73	62.2	7739.5	89.1
V	0.80	77.8	7799.0	90.5

From the above table, scenario V has the highest values in the solar factor 0.8 (an increase by 77.8% from the base system). Additionally, as in the solar fraction, scenario V has the highest values in the annual cost saving 7799 US$ (an increase by 90.5% from the base system). However, that does not mean scenario V is the best choice in terms of payback period because a larger solar fraction and cost saving means a larger collector area, which in turn means larger investment cost (as can be seen from Table 5-4). Figure 5-10 shows the simple payback period for each case and their corresponding amount of change compared with the base system.

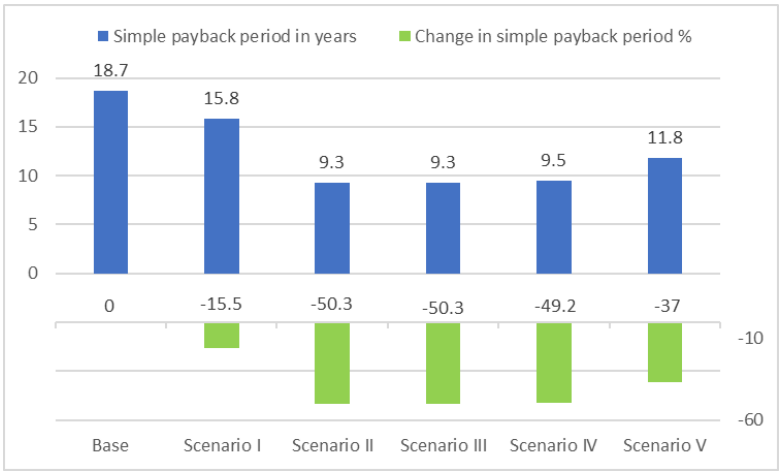

Figure 5-10 Simple payback period for each case and their corresponding amount of change compared with the base system.

As can be seen from Figure 5-10, the shortest payback period is 9.3years in both scenarios II and III (a reduction of 50.3% compared to the base system), and the highest payback period is 18.7years in the base system. As there are two cases with the same payback period, the investment cost will be the indicator to choose the best case. As can been seen from Table 5-4, scenario II has a lower investment cost 66256US$ than scenario II 72071US$. Thus, the scenario II is the best choice in terms of the payback period. But still, even with scenario V, which has the highest investment cost 92289US$, we can reduce the payback period by nearly 40% compared to the non-storage solar absorption system, without any kind of government incentive, in contrast to the study of Hang et al. (2011) that considered incentives in order to reduce the payback period of a non-storage solar absorption system by 40%.

Finally, scenario II will be chosen in this study as the optimally designed solar cooling absorption system that has an efficiently controlled cold thermal energy storage CTES, with exergy efficiency of 69.4%,, investment cost of 66256US$ and total avoided annual CO_2 emissions of 33.9% compared to the base system. Additionally, without any

government incentives, the payback is 9.3years, which is 50% less than the system without CTES.

5.7 Conclusion

A new generic and simple control strategy is proposed for charging and discharging of a water cold thermal energy storage used in a solar absorption cooling system. In order to assess the proposed approach, the solar absorption system is analysed based on exergy efficiency, cost rate and annual CO_2 emissions aspects, as well as the payback period criteria. A case study was conducted to apply this method to a solar cooling absorption system in a residential house in Baghdad, Iraq. The genetic algorithm multiobjective optimisation technique and a decision-making Technique for Order Performance by Similarity to Ideal Solution tool were used to find the optimal design. In order to make the assessment more realistic, the proposed system was also compared with a non-storage (without cold storage tank) solar absorption system. Finally, the chosen optimal system uses an efficient controlled cold thermal energy storage CTES, has exergy efficiency of 69.4%, total cost rate of 4.25US$/hr and total avoided annual CO2 emissions of 33.9% less than system without CTES. Additionally, without any government incentive, the payback was recorded 9.3years, which was 50% less than the system without cold storage tank.

Chapter Six

Conclusions and future work

6.1 Conclusions

With the objective of designing a solar cooling system for the Iraqi climate, solar energy resources were assessed and methods proposed to enhance harvesting the solar energy in the Iraqi climate. A methodology of multi objective optimisation of a solar absorption cooling system was then developed and demonstrated by applying it in a domestic application in Baghdad. Maximising the system performance in exergy, economic and environment were the objectives of the projects. After analysing the optimal configuration of the system, parts that needed more attention were identified. Next, a new control strategy was developed and applied in the system to make it more cost effective. Conclusions of this successive work are:

- Solar energy resources should be assessed in order to find methods to enhance harvesting the solar energy.
- Solar absorption cooling systems are still immature economically, in that the investment payback period is generally greater than the life span of the system, thus the government incentives are necessary to reduce the payback period and make them cost-competitive.
- The focus of previous studies, as design and operation control, is mainly on hot energy (solar collector, the hot thermal energy storage and auxiliary heater) and chiller (absorption chiller and cooling tower) sides, and there is a lack of information about the cold energy side (cold thermal energy storage) in design and

control strategies, especially for residential applications that need cooling during the night in climates, such as in the Middle East.

- After carrying out evaluation of nine models, it was found that a new model to estimate diffuse solar irradiance on a horizontal surface in Baghdad was required.
- ASHRAE 2009 clear sky model could be used to estimate clear sky solar irradiance for Baghdad city with high precision.
- Adopting monthly average optimal tilt angles led to a noticeable increase in the amount of useful solar energy, gaining nearly 9%, representing a possibility of obtaining more energy without harming the environment, merely through a simple change in the tilt angle of solar panels and at no greater cost than the cost of this change.
- A multi-objective optimisation of the solar absorption system technique was used to obtain optimal potential designs. A decision-making tool called TOPSIS was then implemented to select the most suitable design. The optimal proposed system has exergy efficiency of 56%, total cost rate of 4.19US$/hr, annual CO_2 emission of 32199kg and payback period of 18.7years.
- The performances of the individual components of the optimised solar absorption system are analysed, and the results showed that the investment cost rate of the auxiliary heater was 1% of the investment cost rate of the solar collector, while the total cost rate of the auxiliary heater was half the total cost of the solar collector.
- The high cost rate in the auxiliary heater was due to its operation at night, when the house needs the cooling effects and the solar energy is not available.
- A cold storage tank with an appropriate control strategy was required to eliminate or reduce the operation of the auxiliary heater at night through storing the produced cold thermal energy in the day in order to use it at night.

- Reviewing the studies on solar absorption systems revealed no clear procedure or methodology that could describe the control mechanism of the cold thermal energy storage. Additionally, no study has pointed out the benefits of transferring or shifting the demanded cooling load for building from night time (expensive period; when free solar energy is not available to power the solar absorption system) to daytime (when the solar energy is available).
- A generic and simple control strategy for charging and discharging a water cold thermal energy storage CTES unit used in a solar absorption cooling system has been presented, and a multi-object optimisation of a solar absorption cooling system with water cold thermal energy storage CTES according to the exergic, economic and environmental viewpoints has been performed.
- The chosen optimal system that uses efficient controlled cold thermal energy storage, has exergy efficiency of 69.4%, total cost rate of 4.25US$/hr and total avoided annual CO_2 emissions of 33.9% less than system without CTES. Additionally, without any government incentive, the payback is recorded 9.3years, which is 50% less than a system without CTES.

6.2 Future works

- Propose a general model to estimate the diffuse irradiance on horizontal surfaces for all Iraq.
- Evaluate different types of solar collectors with the solar absorption system.
- Using different materials such as phase change materials (PCM) to store the hot thermal energy as well as the cold thermal energy.
- Integrate the solar heating system with a solar cooling absorption system.

- Assess other types of solar cooling technologies, such as adsorption systems, and compare them with the solar absorption system.
- Extend the multi objective methodology to include the energy aspect with exergy, economy and environmental aspects.
- Perform the proposed CTES control strategy on different building, such as hotels and hospitals.

References

Abdullah, Z. I. (2016) *Investigation into design and optimisation of solar adsorption cooling/air conditioning under the Iraq climate*. MPhil thesis. Plymouth University, UK.

Afram, A. & Janabi-Sharifi, F. (2014) 'Theory and applications of HVAC control systems – A review of model predictive control (MPC)'. *Building and Environment*, 72 pp 343-355.

Agyenim, F. (2016) 'The use of enhanced heat transfer phase change materials (PCM) to improve the coefficient of performance (COP) of solar powered LiBr/H2O absorption cooling systems'. *Renewable Energy*, 87, Part 1 pp 229-239.

Agyenim, F., Knight, I. & Rhodes, M. (2010) 'Design and experimental testing of the performance of an outdoor LiBr/H2O solar thermal absorption cooling system with a cold store'. *Solar Energy*, 84 (5). pp 735-744.

Ahmadi, M. H., Sayyaadi, H., Mohammadi, A. H. & Barranco-Jimenez, M. A. (2013) 'Thermo-economic multi-objective optimization of solar dish-Stirling engine by implementing evolutionary algorithm'. *Energy Conversion and Management*, 73 pp 370-380.

Ahmadi, P., Dincer, I. & Rosen, M. A. (2011) 'Exergy, exergoeconomic and environmental analyses and evolutionary algorithm based multi-objective optimization of combined cycle power plants'. *Energy*, 36 (10). pp 5886-5898.

Al-Alili, A., Hwang, Y., Radermacher, R. & Kubo, I. (2010) 'Optimization of a solar powered absorption cycle under Abu Dhabi's weather conditions'. *Solar Energy*, 84 (12). pp 2034-2040.

Al-Alili, A., Islam, M. D., Kubo, I., Hwang, Y. & Radermacher, R. (2012) 'Modeling of a solar powered absorption cycle for Abu Dhabi'. *Applied Energy*, 93 pp 160-167.

AL-Jumaily, K. J., AL-Salihi, A. M. & Al-Tai, O. T. (2010) 'Evaluation of Meteosat-8 measurements using daily global solar radiation for two stations in Iraq'. *International Energy & Environment Foundation*, 1 (4). pp 635-642.

Al-Karaghouli, A., Abood, I. & Al-Hamdani, N. I. (1991) 'The solar energy research center building thermal performance evaluation during the summer season'. *Energy Conversion and Management*, 32 (5). pp 409-417.

Al-Karaghouli, A., Al-Hamdani, N. & Al-Sinan, W. (1989) 'Iraqi solar house cooling season performance evaluation'. *Solar & Wind Technology*, 6 (1). pp 29-40.

Al-Rawahi, N., Zurigat, Y. & Al-Azri, N. (2011) 'Prediction of hourly solar radiation on horizontal and inclined surfaces for Muscat/Oman'. *The Journal of Engineering Research*, 8 (2). pp 19-31.

Al-Riahi, M., Al-Hamdani, N. & Tahir, K. (1992) 'An empirical method for estimation of hourly diffuse fraction of global radiation'. *Renewable Energy*, 2 (4–5). pp 451-456.

Al-Riahi, M., Al-Jumaily, K. & Kamies, I. (2003) 'Measurements of net radiation and its components in semi-arid climate of Baghdad'. *Energy Conversion and Management*, 44 (4). pp 509-525.

Al-Riahi, M., Al-Jumaily, K. J. & Ali, H. Z. (1998) 'Modeling clear weather day solar irradiance in Baghdad, Iraq'. *Energy Conversion and Management*, 39 (12). pp 1289-1294.

Al-Riahi, M. & Al-Kayssi, A. (1998) 'Some comments on time variation in solar radiation over Baghdad, Iraq'. *Renewable Energy*, 14 (1–4). pp 479-484.

AL-Salihi, A. M., Kadum, M. M. & Mohammed, A. J. (2010) 'Estimation of Global Solar Radiation on Horizontal Surface Using Routine Meteorological Measurements for Different Cities in Iraq'. *Asian Journal of Scientific Research*, 3 (4). pp 240-248.

Al-Sanea, S. A., Zedan, M. F. & Al-Ajlan, S. A. (2004) 'Adjustment factors for the ASHRAE clear-sky model based on solar-radiation measurements in Riyadh'. *Applied Energy*, 79 (2). pp 215-237.

Al-Ugla, A. A., El-Shaarawi, M. A. I. & Said, S. A. M. (2015) 'Alternative designs for a 24-hours operating solar-powered LiBr–water absorption air-conditioning technology'. *International Journal of Refrigeration*, 53 pp 90-100.

Al-Zahrani, S. M., Tan, F. L. & Choo, F. H. (2012) 'A TRNSYS Simulation Case Study on Utilization of Heat Pump For both Heating and Cooling'. *Energy Science & Technology*, 2 (2). pp 84-92.

Alasady, A. M. A. (2011) 'Solar energy the suitable energy alternative for Iraq beyond oil'. *International Conference on Petroleum and Sustainable Development*. Singapore: IACSIT Press.

Ali, A. H. H., Noeres, P. & Pollerberg, C. (2008) 'Performance assessment of an integrated free cooling and solar powered single-effect lithium bromide-water absorption chiller'. *Solar Energy*, 82 (11). pp 1021-1030.

Alnaser, W. E. & Alnaser, N. W. (2011) 'The status of renewable energy in the GCC countries'. *Renewable and Sustainable Energy Reviews*, 15 (6). pp 3074-3098.

Amarananwatana, P. & Sorapipatana, C. (2004) 'An assessment of the ASHRAE clear sky model for irradiance prediction in Thailand', *the Joint International Conference on Sustainable Energy and Environment (SEE)*. Hua Hin, Thailand.

APRICUS. http://www.apricus.com/ (Accessed: Jan 2016).

Ardehali, M. M., Shahrestani, M. & Adams, C. C. (2007) 'Energy simulation of solar assisted absorption system and examination of clearness index effects on auxiliary heating'. *Energy Conversion and Management*, 48 (3). pp 864-870.

Armstrong, S. & Hurley, W. G. (2010) 'A new methodology to optimise solar energy extraction under cloudy conditions'. *Renewable Energy*, 35 (4). pp 780-787.

Arsalis, A. & Alexandrou, A. N. (2015) 'Parametric study and cost analysis of a solar-heating-and-cooling system for detached single-family households in hot climates'. *Solar Energy*, 117 pp 59-73.

ASHRAE (2005) 'Fenstration'. *2005 ASHRAE Handbook-Fundamentals (SI).* Atlanta, USA: ASHRAE, pp 31.13-31.17.

ASHRAE (2009) 'Climatic Design Information'. *2009 ASHRAE Handbook-Fundamentals (SI).* Atlanta, USA.

ASHRAE (2012) *2012 ASHRAE Handbook: Heating, Ventilating, and Air-conditioning Systems and Equipment.* Atlanta, USA:

Assilzadeh, F., Kalogirou, S. A., Ali, Y. & Sopian, K. (2005) 'Simulation and optimization of a LiBr solar absorption cooling system with evacuated tube collectors'. *Renewable Energy*, 30 (8). pp 1143-1159.

Atmaca, I. & Yigit, A. (2003) 'Simulation of solar-powered absorption cooling system'. *Renewable Energy*, 28 (8). pp 1277-1293.

Ayadi, O., Mauro, A., Aprile, M. & Motta, M. (2012) 'Performance assessment for solar heating and cooling system for office building in Italy'. *Energy Procedia*, 30 pp 490-494.

Bakirci, K. (2009) 'Estimation of Solar Radiation by Using ASHRAE Clear-Sky Model in Erzurum, Turkey'. *Energy Sources, Part A*, 31 (3). pp 208-216.

Bakirci, K. (2012a) 'Correlations for Optimum Tilt Angles of Solar Collectors: A Case Study in Erzurum, Turkey'. *Energy Sources, Part A: Recovery, Utilization, and Environmental Effects*, 34 (11). pp 983-993.

Bakirci, K. (2012b) 'General models for optimum tilt angles of solar panels: Turkey case study'. *Renewable and Sustainable Energy Reviews*, 16 (8). pp 6149-6159.

Balaras, C. A., Grossman, G., Henning, H.-M., Infante Ferreira, C. A., Podesser, E., Wang, L. & Wiemken, E. (2007) 'Solar air conditioning in Europe—an overview'. *Renewable and Sustainable Energy Reviews*, 11 (2). pp 299-314.

Balghouthi, M., Chahbani, M. H. & Guizani, A. (2005) 'Solar Powered air conditioning as a solution to reduce environmental pollution in Tunisia'. *Desalination*, 185 (1–3). pp 105-110.

Balghouthi, M., Chahbani, M. H. & Guizani, A. (2008) 'Feasibility of solar absorption air conditioning in Tunisia'. *Building and Environment*, 43 (9). pp 1459-1470.

Baniyounes, A. M., Liu, G., Rasul, M. G. & Khan, M. M. K. (2013) 'Comparison study of solar cooling technologies for an institutional building in subtropical Queensland, Australia'. *Renewable and Sustainable Energy Reviews*, 23 pp 421-430.

Batlles, F. J., Rubio, M. A., Tovar, J., Olmo, F. J. & Alados-Arboledas, L. (2000) 'Empirical modeling of hourly direct irradiance by means of hourly global irradiance'. *Energy*, 25 (7). pp 675-688.

Beghi, A., Cecchinato, L., Rampazzo, M. & Simmini, F. (2014) 'Energy efficient control of HVAC systems with ice cold thermal energy storage'. *Journal of Process Control*, 24 (6). pp 773-781.

Bellos, E., Tzivanidis, C. & Antonopoulos, K. A. (2016) 'Exergetic, energetic and financial evaluation of a solar driven absorption cooling system with various collector types'. *Applied Thermal Engineering*, 102 pp 749-759.

Belmonte, J. F., Izquierdo-Barrientos, M. A., Eguía, P., Molina, A. E. & Almendros-Ibáñez, J. A. (2014) 'PCM in the heat rejection loops of absorption chillers. A feasibility study for the residential sector in Spain'. *Energy and Buildings*, 80 pp 331-351.

Benghanem, M. (2011) 'Optimization of tilt angle for solar panel: Case study for Madinah, Saudi Arabia'. *Applied Energy*, 88 (4). pp 1427-1433.

Best B, R., Aceves H, J. M., Islas S, J. M., Manzini P, F. L., Pilatowsky F, I., Scoccia, R. & Motta, M. (2013) 'Solar cooling in the food industry in Mexico: A case study'. *Applied Thermal Engineering*, 50 (2). pp 1447-1452.

Bird, R. E. & Hulstrom, R. L. (1981) *Simplified clear sky model for direct and diffuse insolation on horizontal surfaces.* Colorado, USA: Solar Energy Research Institute. Available at: http://rredc.nrel.gov/solar/pubs/pdfs/tr-642-761.pdf (Accessed: Jan 2016).

Boland, J., Ridley, B. & Brown, B. (2008) 'Models of diffuse solar radiation'. *Renewable Energy*, 33 (4). pp 575-584.

Boland, J., Scott, L. & Luther, M. (2001) 'Modelling the diffuse fraction of global solar radiation on a horizontal surface'. *Environmetrics*, 12 (2). pp 103-116.

Boonnasa, S. & Namprakai, P. (2010) 'The chilled water storage analysis for a university building cooling system'. *Applied Thermal Engineering*, 30 (11–12). pp 1396-1408.

Boopathi Raja, V. & Shanmugam, V. (2012) 'A review and new approach to minimize the cost of solar assisted absorption cooling system'. *Renewable and Sustainable Energy Reviews*, 16 (9). pp 6725-6731.

Brander, M., Sood, A., Wylie, C., Haughton, A. & Lovell, J. (2011) *Technical Paper | Electricity-specific emission factors for grid electricity.* Available at: http://ecometrica.com/assets/Electricity-specific-emission-factors-for-grid-electricity.pdf (Accessed: 8th Jan 2015).

Brown, D. R. (2000) *Thermal energy storage space cooling technology for reducing on-peak electricity demand and cost.* Federal Technology Alert, US-DOE. Available at: http://www.pnl.gov/main/publications/external/technical_reports/pnnl-13607.pdf (Accessed: Sept, 2015).

Bukoski, J., Gheewala, S. H., Mui, A., Smead, M. & Chirarattananon, S. (2014) 'The life cycle assessment of a solar-assisted absorption chilling system in Bangkok, Thailand'. *Energy and Buildings*, 72 pp 150-156.

Calise, F. (2010) 'Thermoeconomic analysis and optimization of high efficiency solar heating and cooling systems for different Italian school buildings and climates'. *Energy and Buildings*, 42 (7). pp 992-1003.

Calise, F., d'Accadia, M. D. & Vanoli, L. (2011) 'Thermoeconomic optimization of Solar Heating and Cooling systems'. *Energy Conversion and Management*, 52 (2). pp 1562-1573.

Calise, F., Dentice d'Accadia, M. & Palombo, A. (2010) 'Transient analysis and energy optimization of solar heating and cooling systems in various configurations'. *Solar Energy*, 84 (3). pp 432-449.

Calise, F., Palombo, A. & Vanoli, L. (2010) 'Maximization of primary energy savings of solar heating and cooling systems by transient simulations and computer design of experiments'. *Applied Energy*, 87 (2). pp 524-540.

Caliskan, H., Dincer, I. & Hepbasli, A. (2013) 'Thermoeconomic analysis of a building energy system integrated with energy storage options'. *Energy Conversion and Management*, 76 pp 274-281.

Chang, T. P. (2008) 'Study on the optimal tilt angle of solar collector according to different radiation types'. *Int. J, Applied Sei. Eng*, 2 pp 151-161.

Chang, T. P. (2009) 'The gain of single-axis tracked panel according to extraterrestrial radiation'. *Applied Energy*, 86 (7–8). pp 1074-1079.

ClimaTemps: Baghdad. http://www.baghdad.climatemps.com/sunlight.php (Accessed: Jan 2016).

Cole, W., Kim, J., Kapoor, K. & Edgar, T. (2015) 'Addressing the Peak Power Problem Through Thermal Energy Storage'. *Case Studies in Operations Research.* Springer, pp 337-353.

Cole, W. J., Powell, K. M. & Edgar, T. F. (2012) 'Optimization and advanced control of thermal energy storage systems'. *Reviews in Chemical Engineering - De Gruyter*, 28 (2-3). pp 81-99.

Cole, W. J., Powell, K. M., Hale, E. T. & Edgar, T. F. (2014) 'Reduced-order residential home modeling for model predictive control'. *Energy and Buildings*, 74 pp 69-77.

Davis, L. W. & Gertler, P. J. (2015) 'Contribution of air conditioning adoption to future energy use under global warming '. *Proceedings of the National Academy of Sciences*, 112 (19). pp 5962-5967.

Davis, P. (2014) *SolarKeymark Certificate.* Fakhraldin, S., [Email].June 2014.

de Miguel, A., Bilbao, J., Aguiar, R., Kambezidis, H. & Negro, E. (2001) 'Diffuse solar irradiation model evaluation in the North Mediterranean Belt area'. *Solar Energy*, 70 (2). pp 143-153.

Dervishi, S. & Mahdavi, A. (2012) 'Computing diffuse fraction of global horizontal solar radiation: A model comparison'. *Solar Energy*, 86 (6). pp 1796-1802.

Dincer, I. & Rosen, M. A. (2011) *Thermal Energy Storage: Systems and Applications.* Wiley.

DOE (2012) *Building Technologies Program: EnergyPlus Energy Simulation Software.* Available at: http://apps1.eere.energy.gov/buildings/energyplus/.

Drosou, V. N., Tsekouras, P. D., Oikonomou, T. I., Kosmopoulos, P. I. & Karytsas, C. S. (2014) 'The HIGH-COMBI project: High solar fraction heating and cooling systems with combination of innovative components and methods'. *Renewable and Sustainable Energy Reviews*, 29 pp 463-472.

Eicker, U. (2009) *Low Energy Cooling for Sustainable Buildings.* UK: Wiley.

Eicker, U. & Pietruschka, D. (2009) 'Design and performance of solar powered absorption cooling systems in office buildings'. *Energy and Buildings*, 41 (1). pp 81-91.

El-Kassaby, M. M. (1988) 'Monthly and daily optimum tilt angle for south facing solar collectors; theoretical model, experimental and empirical correlations'. *Solar & Wind Technology*, 5 (6). pp 589-596.

El-Sebaii, A. A., Al-Hazmi, F. S., Al-Ghamdi, A. A. & Yaghmour, S. J. (2010) 'Global, direct and diffuse solar radiation on horizontal and tilted surfaces in Jeddah, Saudi Arabia'. *Applied Energy*, 87 (2). pp 568-576.

Elminir, H. K. (2007) 'Experimental and theoretical investigation of diffuse solar radiation: Data and models quality tested for Egyptian sites'. *Energy*, 32 (1). pp 73-82.

Elminir, H. K., Ghitas, A. E., El-Hussainy, F., Hamid, R., Beheary, M. M. & Abdel-Moneim, K. M. (2006) 'Optimum solar flat-plate collector slope: Case study for Helwan, Egypt'. *Energy Conversion and Management*, 47 (5). pp 624-637.

Elsayed, M. M. (1989) 'Optimum orientation of absorber plates'. *Solar Energy*, 42 (2). pp 89-102.

Erbs, D. G., Klein, S. A. & Duffie, J. A. (1982) 'Estimation of the diffuse radiation fraction for hourly, daily and monthly-average global radiation'. *Solar Energy*, 28 (4). pp 293-302.

Ertekin, C., Evrendilek, F. & Kulcu, R. (2008) 'Modeling Spatio-Temporal Dynamics of Optimum Tilt Angles for Solar Collectors in Turkey'. *Sensors*, 8 (5). pp 2913-2931.

Fan, Y., Luo, L. & Souyri, B. (2007) 'Review of solar sorption refrigeration technologies: Development and applications'. *Renewable and Sustainable Energy Reviews*, 11 (8). pp 1758-1775.

Florides, G. A., Kalogirou, S. A., Tassou, S. A. & Wrobel, L. C. (2002) 'Modelling and simulation of an absorption solar cooling system for Cyprus'. *Solar Energy*, 72 (1). pp 43-51.

Galanis, N. & Chatigny, R. (1986) 'A critical review of the ASHRAE solar radiation model'. *ASHRAE Trans.*, 92 (part 1).

Gaspar, P. D. & Silva, P. D. d. (2015) *Handbook of Research on Advances and Applications in Refrigeration Systems and Technologies.* IGI Global.

Gebreslassie, B. H., Guillén-Gosálbez, G., Jiménez, L. & Boer, D. (2009) 'Design of environmentally conscious absorption cooling systems via multi-objective optimization and life cycle assessment'. *Applied Energy*, 86 (9). pp 1712-1722.

Genchi, Y., Kikegawa, Y. & Inaba, A. (2002) 'CO2 payback–time assessment of a regional-scale heating and cooling system using a ground source heat–pump in a high energy–consumption area in Tokyo'. *Applied Energy*, 71 (3). pp 147-160.

Ghaddar, N. K., Shihab, M. & Bdeir, F. (1997) 'Modeling and simulation of solar absorption system performance in Beirut'. *Renewable Energy*, 10 (4). pp 539-558.

Ghiaus, C. & Jabbour, N. (2012) 'Optimization of multifunction multi-source solar systems by design of experiments'. *Solar Energy*, 86 (1). pp 593-607.

Goldberg, D. E. (1989) *Genetic Algorithms in Search, Optimization, and Machine Learning.* Addison-Wesley

GoModel Solar. http://solargis.com/ (Accessed: June 2016).

Granjeon, R., Burgun, F., Taylor, R. & Boudehenn, F. (2013) 'Simulation as a Tool for Solar Cooling Systems in Humid, Tropical Climates', *BS2013: 13th Conference of International Building Performance Simulation Association*. Chambéry, France.

Griffiths, S. (2013) 'Strategic considerations for deployment of solar photovoltaics in the Middle East and North Africa'. *Energy Strategy Reviews*, 2 (1). pp 125-131.

Gueymard, C. A. (2008) 'REST2: High-performance solar radiation model for cloudless-sky irradiance, illuminance, and photosynthetically active radiation – Validation with a benchmark dataset'. *Solar Energy*, 82 (3). pp 272-285.

Gueymard, C. A. & Thevenard, D. (2009) 'Monthly average clear-sky broadband irradiance database for worldwide solar heat gain and building cooling load calculations'. *Solar Energy*, 83 (11). pp 1998-2018.

Gunerhan, H. & Hepbasli, A. (2007) 'Determination of the optimum tilt angle of solar collectors for building applications'. *Building and Environment*, 42 (2). pp 779-783.

Habeebullah, B. A. (2007) 'Economic feasibility of thermal energy storage systems'. *Energy and Buildings*, 39 (3). pp 355-363.

Hammad, M. & Zurigat, Y. (1998) 'Performance of a second generation solar cooling unit'. *Solar Energy*, 62 (2). pp 79-84.

Hammer, A., Heinemann, D., Hoyer, C., Kuhlemann, R., Lorenz, E., Müller, R. & Beyer, H. G. (2003) 'Solar energy assessment using remote sensing technologies'. *Remote Sensing of Environment*, 86 (3). pp 423-432.

Hang, Y., Du, L., Qu, M. & Peeta, S. (2013) 'Multi-objective optimization of integrated solar absorption cooling and heating systems for medium-sized office buildings'. *Renewable Energy*, 52 pp 67-78.

Hang, Y. & Qu, M. (2010) 'The impact of hot and cold storages on a solar absorption cooling system for an office building'. *International High Performance Buildings Conference*. Indiana, USA: Purdue University.

Hang, Y., Qu, M. & Ukkusuri, S. (2011) 'Optimizing the design of a solar cooling system using central composite design techniques'. *Energy and Buildings*, 43 (4). pp 988-994.

Hang, Y., Qu, M. & Zhao, F. (2011) 'Economical and environmental assessment of an optimized solar cooling system for a medium-sized benchmark office building in Los Angeles, California'. *Renewable Energy*, 36 (2). pp 648-658.

Hasnain, S. M. & Alabbadi, N. M. (2000) 'Need for thermal-storage air-conditioning in Saudi Arabia'. *Applied Energy*, 65 (1–4). pp 153-164.

Hasnain, S. M., Alawaji, S. H., Al-Ibrahim, A. & Smiai, M. S. (1999) 'Applications of Thermal Energy Storage in Saudi Arabia'. *International journal of energy research*, 23 (2). pp 117-124.

Hassan, H. Z. & Mohamad, A. A. (2012) 'A review on solar cold production through absorption technology'. *Renewable and Sustainable Energy Reviews*, 16 (7). pp 5331-5348.

Hay, J. E. (1979) 'Calculation of monthly mean solar radiation for horizontal and inclined surfaces'. *Solar Energy*, 23 (4). pp 301-307.

Henning, H.-M. (2007) 'Solar assisted air conditioning of buildings – an overview'. *Applied Thermal Engineering*, 27 (10). pp 1734-1749.

Henze, G. P., Dodier, R. H. & Krarti, M. (1997) 'Development of a predictive optimal controller for thermal energy storage systems'. *HVAC&R Research*, 3 (3). pp 233-264.

Hidalgo, M. C. R., Aumente, P. R., Millán, M. I., Neumann, A. L. & Mangual, R. S. (2008) 'Energy and carbon emission savings in Spanish housing air-conditioning using solar driven absorption system'. *Applied Thermal Engineering*, 28 (14–15). pp 1734-1744.

Hollands, K. & Crha, S. (1987) 'An improved model for diffuse radiation: correction for atmospheric back-scattering'. *Solar Energy*, 38 (4). pp 233-236.

Hwang, Y., Radermacher, R., Alili, A. A. & Kubo, I. (2008) 'Review of Solar Cooling Technologies'. *HVAC&R Research*, 14 (3). pp 507-528.

Ineichen, P. (2008) 'Comparison and validation of three global-to-beam irradiance models against ground measurements'. *Solar Energy*, 82 (6). pp 501-512.

Iqbal, M. (1980) 'Prediction of hourly diffuse solar radiation from measured hourly global radiation on a horizontal surface'. *Solar Energy*, 24 (5). pp 491-503.

Iraqi Electricity Ministry. http://www.moelc.gov.iq/ (Accessed: Jan. 2016).

Jacovides, C. P., Boland, J., Asimakopoulos, D. N. & Kaltsounides, N. A. (2010) 'Comparing diffuse radiation models with one predictor for partitioning incident PAR radiation into its diffuse component in the eastern Mediterranean basin'. *Renewable Energy*, 35 (8). pp 1820-1827.

Jacovides, C. P., Tymvios, F. S., Assimakopoulos, V. D. & Kaltsounides, N. A. (2006) 'Comparative study of various correlations in estimating hourly diffuse fraction of global solar radiation'. *Renewable Energy*, 31 (15). pp 2492-2504.

Jafarkazemi, F. & Saadabadi, S. A. (2012) 'Optimum tilt angle and orientation of solar surfaces in Abu Dhabi, UAE'. *Renewable Energy*, 56 pp 44-49.

Joudi, K. A. & Abdul-Ghafour, Q. J. (2003) 'Development of design charts for solar cooling systems. Part I: computer simulation for a solar cooling system and development of solar cooling design charts'. *Energy Conversion and Management*, 44 (2). pp 313-339.

Kacira, M., Simsek, M., Babur, Y. & Demirkol, S. (2004) 'Determining optimum tilt angles and orientations of photovoltaic panels in Sanliurfa, Turkey'. *Renewable Energy*, 29 (8). pp 1265-1275.

Kalogirou, S. A. (2013) *Solar Energy Engineering: Processes and Systems.* Elsevier Science.

Karamangil, M. I., Coskun, S., Kaynakli, O. & Yamankaradeniz, N. (2010) 'A simulation study of performance evaluation of single-stage absorption refrigeration system using conventional working fluids and alternatives'. *Renewable and Sustainable Energy Reviews*, 14 (7). pp 1969-1978.

Kasten, F. & Young, A. T. (1989) 'Revised optical air mass tables and approximation formula'. *Applied Optics*, 28 (22). pp 4735-4738.

Ketjoy, N., yongphayoon, R. & Mansiri, K. (2013) 'Performance Evaluation of 35 kW LiBr–H2O Solar Absorption Cooling System in Thailand'. *Energy Procedia*, 34 pp 198-210.

Khalil, S. A. & Shaffie, A. (2013) 'Performance of Statistical Comparison Models of Solar Energy on Horizontal and Inclined Surface'. *International Journal of Energy and Power*, 2 (1).

Kim, D. S. & Infante Ferreira, C. A. (2008) 'Solar refrigeration options – a state-of-the-art review'. *International Journal of Refrigeration*, 31 (1). pp 3-15.

Klein, S. A. (1977) 'Calculation of monthly average insolation on tilted surfaces'. *Solar Energy*, 19 (4). pp 325-329.

Klein, S. A., Beckman, W. A., Mitchell, J. W., Duffie, J. A. & Duffie, N. A. (2012) *TRNSYS 17: a Transient System Simulation Program.* The Solar Energy Laboratory, University of Wisconsin-Madison, Madison, USA

Available at: http://sel.me.wisc.edu/trnsys.

Kohlenbach, P. & Jakob, U. (2014) *Solar Cooling: The Earthscan Expert Guide to Solar Cooling Systems.* Taylor & Francis.

Koo, C., Park, S., Hong, T. & Park, H. S. (2014) 'An estimation model for the heating and cooling demand of a residential building with a different envelope design using the finite element method'. *Applied Energy*, 115 pp 205-215.

Krarti, M. (2010) *Energy Audit of Building Systems: An Engineering Approach, Second Edition.* CRC Press.

Kwak, H. Y., Kim, D. J. & Jeon, J. S. (2003) 'Exergetic and thermoeconomic analyses of power plants'. *Energy*, 28 (4). pp 343-360.

Labus, J. M., Bruno, C. J. & Coronas, A. (2013) 'Review on absorption technology with emphasis on small capacity absorption machines'. *Thermal Science*, 17 (3). pp 739-762.

Lauret, P., Boland, J. & Ridley, B. (2010) 'Derivation of a Solar Diffuse Fraction Model in a Bayesian Framework'. *Case studies in business, industry and government statistics (CS-BIGS)*, 3 (2). pp 108-122.

Lauret, P., Boland, J. & Ridley, B. (2013) 'Bayesian statistical analysis applied to solar radiation modelling'. *Renewable Energy*, 49 pp 124-127.

Lave, M. & Kleissl, J. (2011) 'Optimum fixed orientations and benefits of tracking for capturing solar radiation in the continental United States'. *Renewable Energy*, 36 (3). pp 1145-1152.

Lazzarin, R. M. (2013) 'Solar cooling: PV or thermal? A thermodynamic and economical analysis'. *International Journal of Refrigeration*, 39

Lentz, A., Renné, D., Eicker, U., Pietruschka, D., Haag, M. & Schmitt, A. (2014) '2013 ISES Solar World CongressEnergy and Economic Performance of Solar Cooling Systems World Wide'. *Energy Procedia*, 57 pp 2581-2589.

Lewis, G. (1987) 'Optimum tilt of a solar collector'. *Solar & Wind Technology*, 4 (3). pp 407-410.

Li, Z. F. & Sumathy, K. (2001) 'Experimental studies on a solar powered air conditioning system with partitioned hot water storage tank'. *Solar Energy*, 71 (5). pp 285-297.

Liu, B. & Jordan, R. (1962) 'Daily insolation on surfaces tilted towards equator'. *Trans ASHRAE*, 67 pp 526-540.

Liu, B. Y. H. & Jordan, R. C. (1960) 'The interrelationship and characteristic distribution of direct, diffuse and total solar radiation'. *Solar Energy*, 4 (3). pp 1-19.

Louche, A., Notton, G., Poggi, P. & Simonnot, G. (1991) 'Correlations for direct normal and global horizontal irradiation on a French Mediterranean site'. *Solar Energy*, 46 (4). pp 261-266.

Lubitz, W. D. (2011) 'Effect of manual tilt adjustments on incident irradiance on fixed and tracking solar panels'. *Applied Energy*, 88 (5). pp 1710-1719.

Mahdi, E. J., Abdul-Wahid, s. N., ShakerAbdulstar, S., Sahab, S. A. & Mosli, A. H. (2011) 'Optimum Orientation of Solar Panels in Baghdad city'. *Journal of Basrah Researches (Sciences)*, 37. (3).

Maluleke, A. (2002) *Optimal control versus conventional control strategies for ice-based thermal storage*. MSc thesis. Rand Afrikaans University.

Mammoli, A., Vorobieff, P., Barsun, H., Burnett, R. & Fisher, D. (2010) 'Energetic, economic and environmental performance of a solar-thermal-assisted HVAC system'. *Energy and Buildings*, 42 (9). pp 1524-1535.

Marc, O., Anies, G., Lucas, F. & Castaing-Lasvignottes, J. (2012) 'Assessing performance and controlling operating conditions of a solar driven absorption chiller using simplified numerical models'. *Solar Energy*, 86 (9). pp 2231-2239.

Marc, O., Lucas, F., Sinama, F. & Monceyron, E. (2010) 'Experimental investigation of a solar cooling absorption system operating without any backup system under tropical climate'. *Energy and Buildings*, 42 (6). pp 774-782.

Marc, O., Sinama, F. & Lucas, F. (2012) 'Decision making tool to design solar cooling system coupled with building under tropical climate'. *Energy and Buildings*, 49 pp 28-36.

Marion, W. & Wilcox, S. (1995) *Solar radiation data manual for buildings.* National Renewable Energy Laboratory. Available at: http://rredc.nrel.gov/solar/pubs/bluebook/ (Accessed: July 2013).

Martínez, J. C. (2014) *Cooling tower in in Alicante (Spain) research.* Fakhraldin, S., [Email].June 2014.

Martínez, P. J., Martínez, J. C. & Lucas, M. (2012) 'Design and test results of a low-capacity solar cooling system in Alicante (Spain)'. *Solar Energy*, 86 (10). pp 2950-2960.

MathWorks, I. (2014) *MATLAB 2014b Optimization Toolbox : User's Guide.* The MathWorks.

MATLAB (2012) (Version 2012b) [Computer Program]. Available at: www.mathworks.com

Maxwell, E. L. (1987) *A quasi-physical model for converting hourly global horizontal to direct normal insolation.* Colorado, USA: Solar Energy Research Institute. Available at: http://rredc.nrel.gov/solar/pubs/PDFs/TR-215-3087.pdf (Accessed: Jan 2016).

Mitchell, M. (1998) *An introduction to genetic algorithms.* MIT press.

Monné, C., Alonso, S., Palacín, F. & Serra, L. (2011) 'Monitoring and simulation of an existing solar powered absorption cooling system in Zaragoza (Spain)'. *Applied Thermal Engineering*, 31 (1). pp 28-35.

Moreno, A. G., Peláez, P. C., Garrido, F. D., Carnicero, J. P., García, R. L. & Peragón, F. C. (2010) 'Results of an experimental study of a solar cooling system in Jaén using single effect lithium bromide absorption chiller'. *RE&PQJ*, 1 (8). pp 915-919.

Mugnier, D. (2015a) *Task 48 Simplified short brochure: Quality assurance and support measures for solar cooling.* IEA Solar Heating and Cooling Programme Available at: http://task48.iea-shc.org/data/sites/1/publications/Task48%20D3%20brochure%20final.pdf (Accessed: Mar 2016).

Mugnier, D. (2015b) *Task 48 Solar Cooling Position paper: Quality Assurance and Support Measures for Solar Cooling.* IEA Solar Heating and Cooling Programme. Available at: https://www.iea-shc.org/data/sites/1/publications/IEA-SHC_Solar-Cooling-Position-Paper_Sep2015.pdf (Accessed: Mar 2016).

Munari Probst, M. & Roecker, C. (2007) 'Towards an improved architectural quality of building integrated solar thermal systems (BIST)'. *Solar Energy*, 81 (9). pp 1104-1116.

Muneer, T., Hawas, M. M. & Sahili, K. (1984) 'Correlation between hourly diffuse and global radiation for New Delhi'. *Energy Conversion and Management*, 24 (4). pp 265-267.

Muneer, T. & Munawwar, S. (2006) 'Improved accuracy models for hourly diffuse solar radiation'. *Trans. ASME*, 128 (1). pp 104.

Muzathik, A. M., Ibrahim, M. Z., Samo, K. B. & Wan Nik, W. B. (2011) 'Estimation of global solar irradiation on horizontal and inclined surfaces based on the horizontal measurements'. *Energy*, 36 (2). pp 812-818.

Nijegorodov, N. (1996) 'Improved ashrae model to predict hourly and daily solar radiation components in Botswana, Namibia, and Zimbabwe'. *Renewable Energy*, 9 (1–4). pp 1270-1273.

Nijmeh, S. & Mamlook, R. (2000) 'Testing of two models for computing global solar radiation on tilted surfaces'. *Renewable Energy*, 20 (1). pp 75-81.

Noorian, A. M., Moradi, I. & Kamali, G. A. (2008) 'Evaluation of 12 models to estimate hourly diffuse irradiation on inclined surfaces'. *Renewable Energy*, 33 (6). pp 1406-1412.

Notton, G., Cristofari, C., Muselli, M. & Poggi, P. (2004) 'Calculation on an hourly basis of solar diffuse irradiations from global data for horizontal surfaces in Ajaccio'. *Energy Conversion and Management*, 45 (18–19). pp 2849-2866.

Onan, C., Ozkan, D. B. & Erdem, S. (2010) 'Exergy analysis of a solar assisted absorption cooling system on an hourly basis in villa applications'. *Energy*, 35 (12). pp 5277-5285.

Orgill, J. F. & Hollands, K. G. T. (1977) 'Correlation equation for hourly diffuse radiation on a horizontal surface'. *Solar Energy*, 19 (4). pp 357-359.

Ortiz, M., Barsun, H., He, H., Vorobieff, P. & Mammoli, A. (2010) 'Modeling of a solar-assisted HVAC system with thermal storage'. *Energy and Buildings*, 42 (4). pp 500-509.

Perez, R., Ineichen, P., Maxwell, E., Seals, R. & Zelenka, A. (1992) 'Dynamic global-to-direct irradiance conversion models', *ASHRAE Winter Meeting*. pp. 354-369.

Perez, R., Ineichen, P., Seals, R. & Zelenka, A. (1990a) 'Making full use of the clearness index for parameterizing hourly insolation conditions'. *Solar Energy*, 45 (2). pp 111-114.

Perez, R., Seals, R., Zelenka, A. & Ineichen, P. (1990b) 'Climatic evaluation of models that predict hourly direct irradiance from hourly global irradiance: Prospects for performance improvements'. *Solar Energy*, 44 (2). pp 99-108.

Pongtornkulpanich, A., Thepa, S., Amornkitbamrung, M. & Butcher, C. (2008) 'Experience with fully operational solar-driven 10-ton LiBr/H2O single-effect absorption cooling system in Thailand'. *Renewable Energy*, 33 (5). pp 943-949.

Posadillo, R. & López Luque, R. (2009) 'Hourly distributions of the diffuse fraction of global solar irradiation in Córdoba (Spain)'. *Energy Conversion and Management*, 50 (2). pp 223-231.

Praene, J. P., Marc, O., Lucas, F. & Miranville, F. (2011) 'Simulation and experimental investigation of solar absorption cooling system in Reunion Island'. *Applied Energy*, 88 (3). pp 831-839.

Qiu, G. & Riffat, S. B. (2003) 'Optimum tilt angle of solar collectors and its impact on performance'. *International Journal of Ambient Energy*, 24 (1). pp 13-20.

Rakovec, J., Zakšek, K., Brecl, K., Kastelec, D. & Topič, M. (2011) *Orientation and Tilt Dependence of a Fixed PV Array Energy Yield Based on Measurements of Solar Energy and Ground Albedo – a Case Study of Slovenia.* Energy Management Systems.

Reda, F., Viot, M., Sipilä, K. & Helm, M. (2016) 'Energy assessment of solar cooling thermally driven system configurations for an office building in a Nordic country'. *Applied Energy*, 166 pp 27-43.

Reindl, D. T., Beckman, W. A. & Duffie, J. A. (1990) 'Diffuse fraction correlations'. *Solar Energy*, 45 (1). pp 1-7.

Ridley, B., Boland, J. & Lauret, P. (2010) 'Modelling of diffuse solar fraction with multiple predictors'. *Renewable Energy*, 35 (2). pp 478-483.

Rismanchi, B., Saidur, R., BoroumandJazi, G. & Ahmed, S. (2012) 'Energy, exergy and environmental analysis of cold thermal energy storage (CTES) systems'. *Renewable and Sustainable Energy Reviews*, 16 (8). pp 5741-5746.

Ruiz-Arias, J. A., Alsamamra, H., Tovar-Pescador, J. & Pozo-Vázquez, D. (2010) 'Proposal of a regressive model for the hourly diffuse solar radiation under all sky conditions'. *Energy Conversion and Management*, 51 (5). pp 881-893.

Said, S. A. M., El-Shaarawi, M. A. I. & Siddiqui, M. U. (2015) 'Analysis of a solar powered absorption system'. *Energy Conversion and Management*, 97 pp 243-252.

Sanaye, S. & Shirazi, A. (2013) 'Thermo-economic optimization of an ice thermal energy storage system for air-conditioning applications'. *Energy and Buildings*, 60 pp 100-109.

Saraf, G. R. & Hamad, F. A. W. (1988) 'Optimum tilt angle for a flat plate solar collector'. *Energy Conversion and Management*, 28 (2). pp 185-191.

Sarbu, I. & Sebarchievici, C. (2013) 'Review of solar refrigeration and cooling systems'. *Energy and Buildings*, 67 pp 286-297.

Sebzali, M. J. & Rubini, P. A. (2006) 'Analysis of ice cool thermal storage for a clinic building in Kuwait'. *Energy Conversion and Management*, 47 (18–19). pp 3417-3434.

Sebzali, M. J. & Rubini, P. A. (2007) 'The impact of using chilled water storage systems on the performance of air cooled chillers in Kuwait'. *Energy and Buildings*, 39 (8). pp 975-984.

Shariah, A., Al-Akhras, M. A. & Al-Omari, I. A. (2002) 'Optimizing the tilt angle of solar collectors'. *Renewable Energy*, 26 (4). pp 587-598.

Shirazi, A., Najafi, B., Aminyavari, M., Rinaldi, F. & Taylor, R. A. (2014) 'Thermal–economic–environmental analysis and multi-objective optimization of an ice thermal energy storage system for gas turbine cycle inlet air cooling'. *Energy*, 69 pp 212-226.

Shirazi, A., Pintaldi, S., White, S. D., Morrison, G. L., Rosengarten, G. & Taylor, R. A. (2016a) 'Solar-assisted absorption air-conditioning systems in buildings: Control strategies and operational modes'. *Applied Thermal Engineering*, 92 pp 246-260.

Shirazi, A., Taylor, R. A., White, S. D. & Morrison, G. L. (2016b) 'Transient simulation and parametric study of solar-assisted heating and cooling absorption systems: An energetic, economic and environmental (3E) assessment'. *Renewable Energy*, 86 pp 955-971.

Silvetti, B. (2002) 'Application Fundamentals Of Ice-Based Thermal Storage'. *ASHRAE journal*, (Feb 2002).

Skartveit, A. & Asle Olseth, J. (1986) 'Modelling slope irradiance at high latitudes'. *Solar Energy*, 36 (4). pp 333-344.

Skartveit, A. & Olseth, J. A. (1987) 'A model for the diffuse fraction of hourly global radiation'. *Solar Energy*, 38 (4). pp 271-274.

Skartveit, A., Olseth, J. A. & Tuft, M. E. (1998) 'An hourly diffuse fraction model with correction for variability and surface albedo'. *Solar Energy*, 63 (3). pp 173-183.

Skeiker, K. (2009) 'Optimum tilt angle and orientation for solar collectors in Syria'. *Energy Conversion and Management*, 50 (9). pp 2439-2448.

Soulayman, S. S. (1991) 'On the optimum tilt of solar absorber plates'. *Renewable Energy*, 1 (3–4). pp 551-554.

Spencer, J. W. (1982) 'A comparison of methods for estimating hourly diffuse solar radiation from global solar radiation'. *Solar Energy*, 29 (1). pp 19-32.

Srikhirin, P., Aphornratana, S. & Chungpaibulpatana, S. (2001) 'A review of absorption refrigeration technologies'. *Renewable and Sustainable Energy Reviews*, 5 (4). pp 343-372.

Stair, R. & Ellis, H. T. (1968) 'The Solar Constant Based on New Spectral Irradiance Data from 310 to 530 Nanometers'. *Journal of Applied Meteorology*, 7 (6). pp 635-644.

Stephenson, D. G. (1965) 'Equations for solar heat gain through windows'. *Solar Energy*, 9 (2). pp 81-86.

Sunderan, P., Ismail, A. M., Singh, B. & Mohamed, N. M. (2011) 'Optimum Tilt Angle and Orientation of Stand-Alone Photovoltaic Electricity Generation Systems for Rural Electrification'. *Journal of Applied Sciences*, 11 (7). pp 1219-1224.

Syed, A., Izquierdo, M., Rodríguez, P., Maidment, G., Missenden, J., Lecuona, A. & Tozer, R. (2005) 'A novel experimental investigation of a solar cooling system in Madrid'. *International Journal of Refrigeration*, 28 (6). pp 859-871.

Tang, R. & Wu, T. (2004) 'Optimal tilt-angles for solar collectors used in China'. *Applied Energy*, 79 (3). pp 239-248.

Thevenard, D. (2012) *Solar clear sky irradiance and related data for Baghdad, Iraq.* [Email].July 2012.

Thirugnanasambandam, M., Iniyan, S. & Goic, R. (2010) 'A review of solar thermal technologies'. *Renewable and Sustainable Energy Reviews*, 14 (1). pp 312-322.

Tiris, M. & Tiris, C. (1998) 'Optimum collector slope and model evaluation: Case study for Gebze, Turkey'. *Energy Conversion and Management*, 39 (3–4). pp 167-172.

Torres, J. L., De Blas, M., García, A. & de Francisco, A. (2010) 'Comparative study of various models in estimating hourly diffuse solar irradiance'. *Renewable Energy*, 35 (6). pp 1325-1332.

Touretzky, C. R. & Baldea, M. (2014) 'Nonlinear model reduction and model predictive control of residential buildings with energy recovery'. *Journal of Process Control*, 24 (6). pp 723-739.

Trading Economics: Iraq Interest Rate. http://www.tradingeconomics.com/iraq/interest-rate (Accessed: June 2016).

Trieb, F. & Müller-Steinhagen, H. (2008) 'Concentrating solar power for seawater desalination in the Middle East and North Africa'. *Desalination*, 220 (1–3). pp 165-183.

TRNSYS. Solar Energy Laboratory, University of Wisconsin, Madison, USA. http://www.trnsys.com/ (Accessed: Jan 2016).

Tsoutsos, T., Aloumpi, E., Gkouskos, Z. & Karagiorgas, M. (2010) 'Design of a solar absorption cooling system in a Greek hospital'. *Energy and Buildings*, 42 (2). pp 265-272.

Tsoutsos, T., Anagnostou, J., Pritchard, C., Karagiorgas, M. & Agoris, D. (2003) 'Solar cooling technologies in Greece. An economic viability analysis'. *Applied Thermal Engineering*, 23 (11). pp 1427-1439.

Tyagi, V. V., Rahim, N. A. A., Rahim, N. A. & Selvaraj, J. A. L. (2013) 'Progress in solar PV technology: Research and achievement'. *Renewable and Sustainable Energy Reviews*, 20 pp 443-461.

Ulgen, K. (2006) 'Optimum Tilt Angle for Solar Collectors'. *Energy Sources, Part A: Recovery, Utilization, and Environmental Effects*, 28 (13). pp 1171-1180.

Ullah, K. R., Saidur, R., Ping, H. W., Akikur, R. K. & Shuvo, N. H. (2013) 'A review of solar thermal refrigeration and cooling methods'. *Renewable and Sustainable Energy Reviews*, 24 pp 499-513.

Wang, R. Z., Ge, T. S., Chen, C. J., Ma, Q. & Xiong, Z. Q. (2009) 'Solar sorption cooling systems for residential applications: Options and guidelines'. *International Journal of Refrigeration*, 32 (4). pp 638-660.

Wessapan, T. & Somsuk, N. (2008) 'Applicability of the ASHRAE Clear Sky Model in Bangkok Metropolitan Area'. *Thammasat Int. J. Sc. Tech*, 13 Special Edition pp 75-79.

Western, B. E. (1990) 'The estimation of solar radiation in New Zealand'. *Solar Energy*, 45 (3). pp 121-129.

Wong, L. T. & Chow, W. K. (2001) 'Solar radiation model '. *Applied Energy*, 69 (3). pp 191-224.

Wu, S. & Eames, I. W. (2000) 'Innovations in vapour-absorption cycles'. *Applied Energy*, 66 (3). pp 251-266.

Xu, Z. Y., Wang, R. Z. & Wang, H. B. (2015) 'Experimental evaluation of a variable effect LiBr–water absorption chiller designed for high-efficient solar cooling system'. *International Journal of Refrigeration*, 59 pp 135-143.

Yang, L., Yan, H. & Lam, J. C. (2014) 'Thermal comfort and building energy consumption implications – A review'. *Applied Energy*, 115 pp 164-173.

Yazaki-airconditioning (2007) 'WFC-SC5 Data Sheet'.[in. Available at: http://www.yazaki-airconditioning.com/fileadmin/templates/pdf_airconditioning/data_sheets/FT_WFC_SC_5_en.pdf (Accessed:Yazaki-airconditioning 11 February 2014).

Yildiz, A. (2011) 'Investigation of Applicability of Ashrae Clear-Sky Model to Izmir, Turkey'. *ISI bilimi ve tekniği dergisi/Journal of Thermal Science and Technology*, 31 (2). pp 25-32.

Yudong, M., Borrelli, F., Hencey, B., Coffey, B., Bengea, S. & Haves, P. (2012) 'Model Predictive Control for the Operation of Building Cooling Systems'. *Control Systems Technology, IEEE Transactions on*, 20 (3). pp 796-803.

Yudong, M., Borrelli, F., Hencey, B., Packard, A. & Bortoff, S. (2009) 'Model Predictive Control of thermal energy storage in building cooling systems', *Decision and Control, 2009 held jointly with the 2009 28th Chinese Control Conference. CDC/CCC 2009. Proceedings of the 48th IEEE Conference on*. 15-18 Dec. 2009. pp. 392-397.

Zakula, T., Armstrong, P. R. & Norford, L. (2014) 'Modeling environment for model predictive control of buildings'. *Energy and Buildings*, 85 pp 549-559.

Zhai, X. Q., Qu, M., Li, Y. & Wang, R. Z. (2011) 'A review for research and new design options of solar absorption cooling systems'. *Renewable and Sustainable Energy Reviews*, 15 (9). pp 4416-4423.

Zhang, Z., Turner, W. D., Chen, Q., Xu, C. & Deng, S. (2011) 'Methodology for determining the optimal operating strategies for a chilled-water-storage system—Part I: Theoretical model'. *HVAC&R Research*, 17 (5). pp 737-751.

Zhao, Y., Lu, Y., Yan, C. & Wang, S. (2015) 'MPC-based optimal scheduling of grid-connected low energy buildings with thermal energy storages'. *Energy and Buildings*, 86 pp 415-426.